

Identification of a cGMP/Ca<sup>2+</sup> crosstalk in cerebellar granule neurons and  
development of a new method for cell-specific NO generation

Dissertation

zur Erlangung des Grades eines  
Doktors der Naturwissenschaften

der Mathematisch-Naturwissenschaftlichen Fakultät  
und  
der Medizinischen Fakultät  
der Eberhard-Karls-Universität Tübingen

vorgelegt

von

Michael Paolillo

geboren in Baltimore, MD, USA

Dezember – 2018

Tag der mündlichen Prüfung: 24.1.2019

Dekan der Math.-Nat. Fakultät: Prof. Dr. W. Rosenstiel

Dekan der Medizinischen Fakultät: Prof. Dr. I. B. Autenrieth

1. Berichterstatter: Prof. Dr. Robert Feil

2. Berichterstatter: PD Dr. Andrea Wizenmann

Prüfungskommission: Prof. Dr. Thorsten Stafforst

PD Dr. Hannes Schmidt

**Erklärung / Declaration:**

Ich erkläre, dass ich die zur Promotion eingereichte Arbeit mit dem Titel:

„Identification of a cGMP/Ca<sup>2+</sup> crosstalk in cerebellar granule neurons and development of a new method for cell-specific NO generation“

selbständig verfasst, nur die angegebenen Quellen und Hilfsmittel benutzt und wörtlich oder inhaltlich übernommene Stellen als solche gekennzeichnet habe. Ich versichere an Eides statt, dass diese Angaben wahr sind und dass ich nichts verschwiegen habe. Mir ist bekannt, dass die falsche Abgabe einer Versicherung an Eides statt mit Freiheitsstrafe bis zu drei Jahren oder mit Geldstrafe bestraft wird.

*I hereby declare that I have produced the work entitled*

*“Identification of a cGMP/Ca<sup>2+</sup> crosstalk in cerebellar granule neurons and development of a new method for cell-specific NO generation”,*

*submitted for the award of a doctorate, on my own (without external help), have used only the sources and aids indicated and have marked passages included from other works, whether verbatim or in content, as such. I swear upon oath that these statements are true and that I have not concealed anything. I am aware that making a false declaration under oath is punishable by a term of imprisonment of up to three years or by a fine.*

Tübingen, den .....

Datum / Date

.....

Unterschrift /Signature

# Table of contents

Zusammenfassung .....	vii
Summary .....	ix
Acknowledgements.....	xi
List of figures .....	xii
List of tables .....	xiv
Abbreviations .....	xv
<b>1 Introduction .....</b>	<b>1</b>
1.1 Cellular signaling .....	1
1.2 cGMP and the Nobel Prize .....	1
1.3 NO-cGMP signal transduction .....	2
1.4 cGMP-modulating drugs for humans.....	7
1.5 NO-cGMP signaling in the nervous system .....	8
1.6 Biological models to investigate NO-cGMP signaling .....	12
1.7 Real-time imaging of signal transduction with biosensors.....	13
1.8 Transgenic mice and the Cre/loxP system .....	16
1.9 A new method to induce cell type specific NO generation .....	18
1.10 Aim of the work .....	20
<b>2 Materials and Methods.....</b>	<b>21</b>
2.1 General Materials .....	21
2.1.1 Common compounds, reagents and antibodies .....	21
2.1.2. Common buffers and solutions .....	22
2.2 Mice .....	23
2.3 Mouse genotyping .....	24
2.4 Cell culture.....	26
2.4.1. Primary culture of vascular smooth muscle cells .....	26
2.4.1. Primary culture of cerebellar granule neurons .....	28
2.5 Transfection of primary VSMCs.....	30
2.6 Preparation of acute brain slices and fixed brain sections .....	30
2.7 Animal procedures for imaging under anesthesia .....	30
2.7.1. Surgical implantation of mouse cranial window .....	30
2.7.2. Microinjection protocol and mouse monitoring .....	31
2.8 Microscopy imaging setups.....	32
2.8.1. Fluorescence microscopy with Axiovert 200 microscope .....	32

2.8.2.	Fluorescence microscopy with Examiner.Z1 spinning disc microscope....	34
2.8.3.	Fluorescence microscopy with a 2-photon microscope .....	35
2.9	Imaging protocols.....	36
2.10	PDE inhibitor experiments .....	37
2.11	Protein isolation and Western blotting .....	37
2.12	Detailed working protocol for Lowry, SDS-Page and Western blotting .....	38
2.12.1.	Lowry protein assay .....	38
2.12.2.	SDS-Page and Western blot .....	40
2.13	Immunostaining .....	44
2.14	X-gal staining .....	44
2.15	$\beta$ -gal-NONOate activity in vivo as determined by VASP phosphorylation .....	44
2.16	Synthesis of $\beta$ -gal-NONOate .....	45
2.17	Data analysis and statistics .....	48
3	Results .....	49
3.1	NO-cGMP signaling in CGNs .....	49
3.1.1.	cGMP imaging in CGNs reveals a NO-induced cGMP response .....	49
3.1.2.	cGMP imaging in acute cerebellar slices reveals a NO-induced cGMP response .....	51
3.1.3.	Simultaneous imaging of $Ca^{2+}$ and cGMP reveals NO potentiation of glutamate-induced $Ca^{2+}$ transients in CGNs .....	52
3.1.4.	cGMP analogues support a cGMP-dependent increase of glutamate-induced $Ca^{2+}$ transients .....	54
3.1.5.	CGN primary cultures do not express cGKI nor cGKII as determined by Western blot analysis .....	55
3.1.6.	Real-time cGMP imaging in CGNs reveals a cGMP degradation via Zaprinast-sensitive PDEs .....	57
3.2	Cell type specific NO release with $\beta$ -gal-NONOate .....	58
3.2.1.	Synthesis of $\beta$ -gal-NONOate .....	59
3.2.2.	Real-time cGMP imaging in VSMCs with $\beta$ -gal-NONOate .....	63
3.2.3.	Real-time cGMP imaging in Purkinje cells in acute cerebellar slices with $\beta$ -gal-NONOate .....	65
3.2.4.	$\beta$ -gal-NONOate-induced VASP phosphorylation in vivo .....	68
3.2.5.	$\beta$ -gal-NONOate-induced vasodilation in the cerebral cortex .....	73
4	Discussion .....	76
4.1	NO-cGMP signaling in CGNs .....	76
4.1.1.	cGMP elevation in CGNs.....	76

4.1.2.	cGMP-Ca <sup>2+</sup> crosstalk in CGNs.....	77
4.1.3.	cGMP analogues to investigate cGMP-Ca <sup>2+</sup> crosstalk in CGNs.....	78
4.1.4.	The role of cGKs in cGMP-Ca <sup>2+</sup> crosstalk in CGNs.....	79
4.1.5.	cGMP degradation in CGNs via PDEs .....	81
4.1.6.	Outlook for cGMP signaling in CGNs .....	83
4.2	Cell type specific generation of NO with $\beta$ -gal-NONOate .....	84
4.2.1.	Synthesis of $\beta$ -gal-NONOate .....	85
4.2.2.	$\beta$ -gal-NONOate-induced cGMP responses in VSMCs.....	86
4.2.3.	$\beta$ -gal-NONOate-induced cGMP responses in cerebellar tissue slices.....	87
4.2.4.	$\beta$ -gal-NONOate-induced VASP phosphorylation in vivo .....	88
4.2.5.	$\beta$ -gal-NONOate-induced vasodilation in the cerebral cortex .....	89
4.2.6.	Outlook for $\beta$ -gal-NONOate as a tool to investigate the role of NO-cGMP signaling in behavior .....	90
5	Appendix.....	94
5.1	Polymerase chain reaction protocols .....	94
5.2	Construct map of pFRT $\beta$ -gal.....	95
6	References .....	96
7	Curriculum vitae .....	108

# Zusammenfassung

Stickstoffmonoxid (NO) und cyclisches Guanosinmonophosphat (cGMP) sind Signalmoleküle, welche an zahlreichen physiologischen Prozessen beteiligt sind. NO stimuliert die lösliche Guanylylcyclase (NO-GC), die cGMP aus Guanosintriphosphat (GTP) synthetisiert. cGMP steuert physiologische Prozesse durch die Aktivierung von cGMP-Effektorproteinen wie cGMP-abhängige Proteinkinasen (cGKs), cyclische Nukleotid gesteuerte Kationenkanäle (cyclic nucleotide gated channels; CNG Kanäle) oder Phosphodiesterasen (PDE). Des Weiteren bauen PDEs cGMP zu GMP ab. Der cGMP Signalweg beeinflusst u.a. den Gefäßtonus, Knochenwachstum, Neurotransmission sowie Lernen und Gedächtnis. Im Gegensatz zum kardiovaskulären System, bei welchem die funktionellen Implikationen der NO-cGMP-Signalkaskade bereits relativ gut erforscht sind, ist die Rolle dieses Signalsystems im Nervensystem weitgehend unbekannt. In dieser Arbeit haben wir Echtzeit-Fluoreszenzmikroskopie und andere biochemische Methoden verwendet, um den NO-cGMP-Signalweg im Nervensystem zu untersuchen. Des Weiteren haben wir eine Methode entwickelt, die eine zelltypspezifische Generierung von NO ermöglicht.

Im ersten Teil der Arbeit wurde die Wechselwirkung zwischen cGMP und  $Ca^{2+}$ , einem weiteren Signalmolekül, welches an neuronalen Funktionen beteiligt ist, weiter aufgeklärt. Für die simultane Messung beider Signalmoleküle in isolierten Kleinhirn Körnerzellen (cerebellar granule neurons; CGNs) haben wir ein mikroskopisches Echtzeit-Imaging Verfahren angewendet. Für die Visualisierung von cGMP wurde der Förster Resonanz Energietransfer (FRET)-basierte Sensor cGi500 verwendet. Für die Aufzeichnung von  $Ca^{2+}$  Signalen wurde der  $Ca^{2+}$ -sensitive Farbstoff Fura-2 eingesetzt. cGMP Signale wurden in kultivierten CGNs oder akut isolierten Kleinhirnschnitten aus transgenen Mäusen gemessen, welche den cGi500 Sensor exprimierten. Die Präparate wurden mit dem NO-Donor DEA/NO stimuliert. DEA/NO erhöhte die intrazelluläre cGMP-Konzentration und verstärkte Glutamat-induzierte  $Ca^{2+}$  Signale in CGNs. Diese DEA/NO-induzierten Effekte fehlten in CGNs, welche aus NO-GC Knockout-Mäusen isoliert wurden. Darüber hinaus konnten die Glutamat-induzierten  $Ca^{2+}$ -Signale in CGNs auch durch Applikation zweier unterschiedlicher cGMP-Analoga (8-Br-cGMP bzw. 8-pCPT-cGMP) verstärkt werden. Diese Analoga aktivieren cGMP-Effektor Proteine wie cGKs oder CNG Kanäle. Mittels Western Blot Analysen mit

spezifischen Antikörpern konnten wir weder für cGK Typ I noch cGK Typ II eine Expression in unseren primären CGN-Kulturen nachweisen. Durch Zugabe von PDE-Inhibitoren während der Messung von cGMP konnte gezeigt werden, dass CGNs cGMP über Zaprinast-sensitive PDEs abbauen, höchstwahrscheinlich durch PDE5 und/oder PDE10, aber nicht über PDE1, 2 oder 3. Zusammenfassend beschreiben diese Daten eine cGK-unabhängige NO-cGMP-Signalkaskade, welche die Glutamat-induzierten  $\text{Ca}^{2+}$ -Signale in CGNs verstärkt. Diese Wechselwirkung zwischen cGMP und  $\text{Ca}^{2+}$  beeinflusst vermutlich Neurotransmitter-stimulierte Funktionen in CGNs.

Im zweiten Teil der Arbeit wurde eine neue Methode entwickelt, die eine zelltypspezifische Generierung von NO ermöglicht. In vitro ist es bereits möglich den NO-cGMP Signalweg in ausgewählten Zelltypen zu untersuchen, jedoch bestand diese Möglichkeit bisher nicht für in vivo-Studien. Hier beschreiben wir eine neue Methode, welche auf der Verwendung von transgenen Mäusen und der Substanz  $\beta$ -Gal-NONOat basiert. Diese Substanz setzt NO nur in Gegenwart des Enzyms  $\beta$ -Galaktosidase frei. Durch eine Cre/loxP gesteuerte Expression des lacZ-Gens, welches für die  $\beta$ -Galaktosidase kodiert, war es möglich, NO in spezifischen Zelltypen freizusetzen. Durch die Zugabe von  $\beta$ -Gal-NONOat wurde nur in  $\beta$ -Galaktosidase exprimierenden glatten Muskelzellkulturen die intrazelluläre Konzentration von cGMP erhöht. Dies haben wir auch bei  $\beta$ -Galaktosidase exprimierenden Purkinje Zellen in Kleinhirnschnitten beobachtet. Weiterhin haben wir in einem transgenen Mausmodell, in dem  $\beta$ -Galaktosidase lediglich in Neuronen exprimiert wird,  $\beta$ -Gal-NONOat verwendet, um Vasodilatation in vivo über neuronal generiertes NO herbeizuführen. Zusammengefasst haben wir in dieser Arbeit den prinzipiellen Nachweis der zelltypspezifischen Generierung von NO durch Verabreichung von  $\beta$ -Gal-NONOat in Zellkultur, Gewebeschnitten und in vivo demonstriert. In Zukunft kann diese Methode dazu verwendet werden, um den Einfluss der Bildung von NO durch spezifische Zelltypen auf diverse biologische Prozesse zu untersuchen.

## Summary

Nitric oxide (NO) and cyclic guanosine monophosphate (cGMP) are signal molecules associated with various physiological processes. NO stimulates soluble guanylyl cyclase (NO-GC), which synthesizes cGMP from guanosine triphosphate (GTP). cGMP triggers physiological processes through the activation of cGMP effector proteins such as cGMP-dependent protein kinases (cGKs), cyclic nucleotide gated (CNG) cation channels, or phosphodiesterases (PDE). Furthermore, PDEs degrade cGMP to GMP. The cGMP signaling pathway influences processes such as vasodilation, bone growth, neurotransmission, and learning and memory. However, in contrast to the cardiovascular system where the functional implications of NO-cGMP signaling have been well described, its detailed role in the nervous system is still relatively unknown. In this thesis, we have used real-time fluorescence microscopy and other biochemical methods to further investigate NO-cGMP signaling in the nervous system. In addition, we have developed a method that enables NO generation in a cell specific manner.

In the first part of the work, we have studied the interaction between cGMP and  $\text{Ca}^{2+}$ , another signaling molecule involved in neuronal functions. We used microscopic real-time imaging techniques for the simultaneous measurement of both signal molecules in isolated cerebellar granule neurons (CGNs). To visualize cGMP, the Förster Resonance Energy Transfer (FRET)-based cGMP sensor, cGi500, was used, whereas the  $\text{Ca}^{2+}$ -sensitive dye Fura-2 was used to record  $\text{Ca}^{2+}$  signals. cGMP signals were measured in primary CGN cultures or acute cerebellar slices from transgenic mice expressing the cGi500 sensor. The preparations were stimulated with the NO donor DEA/NO. DEA/NO increased the intracellular cGMP concentration and augmented glutamate-induced  $\text{Ca}^{2+}$  signals in CGNs. These DEA/NO-induced effects were absent in CGNs isolated from NO-GC knockout mice. In addition, the glutamate-induced  $\text{Ca}^{2+}$  signals in CGNs were enhanced by the application of two different cGMP analogues (8-Br-cGMP and 8-pCPT-cGMP, respectively). These analogues activate cGMP effector proteins such as cGKs or CNG channels. Western blot analyses with specific antibodies could not detect expression of cGK type I or cGK type II in our primary CGN cultures. The addition of PDE inhibitors during cGMP measurements showed that CGNs degrade cGMP via Zaprinast-sensitive PDEs, most likely via PDE5

and/or PDE10, but not via PDE1, 2 or 3. In summary, these data describe a cGK-independent NO-cGMP signal cascade that increases glutamate-induced Ca<sup>2+</sup> signals in CGNs. This interaction between cGMP and Ca<sup>2+</sup> is thought to affect neurotransmitter-stimulated functions in CGNs.

In the second part of this work, a new method was described that enables the cell type-specific generation of NO. It is already possible to study the NO-cGMP signaling pathway in specific cell types in vitro, but this possibility did not exist until now for the in vivo situation. Here, we describe a new method based on the use of transgenic mice and the substance  $\beta$ -gal-NONOate. This compound releases NO only in the presence of the enzyme  $\beta$ -galactosidase. Through Cre/loxP controlled expression of the lacZ gene coding for  $\beta$ -galactosidase, it was possible to release NO in specific cell types. The addition of  $\beta$ -gal-NONOate increased the intracellular concentration of cGMP only in vascular smooth muscle cell cultures expressing  $\beta$ -galactosidase. A  $\beta$ -gal-NONOate-induced cGMP increase was also observed in  $\beta$ -galactosidase-expressing Purkinje cells of acute cerebellar slices. Furthermore, in a transgenic mouse model in which  $\beta$ -galactosidase is expressed only in neurons, we used  $\beta$ -gal-NONOate to induce vasodilatation in vivo via neuronally generated NO. In summary, this work has demonstrated the principle of cell type-specific NO generation by administration of  $\beta$ -gal-NONOate to cultured cells, tissue sections and mice in vivo. In the future, this method can be used to investigate the influence of NO generation by specific cell types on various biological processes.

# Acknowledgements

I thank Prof. Dr. Robert Feil for his guidance and support during my time in his laboratory.

I thank Prof. Dr. Thorsten Stafforst and PD Dr. Andrea Wizenmann for their support as my thesis advisory committee members.

I thank PD Dr. Hannes Schmidt for supporting my thesis defense and serving on the thesis board.

I thank the Graduate Training Centre for Neuroscience for their training, financial support and dedication to science education.

I also thank my colleagues present and past in the lab: Barbara Birk, Jacek Dobrowinski, Susanne Feil, Michael Krämer, Moritz Lehnert, Stefanie Peters, Frank Regler, Hannes Schmidt, Daniel Stehle, Martin Thunemann, Angelos Vachaviolos, Lai Wen, Markus Wolters, among others.

I thank Barbara Birk for her technical support in the lab as well as the animal care takers for their help in the animal facility.

I thank Prof. Dr. Anna Devor and Dr. Martin Thunemann for their collaboration at the University of California San Diego as well as the lab colleagues there.

I thank my collaborators, without whom this work would not have been possible. Including, but not limited to, the working groups of Prof. Dr. Thorsten Stafforst, Prof. Dr. Thomas Ziegler, Prof. Dr. Andreas Friebe, and Prof. Dr. Jens Schlossmann.

I thank my friends for their friendship and the great times shared.

I thank my parents Joan Paolillo and Dr. William Paolillo, sisters Gabrielle Paolillo and Isabelle Paolillo and brother James Paolillo for being there for me. I am lucky to have such an encouraging and supportive family.

And a big thank you goes to Laura Dudek Bothmann for her love and support without which I would be lost.

# List of figures

Figure 1. cGMP signaling and its physiological effects .....	5
Figure 2. Current hypothesis of the role of cGMP signaling in synaptic plasticity .....	10
Figure 3. A model of neurovascular coupling .....	11
Figure 4. FRET-based cGMP sensor cGi500.....	14
Figure 5. Fura-2-AM for intracellular Ca <sup>2+</sup> imaging .....	15
Figure 6. Generation of cell type specific gene expression with the Cre/loxP system....	17
Figure 7. Cell-specific elevation of NO with $\beta$ -gal-NONOate.....	19
Figure 8. Schematic representation of the cGi500 FRET imaging system .....	34
Figure 9. How to set up the Western blot with Whatman papers .....	42
Figure 10. Visualization of cGMP in CGNs reveals a NO-induced cGMP response .....	50
Figure 11. Visualization of cGMP in acute cerebellar slices reveals a NO-induced cGMP response.....	51
Figure 12. Simultaneous measurement of cGMP and Ca <sup>2+</sup> reveals cGMP-Ca <sup>2+</sup> crosstalk in CGNs.....	53
Figure 13. The addition of cGMP analogues confirms cGMP-Ca <sup>2+</sup> crosstalk in CGNs ....	54
Figure 14. Western blot analysis reveals no cGKI expression in primary CGNs .....	56
Figure 15. Western blot analysis reveals no cGKII expression in primary CGNs .....	56
Figure 16. Real-time cGMP imaging in CGNs reveals degradation of cGMP by Zaprinast-sensitive PDEs .....	58
Figure 17. <sup>1</sup> H NMR spectrum of the end product .....	60
Figure 18. Synthesis of $\beta$ -gal-NONOate .....	61
Figure 19. $\beta$ -gal-NONOate elevates cGMP in VSMC cultures expressing $\beta$ -galactosidase .....	64
Figure 20. $\beta$ -gal-NONOate does not elevate cGMP in VSMC cultures lacking $\beta$ -galactosidase.....	65
Figure 21. $\beta$ -gal-NONOate elevates cGMP in Purkinje cells in the presence of $\beta$ -galactosidase.....	67
Figure 22. X-gal staining of isolated tissues from SM-CreERT2 mice and controls. ....	70
Figure 23. $\beta$ -galactosidase-induced VASP phosphorylation .....	72
Figure 24. $\beta$ -gal-NONOate-induced vasodilation in the cerebral cortex.....	74
Figure 25. Summary and outlook of the CGN findings .....	83
Figure 26. Controlled intracranial injection of $\beta$ -gal-NONOate to investigate the role of	

<b>NO signaling in behavior paradigms.....</b>	<b>91</b>
<b>Figure A1. Construct map of pFRT<math>\beta</math>-gal .....</b>	<b>95</b>

# List of tables

<b>Table 1. Selected cGMP-modulating medications available or in development for human use.....</b>	<b>8</b>
<b>Table 2. PCR master mix.....</b>	<b>25</b>
<b>Table 3. Recommended amount of SDS lysis buffer .....</b>	<b>39</b>
<b>Table 4. Composition of polyacrylamide gel .....</b>	<b>41</b>
<b>Table A1. Primer Sequences .....</b>	<b>94</b>
<b>Table A2. Polymerase chain reaction conditions.....</b>	<b>94</b>

# Abbreviations

ANP	Atrial natriuretic peptide
$\beta$ -gal-NONOate	1-O-(1-pyrrolidinyl-ONN-azoxy)- $\beta$ -D-glucopyranose
Bp	Base pairs
BSA	Bovine serum albumin
$[Ca^{2+}]_i$	Intracellular $Ca^{2+}$ concentration
CAG	Cytomegalovirus early enhancer/chicken $\beta$ -actin/rabbit $\beta$ -globin
cAMP	Cyclic 3',5'-adenosine monophosphate
CFP	Cyan fluorescent protein
cGi	cGMP indicator
cGK	cGMP-dependent protein kinase
cGKI	cGMP-dependent protein kinase I
cGKII	cGMP-dependent protein kinase II
cGMP	Cyclic 3',5'-guanosine monophosphate
CGN	Cerebellar granule neuron
CNG	Cyclic nucleotide-gated
CNP	C-type natriuretic peptide
CNS	Central nervous system
Cre	Cyclisation recombination SSR
DEA/NO	2-(N,N-diethylamino)-diazene-2-oxide diethylammonium salt
DMEM	Dulbecco's modified Eagle medium
DMSO	Dimethyl sulfoxide
DNA	Deoxyribonucleic acid
EM-CCD	Electron multiplying charge-coupled device
eNOS	Endothelial NO synthase
ER	Endoplasmic reticulum
F340	Fluorescence intensity at 340 nm excitation
F380	Fluorescence intensity at 380 nm excitation
F480	Emission at 480 nm (CFP emission)
F535	Emission at 535 nm (YFP emission)
FRET	Förster resonance energy transfer
GAF	GAF domains from cGMP-specific phosphodiesterases, <i>Anabaena</i> adenylyl cyclases, and <i>E. coli</i> FhIA
GC	Guanylyl cyclase
GFP	Green fluorescent protein
IBMX	3-Isobutyl-1-methylxanthine
iNOS	Inducible NO synthase
lacZ	$\beta$ -galactosidase encoding gene
loxP	Locus of X-over in P1
mRNA	Messenger RNA
NGF	Nerve growth factor
NGS	Normal goat serum
NMDA	N-methyl-D-aspartate
nNOS	Neuronal NO synthase
NO	Nitric oxide
NO-GC	NO-sensitive guanylyl cyclase
NO-GC KO	NO-sensitive guanylyl cyclase knockout
NOS	Nitric oxide synthase
ODQ	1H-[1,2,4]oxadiazolo[4,3-a]quinoxalin-1-one
PBS	Phosphate-buffered saline
PCR	Polymerase chain reaction
PDE	Phosphodiesterase
PDL	Poly-D-lysine
Pen/Strep	Penicillin/Streptomycin
pGC	Particulate guanylyl cyclase
R	CFP/YFP emission ratio (F480/F535) or ratio of fluorescence intensity at 340 nm/380 nm excitation (F340/F380)
RNA	Ribonucleic acid
ROI	Region of interest

ROSA	Reverse orientation splice acceptor
rt	Room temperature
SDS	Sodium dodecyl sulfate
TBS-T	Tris-buffered saline with Tween-20
tg	transgene
Tris	Tris(hydroxymethyl)aminomethane
VASP	Vasodilator-stimulated phosphoprotein
VSMCs	Vascular smooth muscle cells
YFP	Yellow fluorescent protein

# 1 Introduction

## 1.1. Cellular signaling

Biological systems receive information from the external environment which is then processed internally. This is also true at the cellular level. Extracellular molecules either bind to transmembrane proteins and initiate an intracellular signaling cascade or extracellular molecules themselves pass through the cell membrane and directly bind effector proteins inside the cell. These signal cascades induce physiological reactions such as vasodilation or neuronal firing and ultimately contribute to overarching behavioral processes like learning and memory. Advances in this field of research have resulted in a deeper understanding of biological processes and helped to produce new medications for humans. This thesis further investigates the interaction between the signaling pathways of nitric oxide (NO), cyclic 3',5'-guanosine monophosphate (cGMP), and calcium ( $\text{Ca}^{2+}$ ).

## 1.2. cGMP and the Nobel Prize

The discovery of the second messenger cyclic adenosine monophosphate (cAMP) in 1958 by Rall and Sutherland [1] led to an explosive development of research on cyclic nucleotides and the intracellular second messenger cGMP has proven to be crucial for a variety physiological processes. For example, cGMP plays a vital role in vasodilation [2], bone growth [3], angiogenesis [4], hormone secretion [5], neurotransmission [6], sensory axon bifurcation [7], pain perception [8,9], learning and memory [10,11], among others. Since 1971, research relating to cyclic nucleotides and signal transduction has been awarded with at least five Nobel Prizes [12]. The prizes were awarded in 1971 to Dr. Sutherland Jr. for his work on hormones and cyclic adenosine monophosphate (cAMP) [13]; in 1992 to Dr. Fischer and Dr. Krebs for their work on protein kinases including cAMP regulated proteinkinases and their role in reversible protein phosphorylation [14]; in 1994 to Dr. Gilman and Dr. Rodbell for their work on G protein coupled receptors that regulate cAMP synthesis [15,16]; in 1998 to Dr. Furchgott, Dr. Ignarro and Dr. Murad for their findings about the role of NO and cGMP in vasodilation [17-21]; and in 2000 to Dr. Carlsson, Dr. Greengard, and Dr. Kandel for their contributions to cyclic nucleotide signaling in the nervous system [22-

24]. This field of research has proven itself highly influential across disciplines.

Alfred Nobel himself, the famous scientist and namesake of the Nobel Prize, helped to develop stable nitroglycerin in the mid-19<sup>th</sup> century and reportedly refused nitroglycerin as a treatment for his treat chest pain, so called angina pectoris [25]. NO releasing compounds have been used in the clinic since as early as 1867 to treat angina pectoris without an understanding of the underlying molecular mechanisms [25]. The 1998 Nobel Prize awarded to Dr. Furchgott, Dr. Ignarro and Dr. Murad is of particular interest to this doctoral thesis because they set the framework for NO-cGMP signaling. In their 1977 publication, Murad and colleagues demonstrated that certain nitric oxide releasing compounds, such as sodium nitroprusside, nitroglycerin, sodium azide and hydroxylamine increased cGMP levels via activation of the enzyme NO-sensitive guanylyl cyclase (NO-GC) [21]. A few years later in 1980, Furchgott and colleagues reported that a vasodilating substance was released from the endothelial layer of vessels upon exposure to acetylcholine. The paper termed the substance endothelium-derived relaxing factor (EDRF) [20,26]. Later work by Ignarro revealed that NO and EDRF are indeed one and the same [19], leading to the researcher's shared 1998 Nobel Prize for Physiology or Medicine. Since then a great deal of work conducted on NO has detailed the relevant enzymes and molecules responsible for its wide-ranging physiological effects. The following section outlines the relevant molecular players in cGMP signaling.

### **1.3. NO-cGMP signal transduction**

The enzymes that catalyze NO synthesis are known as nitric oxide synthases (NOSs) and consist of three known members: endothelial NOS (eNOS), neuronal NOS (nNOS) and inducible NOS (iNOS) [27,28]. NOS catalyzes the conversion of L-arginine and oxygen into NO and consists of a bidomain structure containing an N-terminal oxygenase domain that is linked to the C-terminal reductase domain by a Ca<sup>2+</sup>/calmodulin-recognition site and has binding sites for heme, tetrahydrobiopterin (BH<sub>4</sub>) and L-arginine [27,28]. The C-terminal reductase domain contains binding sites for the cofactors flavin adenine dinucleotide (FAD), flavin mononucleotide (FMN) and nicotinamide adenine dinucleotide phosphate (NADPH) [29]. eNOS is present in endothelial cells including those in the central nervous system (CNS) [27]. iNOS is associated with immune responses and has been reported in macrophages and

microglia [27,29]. nNOS generates NO in the central nervous system (CNS) and in specific tissues outside the CNS, for example in skeletal tissue. Both nNOS and eNOS demonstrate calcium-dependent regulation, while iNOS is calcium-insensitive [29,30].

nNOS was the first NOS to be purified and cloned and it is ubiquitously expressed throughout the CNS where it serves as the main source of NO in the brain [29]. Notably, the N-terminal 220 amino-acids of nNOS are distinct from the other NOS isoforms. The N-terminus of nNOS contains a binding site for the post synaptic density protein 95 (PSD-95), termed the PDZ binding domain. The term PDZ comes from the first letters of the first three proteins discovered with said domain, namely PSD-95, Drosophila disc large tumor suppressor (Dlg1), and zonula occludens-1 protein (zo-1) [29]. PSD-95 binds to the C-terminus of N-methyl-D-aspartate (NMDA) receptors and has been evidenced to provide a platform for the functional coupling of nNOS and NMDA receptors [31,32]. Researchers have postulated that agonist-induced NMDA receptor stimulation activates nNOS and thus NO generation in neurons pointing to a neuronal activity dependent modulation of cGMP signaling.

cGMP is generated via activation of guanylyl cyclases (GCs) which exist in two families: the NO-GC proteins, primarily found in the cytosol, and the transmembrane proteins, particulate guanylyl cyclases (pGCs). NO activates NO-GC [33,34], while natriuretic peptides, guanylin, uroguanylin, or enterotoxins activate pGC [35,36]. The enzyme GC-A binds atrial and B-type natriuretic peptide (ANP, BNP), while GC-B binds C-type natriuretic peptide (CNP), and GC-C binds guanylin and uroguanylin [35]. The pGC stimulated pathway is also essential for key neuronal processes. For example, the CNP/GC-B/cGMP pathway is essential for sensory axon bifurcation in the developing spinal cord and is associated with axon guidance [7,37]. However, the main focus of this work is NO-cGMP signaling.

The mammalian NO-GC is a heterodimeric hemoprotein with two known NO-GC isoforms,  $\alpha_1\beta_1$  and  $\alpha_2\beta_1$  [38]. Both isoforms exist in most tissues, but research has shown that while the  $\alpha_2\beta_1$  isoform is more prominently expressed in the brain in general [39], some neuronal regions express the  $\alpha_2$  or  $\alpha_1$  isoforms preferentially [40-43]. This suggests that there could be differential cGMP signaling facilitated by distinct NO-GC isoform distribution. The  $\alpha_2$  isoform has an additional PDZ binding domain, which could facilitate its localization to the presynapse [44]. Another isoform of the  $\beta$  subunit has been reported termed  $\beta_2$ , but it appears to be physiologically inert and is considered to

be a pseudogene [39]. NO-GC is primarily found in the cytosol and is the only known physiological receptor of NO in mammals. NO activates NO-GC via binding to the heme group of the  $\beta_1$  subunit at the axial ligand histidine 105 [45] and the heme-binding motif tyrosine 135 and arginine 139 [46]. Upon NO binding, the heme  $\text{Fe}^{2+}$  forms nitrosyl-heme [47], disrupting the histidine 105-iron bond resulting in enzyme activation and subsequent conversion of GTP into cGMP [45,48-50].

While this work focuses on NO as an activator of NO-GC, it is important to note that NO also can induce cGMP independent effects. For example, NO can generate reactive oxygen species, such as superoxide anion ( $\cdot\text{O}_2^-$ ) or peroxynitrite ( $\text{ONOO}^-$ ), both of which have been shown to cause oxidative injury [51]. This happens when peroxynitrite causes oxidative stress to DNA, proteins, or lipids. For example, these reactions can damage endothelial tissue and contribute to cardiovascular disease [51]. For these reasons, control experiments with tools that disrupt the function of NO-GC are essential to discriminate between the NO-GC mediated effects and NO-GC independent effects of NO.

cGMP signaling imparts its physiological effects via three main types of effectors: cGMP-dependent protein kinases (cGKs), cation channels, such as cyclic nucleotide gated (CNG) channels, and cGMP-regulated phosphodiesterases (PDEs) (**Figure 1**).

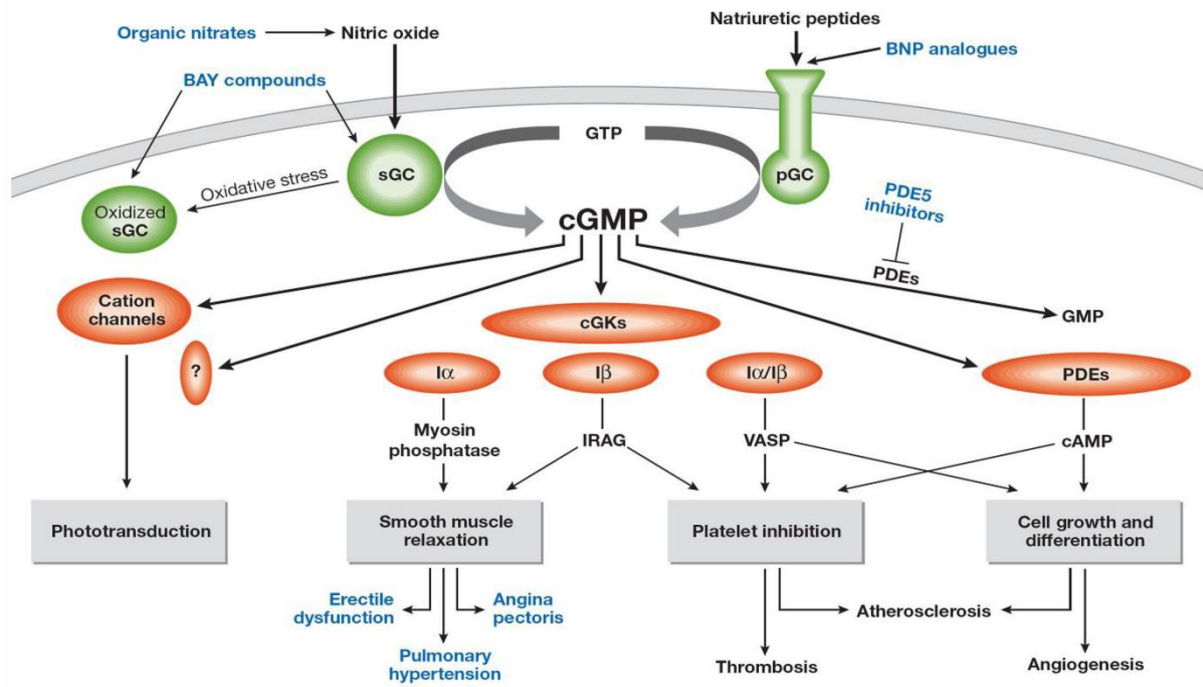


**Figure 1. cGMP signaling and its physiological effects.**

Pictured are cGMP generators (green), effectors (red), and some downstream pathways and cellular functions of cGMP signaling (grey boxes). The blue text represents areas where cGMP-modulating drugs act. The lower part shows some current (blue) and potential future (black) indications for drugs that modulate cGMP levels or cGMP effector pathways. BNP, B-type natriuretic peptide; cGKs, cGMP dependent protein kinases; IRAG, IP<sub>3</sub> receptor-associated cGKII $\beta$  substrate; PDEs, phosphodiesterases; pGC, particulate guanylyl cyclase; sGC, soluble guanylyl cyclase (also known as NO-GC); VASP, vasodilator-stimulated phosphoprotein. Adapted from Feil and Kemp-Harper, 2006 [52].

The cGKs are part of the serine/threonine kinase family and consist of three isoforms: cGK type I $\alpha$  and I $\beta$  (cGKI $\alpha/\beta$ ), and cGK type II (cGKII), these proteins are homodimers and also sometimes termed ‘protein kinase cGMP’ (PKG1 and PKG2) [53]. In this thesis, they will always be referred to as cGKs. The cGKs have two cGMP binding sites [54] and the N-terminus acts as a targeting sequence that influences the subcellular location of the different isoforms, where cGKI is generally in the cytosol and cGKII at the membrane [55,56]. cGKI is highly expressed in smooth muscle, cerebellum, hippocampus, dorsal root ganglia, neuromuscular junctions, kidney, and platelets, and in lower amounts in other tissues [57,58]. cGKII undergoes myristoylation of the Gly2 residue and is located at the plasma membrane. cGKII has been identified in the brain, kidney, adrenal cortex, lung, bone, and other tissues [56,59,60]. Some research suggests distinct functions of the different isoforms [61], but

studies also report that many cGK substrates are phosphorylated by both cGKI and cGKII suggesting that substrate specificity for one isoform is not pronounced in this system [62,63]. That said, differential expression of the cGK isoforms has been observed and cGKI and cGKII are generally not found in the same cell [56,58]. The cGKs also contain N-terminal leucine zipper motifs that form the catalytically active cGK homodimers. Upon cGMP binding, cGK undergoes a conformational change that results in the release of an inhibitory pseudo-substrate domain, located at the N-terminus, enabling the phosphorylation of substrate proteins [54,64]. The cGK substrates exist in a diverse range of tissues and are essential for the regulation of functions, such as cell contractility, motility, proliferation, differentiation, and cellular secretion [55,56]. The typical substrates of cGKs include certain G proteins, ion channels, and cytoskeletal-associated proteins [55].

cGMP can also influence CNG channels, which are found in the plasma membrane and belong to the superfamily of pore-loop cation channels [65,66]. They form heterotetrameric complexes consisting of two or three different subunits. The six different CNG channel genes encode four A subunits (A1, A2, A3, A4) and two B subunits (B1 and B3) [66]. The six homologous proteins display differential tissue expression patterns and varying binding affinities to cGMP and cAMP [66]. The channels open upon binding of cyclic nucleotides to the protein's intracellular region. They are permeable to Na<sup>+</sup>, K<sup>+</sup> and Ca<sup>2+</sup> and show voltage-dependent opening probabilities which are shifted by cyclic nucleotide binding [65]. They have been detected in tissues, such as olfactory bulb, retina, brain, kidneys, and sperm cells [65]. CNG channels are present throughout the mammalian CNS and have been implicated in modulating neuronal synaptic function [65,67,68].

cGMP also interacts with PDEs, which are responsible for cyclic nucleotide degradation. The superfamily of PDE enzymes consists of eleven gene families with some families consisting of multiple members [69-71]. There are a total of 21 PDE genes that also vary with alternative initiation sites and alternative splicing, which generates over 50 different PDE proteins. PDEs hydrolyze both cGMP and cAMP to their respective non-cyclized forms. PDEs 5, 6, and 9 are cGMP-specific; PDEs 4, 7 and 8 are cAMP-specific; and PDEs 1, 2, 3, 10, and 11 degrade both cAMP and cGMP but with varying efficiency [69-71]. PDE activity is regulated by cAMP or cGMP binding. Allosteric binding sites for both cAMP and cGMP known as GAF domains also exist

(cGMP-specific phosphodiesterases, *Anabaena* adenylyl cyclases, and *Escherichia coli* FhIA) and have been identified in PDEs 2, 5, 6, 10, and 11 [69,72]. The existence of GAF domains has resulted in hypothesized cGMP-cAMP crosstalk [73]. Indeed, researchers have reported that the NO-cGMP pathway inhibits transient cAMP signals via activation of PDE2 in striatal neurons demonstrating cGMP-cAMP crosstalk [74]. Furthermore, cAMP binding to PDE10 has been associated with increased cGMP levels [75]. Regarding the other PDEs with GAF domains, PDE 6 is almost exclusively discussed in the context of photoreceptor cells [69], while PDE 5 is reported as functionally relevant for the regulation of cGMP levels in smooth muscle cells, the heart, brain and elsewhere [76,77]. The PDE5 GAF domain has been well studied and a negative feedback loop regulating cGMP levels has been reported at higher cGMP concentrations [78]. This appears to occur due to allosteric binding of cGMP to PDEs which activates the catalytic sites resulting in cGMP hydrolysis [78]. Nearly all of the eleven PDE families have been reported in the CNS [69,79,80]. Research investigating PDEs in rodents and humans has suggested that PDEs 9, 10, and 11 play a role in neurological diseases, such as PDE9 in bipolar affective disorder [81], PDE10 in social interaction, schizophrenia, and bipolar disorder [82-84], and PDE11 in major depression [85]. The following sections discuss cGMP-modulating medications, NO-cGMP signaling in the nervous system, and the modern methods used to investigate cGMP signaling.

#### 1.4. cGMP-modulating drugs for humans

In the past decades, the cGMP signaling cascade has proven itself highly drugable, with the approval of various cGMP-modulating drugs for humans and many more cGMP-modulating substances are in late stage clinical development (**Table 1**). With greater understanding of the cGMP signaling pathway, it will be possible to design new medications that target different aspects of the signaling cascade. These targets include: NO releasing compounds; GC stimulators and activators; inhibitors of neprilysin, a natriuretic peptide degrading enzyme; PDE inhibitors and more could be discovered with further research. The PDE5 inhibitor sildenafil, one of the most famous medications, known commercially as Viagra, is prescribed to treat erectile dysfunction. Further PDE5 inhibitors exist to treat diseases in different therapeutic areas, such as cardiology [86]. Other cGMP-modulating medications include the GC-C agonist

linaclotide to treat chronic idiopathic constipation and irritable bowel syndrome, as well as NO-GC stimulators (e.g. Riociguat, IW-1701, and Ataciguat) which are designed to treat diseases, such as pulmonary hypertension, sickle cell anemia, and cardiovascular disease. Many companies have additional NO-GC stimulators in human clinical trials [87]. Pharmaceutical companies such as Bayer, Ironwood Pharmaceuticals, Abbot Labs, GlaxoSmithKline, Yung-Shin Pharmaceutical, Novartis, Boehringer Ingelheim, Sanofi-Aventis and others have invested time and money into the research and development of cGMP-modulating medications [87]. Indeed, preclinical and clinical research is currently underway on a multitude of cGMP-modulating drugs to determine their therapeutic value as treatments for diseases such as cardiovascular disease, sickle cell anemia, dwarfism, and others (**Table 1**).

**Table 1. Selected cGMP-modulating medications available or in development for human use.**

cGMP-modulating medications act on various parts of the cGMP signaling cascade and are approved for use in several therapeutic areas. The table provides examples of cGMP-modulating medications that are in late-stage clinical development or available in the clinic. See cited papers for more information [52,86-97].

Drug	Mechanism of action	Status	Therapeutic use	Citation
Ataciguat	NO-GC stimulator	Phase II	Cardiovascular	[87,90]
Cenderitide	GC-A and GC-B activator	Phase II	Cardiovascular	[92]
IW-1701	NO-GC stimulator	Phase II	Sickle cell anemia	[87]
Linaclotide	GC-C agonist	In clinical use	Irritable bowel syndrome	[93,94]
Riociguat	NO-GC stimulator	In clinical use	Pulmonary hypertension	[87,97]
Sacubitril	Neprilysin inhibitor	In clinical use	Cardiovascular	[95]
Sildenafil	PDE5 inhibitor	In clinical use	Erectile dysfunction and pulmonary hypertension	[86]
Vosoritide	CNP analogue	Phase II	Dwarfism	[96]

### 1.5. NO-cGMP signaling in the nervous system

Initially, the scientific community did not accept NO as a true neurotransmitter because it is not stored within the brain like other neurotransmitters. Perhaps even more perplexing was the idea that an unstable, gaseous molecule capable of diffusing

across both aqueous and lipid environments is able to serve a targeted function [98]. NO is now recognized as a neurotransmitter and NO-cGMP signaling has been documented in numerous regions of the CNS [6-8,10,30,98]. Both NO-GCs and pGCs have been reported in various neural regions including the cerebellum, striatum, cortex, olfactory bulb, and spinal cord [10]. Downstream targets of cGMP, including cGKI and cGKII, have been described in diverse areas of the nervous system [57,60,99]. CNG cation channels and PDEs have also been demonstrated to play a role in cGMP signaling in the CNS [65,67,69]. The NO-cGMP signaling pathway is implicated in neurological disorders, such as depression, addiction, schizophrenia, and cognition [10].

Modulation of cGMP signaling in the CNS alters learning and memory, as investigated with experimental paradigms, such as long-term potentiation (LTP) and long-term depression (LTD) [11,100]. LTP is a strengthening of synaptic communication between two neurons that persists long-term. LTD is an activity-dependent synaptic weakening that lasts for hours or longer. Both LTP and LTD are paradigms used to investigate learning and memory, or so-called synaptic plasticity. Learning and memory occurs via changes in synaptic efficiency contingent upon the relative frequency at which neurons fire together [101]. This process is referred to as Hebbian plasticity, named after the researcher Donald Hebb who first proposed the theory [102]. As written by Hebb, 'When an axon of cell A is near enough to excite a cell B and repeatedly or persistently takes part in firing it, some growth process or metabolic change takes place in one or both cells such that A's efficiency, as one of the cells firing B, is increased' [103]. Or as succinctly paraphrased by Carla Shatz 'what fires together, wires together', often quoted as 'neurons that fire together, wire together' [104,105].

As it currently stands, the hypothesis of NO-cGMP signaling in the brain begins with NO generation by nNOS, or perhaps eNOS. Then, cGMP is elevated by activated NO-GCs, whereby cGMP targets downstream molecules and ultimately initiates receptor recruitment to, or removal from, the synaptic membrane. Examples of such receptors are NMDA receptors or  $\alpha$ -amino-3-hydroxy-5-methyl-4-isoxazolepropionic acid (AMPA) receptors. Their addition to or removal from the synaptic membrane modulates synaptic firing sensitivities depending on the brain region (**Figure 2**). Due to the gaseous nature of NO, a signaling effect has been proposed whereby NO is

synthesized in the synapse and diffuses across the synaptic cleft to the other synapse elevating cGMP. Depending on the direction, this process is termed retrograde or anterograde NO signaling (**Figure 2**).

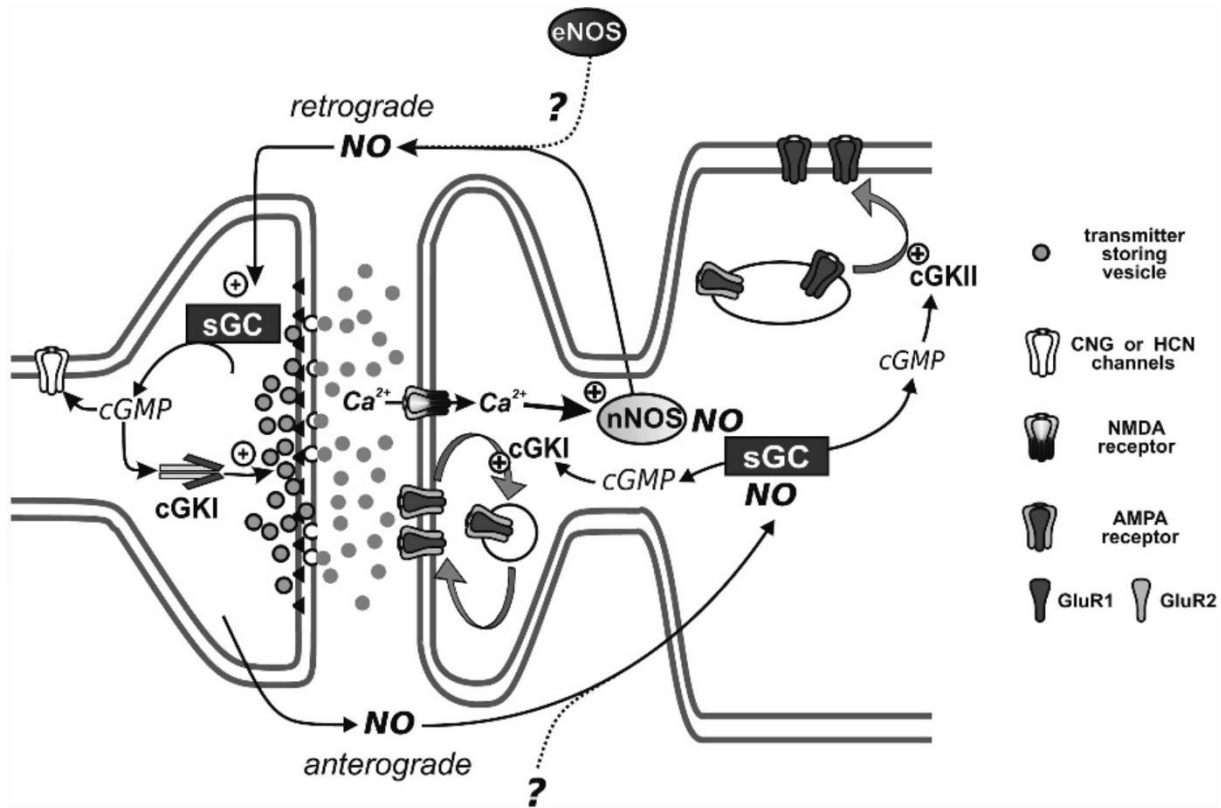


**Figure 2. Current hypothesis of the role of cGMP signaling in synaptic plasticity.**

NO is generated by a  $\text{Ca}^{2+}$ /calmodulin-regulated nNOS or possibly by eNOS from endothelial cells or neighboring neurons (indicated by the question marks). Cellular cGMP concentrations are elevated by sGC (also known as NO-GC) via activation by NO. The cGMP-dependent protein kinases (cGKI and cGKII) and members of two ion channel families (cyclic-nucleotide gated channels (CNG) and hyperpolarization-activated cyclic nucleotide-gated channels (HCN)) have been identified as downstream effectors of cGMP in synaptic plasticity. Depending on the brain region, NO is either produced in the postsynapse and then diffuses into the presynaptic terminal (retrograde signaling) or *vice versa* (anterograde signaling). Retrograde NO signaling has been implicated in LTP in the hippocampus and amygdala. Anterograde NO signaling has been proposed for LTD in the cerebellum. In this figure, the cGKI in the postsynapse may enhance the internalization of AMPA receptors indirectly through phosphorylation of G-substrate (not shown), which, in its phosphorylated form, serves as an inhibitor of protein phosphatases. This increases the level of phosphorylated AMPA receptors, which are removed from the postsynaptic membrane, ultimately, resulting in LTD of synaptic transmission. Adapted from Kleppisch and Feil, 2009 [10].

In addition to learning and memory, the NO-cGMP pathway might be involved in a process known as neurovascular coupling. Neurovascular coupling refers to changes in neuronal activity that result in modulated local blood perfusion and thus

changes in glucose and oxygen supply (**Figure 3**). Disruption of this process has been associated with various neurological diseases such as stroke, Alzheimer's Disease and cortical spreading depression [106,107]. While the exact molecular players involved in neurovascular coupling remain controversial, one candidate is NO [108,109]. Given the gaseous nature of NO, it could be synthesized by nNOS in neurons and diffuse across membranes to induce vasodilation in nearby vessels via elevation of cGMP. Previous work has demonstrated a relationship between NO, cerebral blood flow and oxygen levels in hippocampal slices [108]. Nevertheless, the significance of NO in neurovascular coupling in vivo is unclear.

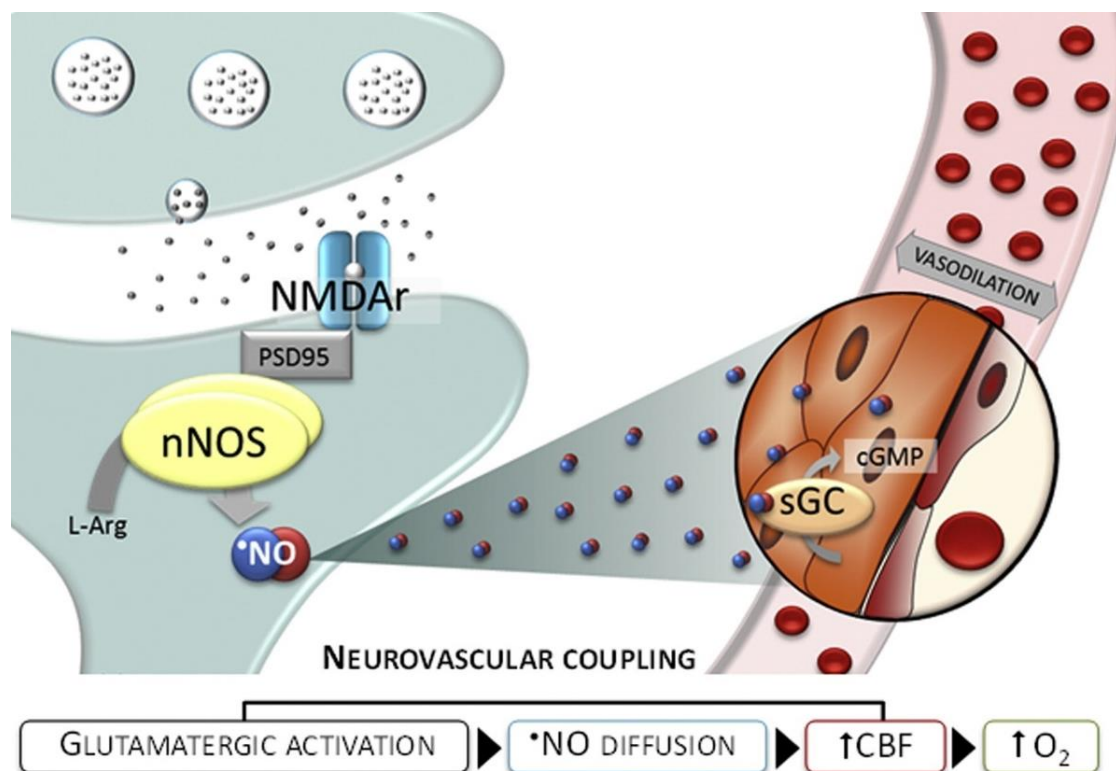


**Figure 3. A model of neurovascular coupling**

The model depicts the sequence of events leading to NO-modulated neurovascular coupling. NO is synthesized by nNOS in the neuron upon glutamate-induced stimulation of NMDA receptors and subsequent nNOS activation. NO then diffuses to nearby vessels, activates NO-GC (pictured sGC), which then elevates cGMP levels. cGMP then activates downstream targets and ultimately induces vasodilation. The resulting increased cerebral blood flow (CBF) provides neurons with more nutrients such as oxygen and glucose. Adapted from Lourenço et. al., 2014 [108].

Although the cGMP signaling cascade has been widely reported in the nervous system, its functional influence is understood in limited contexts. One can argue that the dearth of data on cGMP signaling in the CNS is a large hindrance to the development of cGMP-modulating medications for neurological disorders. Given the success of cGMP-modulating medications in other therapeutic areas (**Table 1**) and the clear relevance of cGMP signaling to neurological processes, it is imperative that researchers continue to delineate the cGMP signaling pathway in the CNS. Such research is of high clinical relevance, given that companies are developing CNS active cGMP-modulating molecules. For example, Ironwood pharmaceuticals has a CNS-penetrant NO-GC stimulator in preclinical development named IW-6463 [87]. Ultimately, a detailed understanding of NO-cGMP signaling is necessary to assess specificity and off-target effects of such treatment avenues. In the following sections, a number of tools will be presented that enable cell type specific generation of NO and the real-time visualization of cGMP in living cells, tissues, and animals allowing for improved spatiotemporal investigation of NO-cGMP signaling.

### **1.6. Biological models to investigate NO-cGMP signaling**

Researchers employ different models to investigate cell signaling pathways. Cell culture, tissue slices, and in vivo models all have their advantages and disadvantages. In this thesis we utilized primary vascular smooth muscle cell (VSMC) cultures isolated from mice. VSMCs are located in blood vessels and can contract to regulate blood flow. The vessel wall consists of three layers: tunica adventitia, tunica media, and tunica intima. The adventitial layer is made up of connective tissue; the intimal layer contains a layer of endothelial cells; the medial layer contains VSMCs. The endothelial cells generate NO which diffuses into the VSMCs and stimulates NO-GC resulting in cGMP elevation [2]. Then cGMP activates cGKI, which likely results in phosphorylation of several substrate proteins, although the in vivo relevance of some substrates is contested, and ultimately vasodilation [62,110]. NO-cGMP signaling has been extensively investigated in VSMCs [2], but its role in the CNS is less well documented.

For our neuronal cell model, we used primary cerebellar granule neurons (CGNs) isolated from mice. CGNs are the most abundant neuronal cell type in the brain. In the cerebellum, more than 90% of the neurons are granule neurons [111].

They are small with a soma of about 10  $\mu\text{m}$  in diameter containing a large nucleus that nearly encompasses the entire soma. CGNs usually have four extending dendrites that form synaptic connections with mossy fibers and Golgi cells in specialized structures referred to as glomeruli [112]. CGN axons, called parallel fibers, interact with another neuronal cell type known as Purkinje cells. CGNs are an established cell model in laboratories across the world and NO-cGMP signaling has been reported in these cells [111,113-116]. While they are highly useful in the laboratory setting, cell culture models are not always representative of the *in vivo* situation. For this reason, we also used acute brain tissue slices and *in vivo* models to investigate NO-cGMP signaling in more biologically relevant models.

### 1.7. Real-time imaging of signal transduction with biosensors

Endpoint assays such as Western blots, mRNA analysis, or immunoassays are often used to investigate signaling cascades. These techniques are limited in that they can only view living systems at single time points. Excitingly, live-cell microscopy has advanced in recent decades and numerous biosensors have been developed to visualize the spatiotemporal dynamics of signaling molecules in living cells and animals in real time [117-119].

Traditionally, cGMP has been measured via enzyme-linked immunosorbent assay (ELISA) or radioimmunoassays, but these are end-point assays meaning they only provide single values and, due to technical restrictions, their temporal resolution is low and they lack tissue or subcellular spatial information about the dynamic signaling processes [120,121]. Recently, the Feil lab has generated mouse lines that express fluorescent biosensors capable of measuring changes in intracellular cGMP concentrations ( $[\text{cGMP}]_i$ ) with high spatiotemporal resolution in real time in living cells, tissues, and mice providing a valuable tool to further investigate this cascade [118,122,123]. The new technology uses a Förster resonance energy transfer (FRET)-based cGMP sensor with an  $\text{EC}_{50}$  of  $\approx 500$  nM (cGi500) created by Russwurm and colleagues (**Figure 4**) [124]. The FRET phenomenon was first described by Theodor Förster in 1946 and operates based on radiationless energy transfer from a light sensitive donor fluorophore to a light sensitive acceptor fluorophore in a proximity and orientation dependent manner [125]. cGi500 is a ratiometric sensor that allows for quantitative measurements of  $[\text{cGMP}]_i$ . The sensor consists of cGMP binding domains

from cGKI flanked by a cyan and yellow fluorescent protein (CFP and YFP). When cGMP binds to cGi500, a conformational change occurs distancing and/or reorienting the two fluorescent proteins and reducing FRET. Specifically, binding of cGMP causes a decreased YFP emission (535 nm) and increased CFP emission (480 nm) in response to CFP excitation (445 nm) (**Figure 4**). The ratio of CFP/YFP emission is used as a measure of FRET efficiency and thus  $[cGMP]_i$ . Different transgenic knock-in mouse lines have been generated that express the cGMP sensor in different forms, for example cytosolic [118] or membrane bound. Furthermore, a cGi500 variant with a stop cassette (mT/cGi500-L2) has been developed that expresses the membrane-targeted tandem-dimer tomato red fluorescent protein (mT) before Cre recombination and contains the L2 allele, where “L2” stands for “two loxP sites” and the stop cassette is excised upon recombination. By using cell specific Cre mouse lines, it is possible to visualize cGMP in specific cells with the cGi500 sensor.

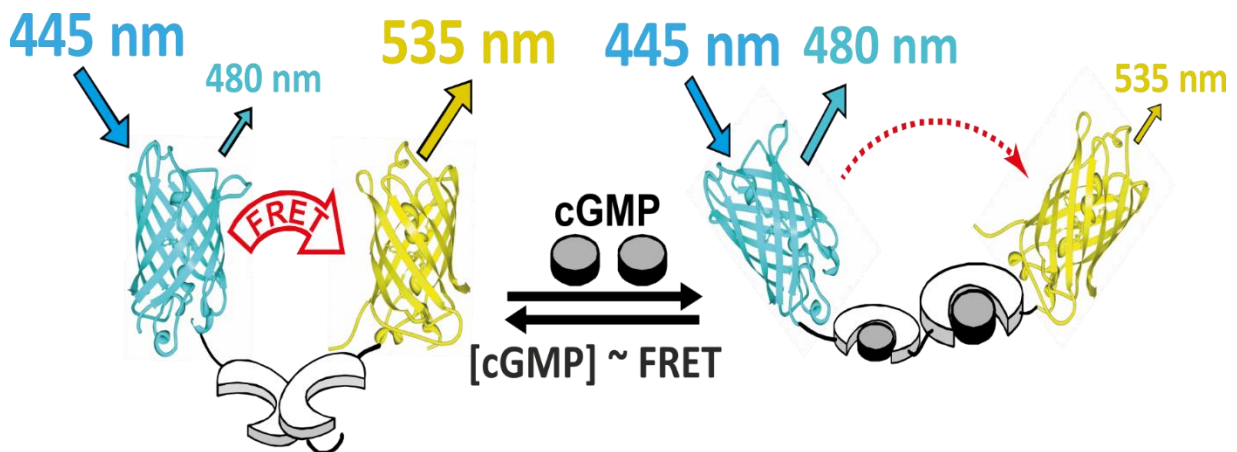


**Figure 4. FRET-based cGMP sensor cGi500.**

cGi500 is a ratiometric cGMP biosensor consisting of the cGMP-binding domain of bovine cGKI flanked by CFP and YFP. The left image depicts the sensor in the non-cGMP bound state where FRET efficiency is high. The right image depicts the cGMP bound state. Binding of cGMP causes a conformational change that reorients and/or distances CFP and YFP. Thereby, after excitation of CFP light emission from YFP at 535 nm is reduced, while emission from CFP at 480 nm is increased. The ratio of emission at 480 nm and 535 nm ( $F_{480}/F_{535}$ ) is used as a measure of FRET efficiency, which represents the  $[cGMP]_i$ . Adapted from Thunemann and Wen et. al., 2013 [118].

To visualize changes of the intracellular  $Ca^{2+}$  concentration ( $[Ca^{2+}]_i$ ), this work employed the fluorescent  $Ca^{2+}$  indicator Fura-2-acetoxymethyl ester (Fura-2-AM). This and other cell permeable  $Ca^{2+}$  sensors have been developed by the Tsien group and others since the 1980s [126]. Fura-2 itself is not membrane permeable but further

chemical modification by researchers led to Fura-2-AM, which is membrane-permeable [126]. When Fura-2-AM enters the cell, it is de-esterified by cellular esterases and the resulting Fura-2 then binds intracellular  $\text{Ca}^{2+}$  (**Figure 5A**). Fura-2 undergoes a shift in excitation maximum from 370 nm to 340 nm upon  $\text{Ca}^{2+}$  binding, while the emission maximum remains at 515 nm independent of  $\text{Ca}^{2+}$  binding (**Figure 5B**) [126]. The Fura-2-AM sensor was chosen because its fluorescence spectrum is compatible with cGi500, it is cell permeable, ratiometric and commonly used in neuronal cultures. By combining Fura-2 and cGi500, both  $\text{Ca}^{2+}$  and cGMP can be visualized in the same cell simultaneously to investigate potential crosstalk between these signaling molecules.

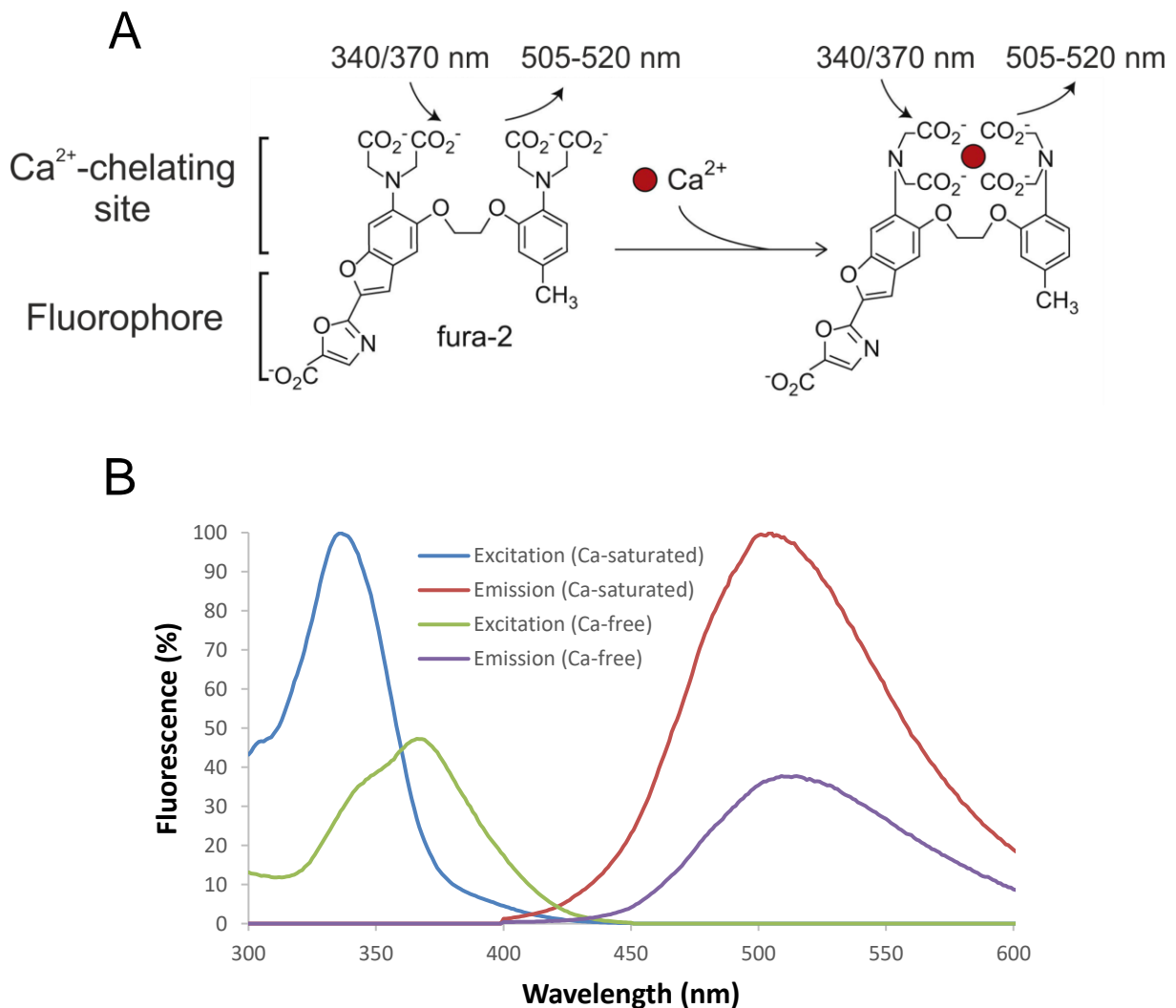


**Figure 5. Fura-2-AM for intracellular  $\text{Ca}^{2+}$  imaging.**

(A) The  $\text{Ca}^{2+}$  indicator Fura-2 is a  $\text{Ca}^{2+}$ -chelating agent and fluorophore. Intracellular free  $\text{Ca}^{2+}$  (red) binds to Fura-2 and induces a conformational change which modulates the excitation maximum of Fura-2 from 340 nm to 370 nm while emission remains between 505-520 nm. Adapted from Grienberger

and Konnerth, 2012 [127]. **(B)** Ca<sup>2+</sup> free Fura-2 exhibits an excitation maximum at 370 nm (green, Ca<sup>2+</sup>-free) and an emission peak maximum at 515 nm (purple, Ca<sup>2+</sup>-free). Upon Ca<sup>2+</sup> binding, Fura-2's excitation maximum changes to 340 nm (blue, Ca<sup>2+</sup>-saturated) while the emission peak remains at 515 nm (red, Ca<sup>2+</sup>-saturated). The [Ca<sup>2+</sup>]<sub>i</sub> correlates with the F<sub>340</sub>/F<sub>380</sub> emission ratio. Credit for Figure B, Markus Wolters.

### 1.8. Transgenic mice and the Cre/loxP system

Transgenic mice are an essential tool to investigate signaling cascades in mammals. Genetic analysis suggests that about 80% of mouse genes have a single orthologue in humans and that less than 1% of mouse genes have no human homologue currently detected [128,129]. Additionally, large mouse breeding colonies are possible to maintain given the relative low costs compared to other mammalian species, a plethora of literature exists on the characterization of mouse lines, and genetic modification techniques are highly advanced for mice. A world-wide effort to develop a knock-out mouse line for every gene to determine its biological function is underway [130]. Excitingly, new gene editing technologies, such as CRISPR-Cas9, make it possible to essentially genetically modify any organism and it is likely that new experimental animal models will emerge in the coming years [131,132].

The combination of genetic mouse models and pharmacological substances allows for the detailed elucidation of cell signaling cascades. However, using transgenic mice that have genetic modifications from conception can influence or even halt the animal's development [133]. For this and other reasons, it is desirable to have a genetic modification of interest controlled in both time and space, also known as spatiotemporal control. Such genetic modification is possible with the cyclization recombination (Cre) enzyme, which recombines two 34 bp-long, semi-palindromic DNA sequences referred to as 'loxP' sites, named after the locus of crossing-over (X-over) in P1 bacteriophages [134]. Upon recombination, the genetic sequence between the loxP sites can be removed or inverted depending on the orientation of the loxP sites (**Figure 6**).

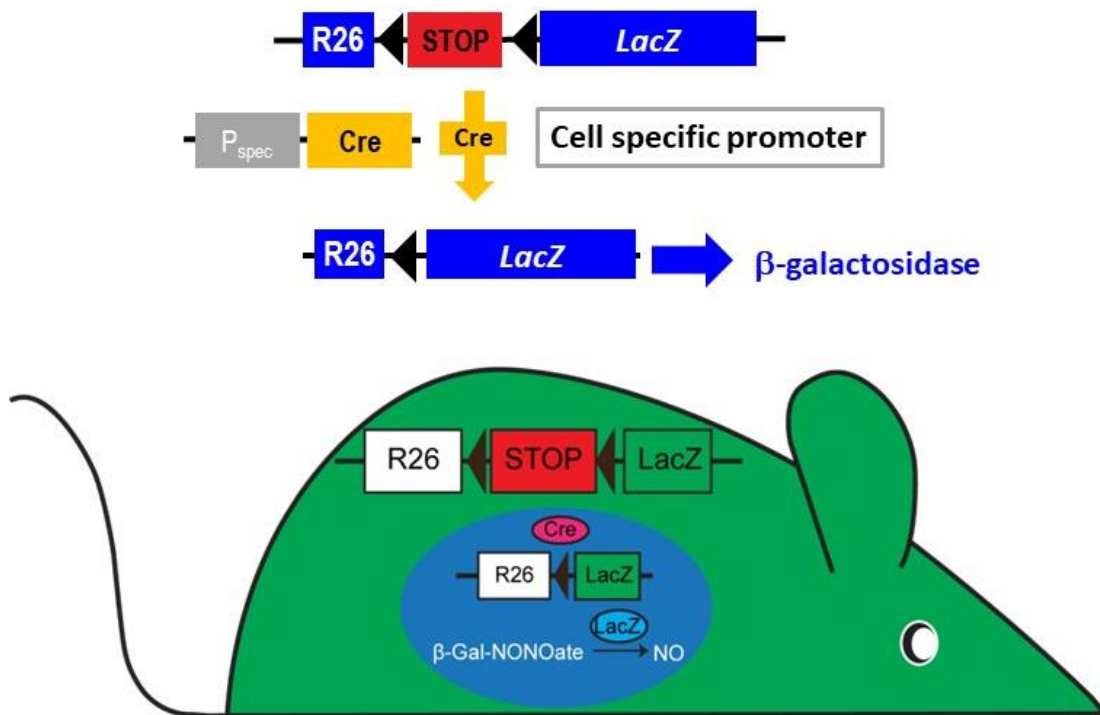


**Figure 6. Cell type specific gene expression with the Cre/loxP system.**

The Cre/loxP-directed gene modification occurs by flanking an exon of the gene of interest with two loxP (black triangles) sites and then Cre excises that portion of the DNA resulting in genetic modification. A possible strategy shown here is to place the gene of interest (e.g. lacZ) under the control of a ubiquitous promoter, such as ROSA26 (R26), with a floxed stop codon (red box). Cell specific expression of lacZ can be achieved by cell type specific expression (blue oval) of a Cre recombinase. In this mouse, lacZ is expressed in specific cells and  $\beta$ -gal-NONOate is cut by the resulting enzyme  $\beta$ -galactosidase. This then generates NO only in the cells where Cre is active. Lai Wen (Interfaculty Institute of Biochemistry, University of Tübingen) provided the mouse image.

Research conducted by Feil, Metzger, Chambon and others led to the development of ligand-activated CreER<sup>T</sup> and CreER<sup>T2</sup> fusion proteins, which bind the synthetic drug 4-hydroxytamoxifen (4-OHT), but not estradiol, the endogenous estrogen receptor ligand [135-137]. By using transgenic mice with cell type specific expression of CreER recombinases and timed exposure to tamoxifen, the prodrug of 4-OHT, highly specific spatiotemporal control over gene expression is possible. It is important to note that, as with any genetic tool, the Cre/loxP system is not always inert in mouse lines as indicated by research demonstrating differences between Cre mouse lines and wild type mouse lines, for example on behavior [138,139]. The influence of the Cre/loxP system can be controlled by comparison of transgenic Cre mice to wild type mice.

Numerous tissue specific Cre mouse lines, also known as a 'Cre-zoo', are

available and can be bred with other genetically modified mice, for example, Cre-activatable lacZ mouse lines. Laboratories with mouse generation expertise can also develop specific mouse lines for their unique experiments as was done by Thunemann, Wen and colleagues [118]. A 'Cre-zoo' allows for interesting genetic combinations, for instance cell specific lacZ expression selectively in the Purkinje cells of the cerebellum. Furthermore, live cell microscopy is an advantageous method when investigating signal cascades with these mouse models. For example, we have a microscopy setup that functions as a continuous flow system and facilitates the application and wash out of substances to measure dynamic cell responses (e.g. [cGMP]<sub>i</sub>) in real-time.

### **1.9. A new method to induce cell type specific NO generation**

Current research investigating the NO signaling pathway generally employs global elevators of NO. That is to say, the current NO donors that are used to increase biological levels of NO act indiscriminately on all tissues and cell types [140]. Even if one uses stereotactic guided injection of a NO-releasing substance to target a specific neuronal region, all cell types are affected, which makes conclusions about the role of NO in specific cell types uncertain. For example, the NO pathway in Purkinje cells in the cerebellum is thought to play a role in LTD [100], but global NO elevators do not allow researchers the cell type precision needed to draw such conclusions. One aim of this work is to develop a method that allows for cell-specific NO generation in order to investigate the role of NO in complex biological processes such as learning and memory at the level of specific cell types.

This aim will be accomplished with transgenic mice and targeted NO generation, facilitated by cell type specific lacZ expression and a synthetic compound that releases NO upon cleavage by  $\beta$ -galactosidase. By placing the relevant gene (e.g. lacZ) under the control of a cell specific promoter with the Cre/loxP system, cell specific expression of lacZ, and thus  $\beta$ -galactosidase, is attainable. The NO-releasing compound 1-O-(1-pyrrolidinyl-ONN-azoxy)- $\beta$ -D-glucopyranose ( $\beta$ -gal-NONOate) is cleaved by the enzyme  $\beta$ -galactosidase at the anomeric carbon freeing the nitrogen salt NONOate from the sugar, after which the NONOate spontaneously degrades into two molecular equivalents of NO [141].  $\beta$ -gal-NONOate is only cleaved in the presence of  $\beta$ -galactosidase thus allowing for cell type specific generation of NO (**Figure 7**). One possible strategy is to use mouse lines with constitutive Cre expression, but this

creates potential problems with the animal's development and might result in complex phenotypes [137]. For this reason, we have used the Cre/loxP system and tamoxifen to induce time-specific gene modification when such mouse lines were available. Otherwise, we have employed mouse lines that have constitutive Cre expression. By combining this genetic manipulation strategy, the cGi500 biosensor, real-time microscopy, and traditional biochemical methods it is possible to investigate the NO-cGMP signaling in a cell specific manner. Our strategy is to apply  $\beta$ -gal-NONOate in a mouse line that has cell type specific lacZ and cGi500 expression. This would enable NO generation and cGMP visualization in only those cell types. Downstream physiological effects influenced by the addition of  $\beta$ -gal-NONOate could also be investigated via real-time microscopy, such as vasodilation (**Figure 7**).

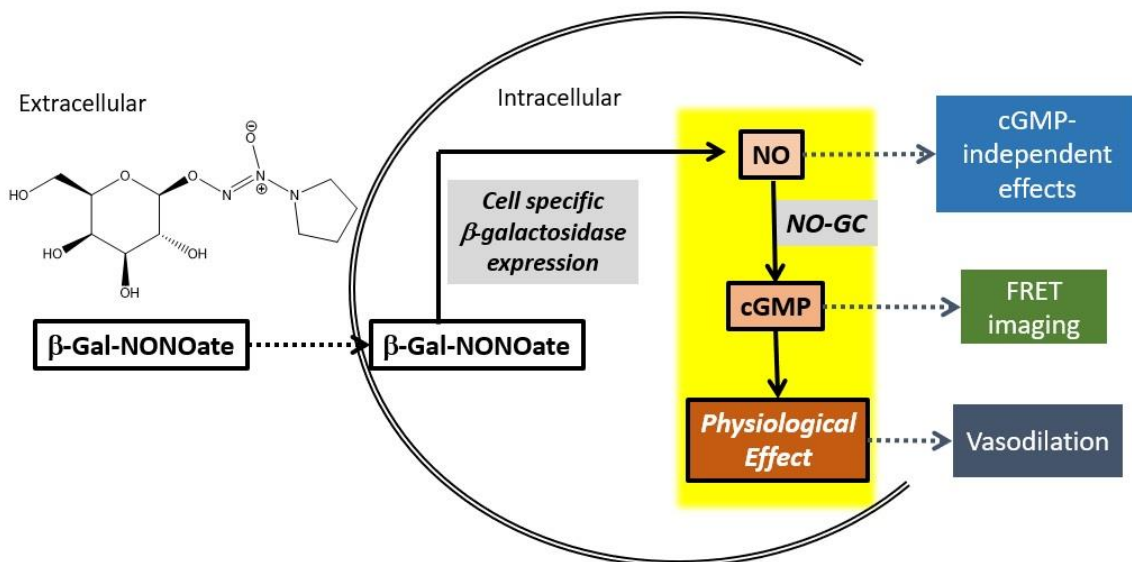


**Figure 7. Cell-specific elevation of NO with  $\beta$ -gal-NONOate.**

NO can be elevated in a cell specific manner via the addition of  $\beta$ -gal-NONOate, which releases NO in the presence of  $\beta$ -galactosidase. By using the Cre/loxP system under a cell type specific promoter, cell-specific lacZ, and thus  $\beta$ -galactosidase, expression is possible. The cGi500 sensor can be used to visualize any changes in  $[cGMP]_i$  upon the addition of  $\beta$ -gal-NONOate. Physiological effects can be investigated via advanced methods, such as real-time microscopy to measure vasodilation.

It is our aim to further elucidate NO-cGMP signaling in the CNS and other biological systems and the work presented here is a large step in exactly that direction. We believe this new method that allows for cell type specific NO generation provides the scientific community with a method to illuminate the role NO plays in specific cell types during modulation of physiological processes.

## 1.10 Aim of the work

The role of cGMP in numerous physiological processes is well documented and with the development of cGMP-modulating medications for human use there is no doubt about the molecule's biological significance. Together with other signaling molecules, such as  $\text{Ca}^{2+}$ , cGMP serves as a crucial molecule in the nervous system, however the minutia of the signal transduction cascades involved need to be further elucidated. Given the great success that cGMP-modulating molecules have seen in the cardiovascular system (**Table 1**) there is high potential for cGMP-modulating medications for CNS diseases.

The major objective of this thesis was to further investigate NO-cGMP signaling in the nervous system. With simultaneous real-time imaging of  $\text{Ca}^{2+}$  and cGMP signaling, we have studied a crosstalk between these two signaling pathways and further described the molecular pathway in CGNs. Furthermore, we sought to develop a new strategy based on the use of the Cre/loxP site-specific recombination system and the compound  $\beta$ -gal-NONOate that enables cell type specific NO generation, thus facilitating greater spatiotemporal resolution when investigating NO-cGMP signaling (**Figure 7**). The cell type specific generation of NO would allow researchers to investigate previously difficult address subjects, for example, the role of neuron generated NO on vasodilation, or so-called neurovascular coupling. The  $\beta$ -gal-NONOate strategy would enable scientists to gain in vivo evidence for a long-hypothesized, yet poorly investigated scientific idea, namely that neurons release vasoactive messengers (e.g. NO), which act directly on the vasculature to a cause a region-specific increase in blood flow. This new methodology can help delineate a signaling cascade from the molecular level up to the behavioral level. While this work focused primarily on the nervous system, the new method could be applied to any cell type of interest and biological process by using the appropriate cell type specific Cre expressing mice. To our knowledge, this is the first reported method that allows for the spatiotemporal controlled, cell type specific generation of NO.

## 2 Materials and Methods

### 2.1 General materials

#### 2.1.1 Common compounds, reagents and antibodies

0.4% Trypan blue	Life Technologies
10xTrypsin/EDTA	Life Technologies
100xPenicillin/Streptomycin (Pen/Strep)	Life Technologies
2-propanol	Carl Roth
30 mm glass coverslips	VWR
37% Hydrochloric acid (HCl)	Carl Roth
8-Br-cGMP	Biolog
8-pCPT-cGMP	Biolog
Agarose	Biozym Biotech
ANP	Tocris
$\beta$ -gal-NONOate	Self-synthesized
Boric acid	Carl Roth
Bovine serum albumin (BSA)	Carl Roth
Chloroform/isoamyl alcohol	Carl Roth
CNP	Tocris
DEA/NO	Axxora
D-Glucose	Carl Roth
DMEM Glutamax <sup>TM</sup>	Life Technologies
Dimethyl sulfoxide (DMSO)	Carl Roth
Diethylether	Carl Roth
EHNA	Axxora
Ethanol	Carl Roth
Fetal Bovine Serum (FBS)	Life Technologies
Glutamate	Sigma
Glutamine	Life Technologies
Hoechst 33258	Sigma-Aldrich
IBMX	Sigma
Milrinone	Sigma
Paraformaldehyde (PFA)	Carl Roth
Phenol/chloroform/isoamyl alcohol	Carl Roth
Sildenafil	Cayman
Vinpocetine	Cayman
Zaprinast	Santa Cruz
<b>Antibodies</b>	
Alexa 488, Goat anti-mouse	Cell Signaling, A-11029,
Mouse anti-mouse $\beta$ -III-Tubulin	Cell Signaling, 4466
Rabbit polyclonal anti-cGKI	Customized [142]
Rabbit polyclonal anti-cGKII	Customized [143]
Rabbit monoclonal anti-GAPDH	Cell Signaling, 2118
Rabbit polyclonal anti- $\beta$ -actin	Abcam, 8227
Hoechst	Sigma, 33258

### 2.1.2. Common buffers and solutions

#### 0.5 M EDTA pH 8.0

Dissolve 186.1 g disodium ethylenediaminetetraacetic acid dihydrate ( $\text{Na}_2\text{EDTA}\cdot 2\text{H}_2\text{O}$ ) in 800 mL  $\text{H}_2\text{O}$ , add NaOH pellets until the solution reaches pH 8.0 and EDTA is dissolved. Adjust volume to 1 L. Autoclave and store at room temperature (rt).

#### 1× Trypsin/EDTA

10×Trypsin/ETDA (0.5% / 0.2%, Life Technologies) 3 mL, add 27 mL PBS, store at 4 °C.

#### 10× TE pH 8.0

100 mM Tris-Cl (100 mL/L 1 M Tris-Cl pH 8.0), 10 mM EDTA (20 mL/L 0.5 M EDTA, pH 8.0), autoclave and store at rt.

#### 10× RT buffer

10×RT-buffer (pH 8.0) contains 500 mM KCl, 100 mM Tris, 15 mM  $\text{MgCl}_2$  and 2 mM dNTP-mixture. Store at  $-20^\circ\text{C}$ .

#### 10× Reaction buffer S

10×Reaction buffer S (Bioron) contains 100 mM Tris-HCl pH 8.8, 500 mM KCl, 0.1% Tween-20, 15 mM  $\text{MgCl}_2$ , store at  $-20^\circ\text{C}$ .

#### 1000× Hoechst 33258

Dissolve Hoechst 33258 (Sigma-Aldrich) at 1 mg/mL in  $\text{H}_2\text{O}$ , store 1 mL aliquots at  $-20^\circ\text{C}$ .

#### 1 kb ladder DNA marker

Add 250  $\mu\text{L}$  1 kb ladder (Life Technologies) to 8.25 mL 1×DNA loading dye, store 500  $\mu\text{L}$  aliquots at 4°C.

#### 1 M Tris-HCl pH 6.8/7.4/8.0

Dissolve 121.14 g tris(hydroxymethyl)aminomethane (Tris) in 1 L  $\text{H}_2\text{O}$ , adjust pH to 6.8/7.4/8.0 with concentrated HCl. Autoclave and store at rt.

#### 20% SDS

Dissolve 200 g sodium dodecyl sulfate (SDS) in 1 L  $\text{H}_2\text{O}$  at  $60^\circ\text{C}$  in a water bath. Store at rt.

#### 5× TBE

Make 450 mM Tris-borate, 10 mM EDTA by weighing 54 g Tris and 27.5 g boric acid and dissolving both in approximately 900 mL  $\text{H}_2\text{O}$ . Add 20 mL of 0.5 M EDTA (pH 8.0) and adjust the solution to a final volume of 1 L. Store at rt.

#### 5 M NaCl

Dissolve 292.2 g NaCl in 1 L  $\text{H}_2\text{O}$ . Autoclave and store at rt.

#### 6× DNA loading dye

30% glycerol, 10% 10×TE, 0.05% bromophenol blue, 0.05% xylene cyanol. Store at 4 °C.

#### 70% Ethanol

Mix 70 mL ethanol and 30 mL  $\text{H}_2\text{O}$

#### Proteinase K

Prepare 50 mg/mL proteinase K in 1×TE, store at  $-20^\circ\text{C}$ .

#### PBS Buffer

NaCl (135 mM), KCl (3 mM),  $\text{Na}_2\text{HPO}_4\cdot 2\text{H}_2\text{O}$  (8 mM),  $\text{KH}_2\text{PO}_4$  (2 mM), in 10 L  $\text{H}_2\text{O}$ . Adjust pH to 7.4 and autoclave.

## 2.2. Mice

All mouse lines were housed in the animal facility of the Interfaculty Institute of Biochemistry at the Eberhard-Karls University of Tübingen, Germany or the Neuroscience Department at the University of California San Diego (UCSD). Experiments at UCSD were performed according to protocols that are in strict accordance with the recommendations in the Guide for the Care and Use of Laboratory Animals of the National Institutes of Health and in accordance with the guidelines established by the UCSD Institutional Animal Care and Use Committee (IACUC). All animal procedures were performed in compliance with the humane care and use of laboratory animals and approved by the local authorities.

Mice were housed at 22 °C and 50–60% humidity in a 12 h light/12 h dark cycle with permanent access to standard rodent chow (Altromin Spezialfutter GmbH & Co. KG, Lage, Germany and Sniff Spezialdiäten GmbH, Soest, Germany) and tap water. Type II cages (360 cm<sup>2</sup>) were used for housing of single animals or groups with a maximal size of 2 – 3 animals. Type III (810 cm<sup>2</sup>) were used for groups of maximum eight animals. The bedding of a cage consists of autoclaved shredded wood chips (Tapvei). Wooden tunnels and tissues were provided (Tapvei) for environmental enrichment. The animal care takers changed the water and put the mice into clean cages weekly. For breeding, one or two female mice were housed together with one male mice in a Type II cage. The breeding period lasts for a maximum of twenty days. To prevent uncontrolled breeding, female mice were separated into a Type III cage before they gave birth. The pregnant animals were given access to breeding chow (Altromin and Sniff). The newborn animals were separated from their mothers and housed in cages with all female or all male littermates at 21 days of age. During the separation process animals were ear tagged and the tissues are used for subsequent genotyping.

The following mouse lines were used: R26-CAG-cGi500(L1) [118], R26-CAG-mT/cGi500(L2) [118], NO-GC KO of the  $\beta_1$  subunit [144], L7-Cre [145], Wnt1-Cre [146], SM-CreER<sup>T2</sup> [147], Camk2 $\alpha$ -CreBAC [148], and R26-lacZ [149]. The R26-CAG-cGi500(L1) (R26-cGi500-L1) mice express the cGMP sensor cGi500 in all cells and R26-CAG-mT/cGi500(L2) (R26-cGi500-L2) mice express membrane-targeted tandem-dimer tomato red fluorescent protein (mT) before Cre recombination and contain the L2 allele, where “L2” stands for “two loxP sites”. The R26-cGi500-L2 recombines in a cell type specific manner after breeding with appropriate Cre mice.

Both mouse lines contain the strong chicken actin/ $\beta$ -globin (CAG) promoter to enhance biosensor expression [150].

Genotyping of the animals was performed by PCR analysis of ear puncture DNA using the following primers: for detection of the R26-cGi500-L1 and R26-cGi500-L2 allele, BB01, BB02 and BB03, which amplify a 330-bp fragment of the wild type allele (BB01 and BB02) and a 250-bp fragment of the transgene (BB01 and BB03); for NO-GC KO mice, BB19, BB20 and BB21, which amplify a 680-bp fragment of the wild type allele (BB19 and BB20) and a 830-bp fragment of the knockout allele (BB19 and BB21); for Cre allele (L7-Cre and Wnt1-Cre), Cre800 and Cre1200, which amplify a 402-bp fragment of the Cre transgene; for the Camk2 $\alpha$ -CreBAC allele, Camk1, Camk2, and Camk5, amplify a 300-bp fragment of the wild type allele and a 350-bp fragment of the transgene; for R26-lacZ allele, BB01, BB02 and RF 127, which amplify a 330-bp fragment of the wild type allele (BB01 and BB02) and a 210-bp fragment of the transgene (BB01 and RF127). Detailed information on genotyping protocols can be found in the appendix (**Tables A1 and A2**). Andreas Friebe (Institute of Physiology, Julius-Maximilians-University) developed the NO-GC KO mouse lines [144]. Hannes Schmidt (Interfaculty Institute of Biochemistry, University of Tübingen) provided the Camk2 $\alpha$ -CreBAC mice [148] that were originally developed by Günther Schütz (German Cancer Research Center, Heidelberg University).

### 2.3 Mouse genotyping

Polymerase chain reaction (PCR) was performed to genotype the mice. The template DNA has to be extracted from the ear punches of the 21-day old mice.

- 1 Place each ear punch into 50  $\mu$ L PCR lysis buffer and incubate over night at 55°C.
- 2 After overnight incubation vortex the sample to dissolve the ear punch completely.
- 3 Centrifuge the sample at 15200 rcf for 5 minutes.
- 4 Transfer the supernatant into a 0.5 mL PCR tube.
- 5 Denature the DNA and inactivate the Proteinase K at 95°C for 15 minutes.
- 6 Store the DNA containing solution at -20°C or use 1–3  $\mu$ L of this sample (depending on the PCR) immediately for genotyping PCR.

#### Materials

- Proteinase K (Genaxxon): 50 mg/mL proteinase K in 1x TE buffer, store at -20°C

- 10x Reaction buffer S (Bioron), store at -20°C
- PCR lysis buffer – 10x reaction buffer S (5 µL), proteinase K (1 µL), H<sub>2</sub>O to 50 µL, store at -20°C

Every genotyping PCR has specific conditions depending on the respective annealing temperature of the primer set and the expected PCR Product length (**Table A2**). The master mix was prepared as shown below (**Table 2**).

1. Pipette 2 µL genomic DNA into a new PCR tube.
2. Prepare the appropriate volume of the master mix.
3. Add 23 µL of the master mix to your DNA sample and pipette up and down.
4. Prepare a positive control from an already genotyped DNA sample and a negative control with a negative DNA sample and a H<sub>2</sub>O negative control.
5. Transfer the samples into the thermocycler (PEQLAB Peqstar 2x; PEQLAB Primus 96 Advanced) and run the respective program.
6. After the PCR is complete add 5 µL of 6x DNA loading dye to the samples.
7. Run the PCR products (12 µL) with a 1 kb plus ladder (7 µL) on a Midori Green containing (2 µL per 50 mL agarose gel) 2% agarose gel.

**Table 2. PCR master mix (one reaction)**

DNA	2.0 µL
10x RT buffer	2.5 µL
Primer 1	0.3 µL
Primer 2	0.3 µL
Primer 3	0.3 µL
Taq Polymerase	0.3 µL
H <sub>2</sub> O	19.3 µL
<b>Total volume</b>	<b>25 µL</b>

- dNTP stocks: 100 mM dATP, 100 mM dCPT, 100 mM dGTP, 100 mM dTTP (Genaxxon), store at -20°C
- 10x RT buffer: 100 mM Tris-HCl pH 8.0, 500 mM KCl, 15 mM MgCl<sub>2</sub>, 2 mM of each dNTP (dATP, dCPT, dGTP, dTTP), in H<sub>2</sub>O, store at -20°C
- Primer (**Table A1**): 25 pmol/µL (Eurofins Genomics) in H<sub>2</sub>O, store at -20°C
- Taq Polymerase (Bioron), store at -20°C
- Molecular size marker: Dilute 250 µL 1kb plus ladder (Life Technologies) in 8.25 mL 1x DNA loading dye. Prepare aliquots with a volume of 500 µL and store one aliquot ready to use at 4°C while the others are stored at -20°C
- Midori Green (nucleic acid staining solution, Nippon Genetics), store at 4°C
- 6x DNA loading dye: Glycerol 30%, 10x TE buffer 10%, bromphenol blue 0.05 %, Xylene cyanol 0.05%, store at 4°C
- 1x TBE buffer: Dilute 2 L of 5x TBE buffer with 8 L H<sub>2</sub>O, store at rt
- LE Agarose (Biozym), store at rt

- 2% agarose gel: Weigh 1 g LE agarose (Biozym) into 50 mL 1x TBE buffer. Put it into the microwave and heat it until the agarose is completely dissolved. Let it cool down (The outside of the Erlenmeyer flask should be a temperature that you can touch without pain) and add 2  $\mu$ L of Midori Green (Nippon Genetics). Mix in the Midori Green with a magnetic stirrer and then pour the agarose gel into a chamber to let polymerize.

## 2.4. Cell culture

### 2.4.1. Primary culture of vascular smooth muscle cells

Jacek Dobrowinski (Interfaculty Institute of Biochemistry, University of Tübingen) helped clean the isolated aortae. Primary VSMCs were isolated from the thoracic aortae of mice aged 6-12 weeks as previously reported [122]. Approximately 150,000 VSMCs per aorta were isolated. Cells were grown in culture medium at 37 °C and 5% CO<sub>2</sub>. Primary VSMCs started to grow and spread after 24-48 hours and were generally confluent about five days after isolation. Petri dishes (100 mm) with PBS and a 33 mm dish with Ca<sup>2+</sup>-free medium (85 mM L-glutamate, 60 mM NaCl, 10 mM HEPES, 5.6 mM KCl, 1 mM MgCl<sub>2</sub>, adjust pH to 7.4 with HCl, autoclave and store at 4 °C) were put on ice. Animals were sacrificed with CO<sub>2</sub> or diethyl ether inhalation. The fur was made damp with 70% ethanol and the abdominal and thoracic cavity were opened with an incision beginning at the pelvis and ascending to the throat. The diaphragm, remaining intestines, esophagus and liver as well spleen and lung were removed. The heart was carefully lifted out of the body cavity to reveal the aorta. Then the aorta was removed by carefully cutting along the spine to free the aorta down towards the pelvis area. The aorta was transferred with the still attached heart into the petri dish with PBS on ice. Using two forceps, the heart was removed from the aorta. Under a stereomicroscope (Stemi 2000C), the surrounding fat tissue was carefully removed from the aorta. The aorta was then transferred into the 35 mm dish with Ca<sup>2+</sup>-free medium. It is especially important to place this dish on ice to delay degradation during the isolation of tissues from multiple animals. The cleaned, isolated aorta was then cut into ~3 mm length pieces.

The following steps were performed under sterile conditions in a laminar flow hood. The aorta pieces were transferred into a 15 mL tube with enzyme solution A (e.g. 0.5 mL solution for 2 aortae) and incubated for 60 minutes in a 37°C water bath with gentle mixing every 10 minutes (the mixing will reduce time for the critical incubation in solution B and thereby increase viable cell yield). The 15 mL tube was

then centrifuge at 150 rcf for 3 minutes. The supernatant was carefully discarded via aspiration and the tissue pellet was suspended in enzyme solution B (same volume as for enzyme solution A). The sample was then incubated for a maximum of 12 minutes at 37°C in a water bath. After the first 3 minutes of incubation a 1000 µL pipette was used to pipet the mixture up and down to assist tissue dissociation. This step is critical and should be performed as quickly as possible. The reaction was quenched with FCS containing culture medium using 3-4 times the volume of enzyme solution B. The solution was centrifuged at 140 rcf for 8 minutes. The supernatant was discarded via aspiration and the pellet suspended in an appropriate volume of medium (~0.5 mL per 2 aortae). 18 mL of the solution was combined with 2 mL of Trypan blue solution and pipetted into a Neubauer counting chamber to determine the number of viable and dead cells (blue positive). VSMCs were then plated according to the experimental requirements and grown at 37°C and 6% CO<sub>2</sub>. Medium was changed as necessary (about every 3 days). Cells were serum-starved in culture medium without serum for 24 h prior to imaging experiments or protein isolation.

Materials for primary VSMC isolation:

- Ca<sup>2+</sup>-free medium (pH 7.4): 85 mM L-glutamate, 60 mM NaCl, 10 mM HEPES, 5.6 mM KCl, 1 mM MgCl<sub>2</sub>, adjust pH to 7.4 with HCl, autoclave and store at 4°C
- VSMC culture medium: 500 mL DMEM medium -GlutaMAX™ (Gibco) including 50 mL FCS and 5 mL Pen/Strep, store at 4°C
- 10 mg/mL Collagenase: Dissolve 100 mg Collagenase (Sigma-Aldrich) in 10 mL Ca<sup>2+</sup>-free medium, prepare 0.5 mL aliquots and store at -20°C
- 10 mg/mL Hyaluronidase: Dissolve 100 mg Hyaluronidase (Sigma-Aldrich) in 10 mL Ca<sup>2+</sup>-free medium, prepare 0.5 mL aliquots and store at -20°C
- 7 mg/mL Papain: Dissolve 100 mg Papain (Sigma-Aldrich) in 14.29 mL Ca<sup>2+</sup>-free medium, prepare 0.5 mL aliquots and store at -20°C
- 100 mg/mL BSA: Dissolve 0.5 g BSA (Roth) in 5 mL Ca<sup>2+</sup>-free medium, sterilize by filtration, prepare 0.5 mL aliquots and store at -20°C
- 100 mg/mL DTT: Dissolve 0.5 g DTT (Roth) in 5 mL Ca<sup>2+</sup>-free medium, sterilize by filtration, prepare 0.5 mL aliquots and store at -20°C
- Enzyme solution A (0.5 mL per 2 aortae): Dilute Papain stock 1/10, BSA stock 1/100 and DTT stock 1/100 in Ca<sup>2+</sup>-free medium
- Enzyme solution B (0.5 mL per 2 aortae): Dilute Collagenase stock 1/10, Hyaluronidase stock 1/10 and BSA stock 1/100 in Ca<sup>2+</sup>-free medium

#### 2.4.2. Primary culture of cerebellar granule neurons

To establish primary cultures of cerebellar granule neurons (CGNs) from mice, the following solutions and “tubes” were prepared: 0.3% bovine serum albumin (BSA, Roth) solution in 1× Krebs buffer, 14.3 mM D-glucose, 2.5 mM MgSO<sub>4</sub>, sterilized by filtration; “tube 1” contained 30 mL 0.3% BSA solution; “tube 2” contained 30 mL 0.3% BSA solution and 300 µL trypsin solution [2.5x trypsin-EDTA (Thermo Scientific) in PBS], added shortly before use; “tube 3” contained 7.8 mg trypsin inhibitor (Life Technologies) in 15 mL 0.3% BSA solution, 3.1 mM MgSO<sub>4</sub>, and 0.1 mg/mL DNase (Roche), added shortly before use); in “tube 4”, 17 mL 0.3% BSA solution were mixed with 8 mL solution from “tube 3” and then 10 mL were discarded, so that 15 mL remained in “tube 4”; “tube 5” contained 12.5 mL 0.3% BSA solution, 2.5 mM MgSO<sub>4</sub>, and 0.1 mM CaCl<sub>2</sub>. Two to five cerebella from 7-day-old mice were isolated and the surrounding meninges were removed in 0.3 % BSA solution. Then, the cerebella were homogenized in 2 mL 0.3% BSA solution with a pipette, transferred into “tube 1” and centrifuged at 170 g for 5 min at room temperature. The supernatant was removed and the pellet was resuspended in the solution from “tube 2” and incubated for 15 min at 37 °C with gentle shaking every 5 min. Then, the suspension was transferred into “tube 4”, mixed and centrifuged at 170 g for 5 min at room temperature. The supernatant was removed and the cell pellet was resuspended in the solution from “tube 3” by pipetting 10 times with a Pasteur pipette. Then, the suspension was transferred into “tube 5”, mixed, passed through a netwell mesh (70 µm), and centrifuged at 170 g for 5 min at room temperature. The pellet was resuspended in CGN medium [Minimal Essential Medium (Life Technologies) containing 0.22 mM KCl, 2% B27 supplement (Thermo Scientific), 9% fetal bovine serum (Thermo Scientific), 0.3 mM glutamine (Thermo Scientific), and 0.1 mM gentamicin (Thermo Scientific)] and plated on 24-well plates (100 k cells per well, viability >95% as determined by trypan blue staining). Wells were equipped with glass coverslips, which had been coated overnight with poly-D-lysine (20 µg/mL, Thermo Scientific). CGNs were grown at 37 °C and 5% CO<sub>2</sub> and after 24 h cytosine arabinoside (5 µM, Sigma) was added. Every 3 days half of the medium was changed.

Materials for primary CGN isolation:

- 10× Krebs buffer: 1.24 M NaCl, 54 mM KCl, 5 mM NaH<sub>2</sub>PO<sub>4</sub>, pH 7.4, autoclave and store at 4 °C.

- 1 M D-glucose: 19.8 g D-glucose · H<sub>2</sub>O in 100 mL H<sub>2</sub>O, sterilize by filtration, store at 4 °C.
- 1.2% CaCl<sub>2</sub>: 1.2 g CaCl<sub>2</sub> · 2H<sub>2</sub>O in 100 mL H<sub>2</sub>O, sterilize by filtration, store at 4 °C.
- 3.82% MgSO<sub>4</sub>: 3.82 g MgSO<sub>4</sub> · 7H<sub>2</sub>O in 100 mL H<sub>2</sub>O, sterilize by filtration, store at 4 °C.
- 0.3% BSA solution (prepare always fresh on the day of use): 450 mg BSA into a beaker glass, 132.84 mL H<sub>2</sub>O, 15 mL 10xKrebs buffer, 2.16 mL 1 M D-glucose and 1.2 mL 3.82% MgSO<sub>4</sub>. Adjust the pH to 7.4 with NaOH, sterilize by filtration, store at 4 °C.
- 50 mg/mL Gentamicin (GIBCO, Life Technologies).
- High K<sup>+</sup> (HK) medium: 825 mg KCl in an autoclaved beaker glass, 50 mL MEM, sterilize by filtration and transfer it back into the original medium bottle (total volume 500 mL MEM). Add 1 mL of gentamicin (50 mg/mL), store at 4 °C.
- CGN medium: 88 mL HK medium, 9 mL FBS, 0.9 mL 100xL-glutamine, 2 mL 50x B27 supplement, store at 4 °C for up to 1 month.

On the day of preparation (postnatal day 7), prepare 5 × 50 mL centrifuge tubes in the tissue culture hood:

Tube 1: 30 mL 0.3% BSA solution.

Tube 2: 30 mL 0.3% BSA solution and, shortly before use add 300 µL 2.5% trypsin.

Tube 3: Dissolve 7.8 mg trypsin inhibitor in 15 mL 0.3% BSA solution (thorough mixing and warming to 37°C facilitates its dissolution), add 150 µL 3.82% MgSO<sub>4</sub>, and shortly before use add 150 µL 1% DNase.

Tube 4: 17 mL 0.3% BSA solution and 8 mL from tube 3; discard 10 mL, so that 15 mL remain in the tube.

Tube 5: 12.5 mL 0.3% BSA solution, 100 µL 3.82% MgSO<sub>4</sub> and 15 µL 1.2% CaCl<sub>2</sub>.

Distribute part of the remaining 0.3% BSA solution into 10 × 35 mm culture dishes (~3 mL/dish); keep on ice for preparation of the brains.

### 2.5. Transfection of primary VSMCs

Isolated primary VSMCs were transfected with the lacZ encoding plasmid pFRTβ-gal (**Figure A1**). Cells had a confluence of 80% or higher upon transfection. Here the lipofection method was used to transfect the construct pFRTβ-gal into VSMCs grown in 6-well plates. The cell medium was aspirated and pre-warmed (37 °C) VSMC culture medium was added (1.25 mL per 6-well). The transfection mixtures of ScreenFect A Transfection kit (Genaxxon Bioscience) were prepared fresh. Tube A contained 120 µL of dilution buffer with 6 µL ScreenFect A. Tube B contained 120 µL dilution buffer with 1 µg plasmid DNA. 'Tube A' was added to 'tube B' and pipetted up and down to mix them well and then incubated for 20-30 min at rt. Thereafter, 240 µL of the transfection mixture were added per well in a 6-well plate on top of the 1.25 mL VSMC culture medium. There might be a color change in the medium of the cells. The cells were incubated overnight at 37 °C and 5% CO<sub>2</sub>. 15-20 h after the transfection,

the medium was replaced with VSMC culture medium. (Do not wash with PBS). The cells were analyzed two days after transfection.

**Materials:**

- VSMC culture medium: 500 mL DMEM medium -GlutaMAX™ (Gibco) including 50 mL FCS and 5 mL Pen/Strep, store at 4°C.

**2.6. Preparation of acute brain slices and fixed brain sections**

For the preparation of acute brain slices, brains were dissected and cut in ice-cold carbogen-gassed Ringer buffer (126 mM NaCl, 2.5 mM KCl, 1 mM MgCl<sub>2</sub>, 1 mM CaCl<sub>2</sub>, 1.25 mM NaH<sub>2</sub>PO<sub>4</sub>, 26 mM NaHCO<sub>3</sub>, 20 mM D-glucose). Slicing was performed with a vibratome (VT1200, Leica, BuffaloGrove, IL, USA). Brains were cut sagittally into 300- $\mu$ m slices. Then, slices were incubated in 37 °C pre-warmed carbogen-gassed Ringer buffer and imaging experiments were performed 45-60 min after slicing.

**2.7. Animal procedures for imaging under anaesthesia**

*2.7.1. Surgical implantation of mouse cranial window*

Surgeries were performed by Martin Thunemann and Qun Cheng (Department of Neurosciences, University of California, San Diego). Experiments performed according to these protocols were in strict accordance with the recommendations in the Guide for the Care and Use of Laboratory Animals of the National Institutes of Health. The experiments at the University of California San Diego were all performed in accordance with the guidelines established by the UCSD Institutional Animal Care and Use Committee (IACUC). Surgeries were performed as described in this section and as previously described [151]. We used adult female mice on a C57BL/6 background. Surgical installation of the cortical window was performed while the mice were anesthetized with isoflurane (2% initially, 0.5–1% during all procedures). A cannula was inserted into the femoral artery. A metal holding bar was glued to the temporal bone for immobilization of the head during imaging. An area of skull overlying the Barrel cortex region contralateral to the holding bar was exposed and dura mater removed. A ~2 × 2 mm cranial window was centered on the Barrel cortex region's stereotactic coordinates: antero-posterior coordinates –1.5, medial-lateral coordinates 2. Cold ACSF (142 mM NaCl, 5 mM KCl, 10 mM glucose, 10 mM HEPES, 3.1 mM

CaCl<sub>2</sub>, 1.3 mM MgCl<sub>2</sub>, pH 7.4) was used during surgery to keep the skull cool during drilling. A drop of agarose (1% wt/vol, A9793, Sigma) in ACSF was applied on the brain surface, and the exposure was covered with a round glass coverslip (5 mm, WPI). To avoid herniation of the exposed brain due to excessive intracranial pressure, the dura mater over the 4th cerebral ventricle was punctured, thus allowing drainage of CSF. After the exposure was closed, the drainage hole was sealed with agarose.

To allow for the addition of pharmacological agents directly into the brain, the round glass coverslip was cut straight on one side facing a gap in the dental acrylic seal. The agar was cut down along the cut side forming a vertical wall. The exposure was aligned with the agar wall such that ACSF under the objective was in direct contact with the cortical surface allowing drugs to penetrate into the cortical tissue.

After closing of the exposure, mice were left to rest under 1% isoflurane for 45 min. Waiting for 45 min between closing the exposure and drug injections minimizes leakage of the drugs onto the cortical tissue exposed through the cut dural blood vessels. Isoflurane was then discontinued and further anesthesia was maintained with  $\alpha$ -chloralose (50 mg/kg/h IV, C0128, Sigma or 100459, MP Biochemicals). Mice were paralyzed with pancuronium bromide (0.4 mg/kg/h IV, P1918, Sigma) [152] and ventilated ( $\sim 110 \text{ min}^{-1}$ ) with 30% O<sub>2</sub> in air. Fluorescein isothiocyanate (FITC)-labeled dextran (MW = 2 MDa, FD-2000S, Sigma) was retro-orbitally injected (50–100  $\mu\text{l}$  of 5% (w/v) solution in phosphate-buffered saline) to visualize the vasculature and control for the integrity of the capillary bed. Expired CO<sub>2</sub> was measured continuously using a micro-capnometer (CI240, Columbus instruments). Heart rate, blood pressure, and body temperature were monitored continuously. Blood gas was analyzed to cross-validate the micro-capnometer measurements. Respiration was adjusted to achieve PaCO<sub>2</sub> between 30 and 40 mmHg and pH between 7.35 and 7.45.  $\alpha$ -chloralose and pancuronium in 5% dextrose saline were supplied through the femoral line every 30 min for the duration of data acquisition.

### *2.7.2. Microinjection protocol and mouse monitoring*

The microinjection pipette was guided under the glass coverslip and positioned  $\sim 200 \mu\text{m}$  below the cortical surface using a Luigs & Neumann translation stage (380FM-U) and manipulation equipment integrated into the Ultima system. The red fluorescent

dye Alexa 594 (A-10442, Alexa Fluor 594 hydrazide, sodium salt, Invitrogen) was added to the solution in order to visualize the micropipette during manipulation and to provide visual feedback during pressure-microinjection into the cortical tissue [153]. The injection pressure was manually adjusted to ensure visible spread of Alexa 594 while avoiding movement artifacts. The injection occurred locally with a volume between 5-10  $\mu\text{L}$  depending on the diameter of the quartz needle, the duration of injection, and the pressure during injection. A video camera (Lifecam Studio, Microsoft; IR filter removed) with an NIR longpass filter (Midwest Optical LP920-25.5) was used for continuous observation of the mouse during measurement. The IR illumination (M940L3 - IR (940 nm) LED, Thorlabs) was invisible to the PMT photodetectors and does not generate imaging artifacts. The camera frames were synchronized with two-photon imaging and recorded. Periods with extensive body movement (e.g., grooming behavior) were excluded during data analysis. Analysis was performed as a pseudo line scan in Fiji (NIH) [154] by measuring the diameter of the vessel across time. A line of interest was drawn followed by the command: Image  $\rightarrow$  Stacks  $\rightarrow$  Reslice which then generates a pseudo line scan “stack”. The resulting image is depicted as a series of slices, each a single-pixel in width along the line of interest. The total area analysis was performed in MATLAB. The analysis measured the total vessel area across time with a region of interest (ROI) that determined the percent area the vessel changes in the ROI over time.

## 2.8. Microscopy imaging setups

FRET/cGMP and  $\text{Ca}^{2+}$  imaging of cultured cells was performed as described here and previously [40,116,118,122,155].

### 2.8.1. Fluorescence microscopy on Axiovert 200 microscope

A schematic representation of the setup is shown below (**Figure 8**). The setup consisted of an inverted Axiovert 200 microscope (Zeiss) equipped with a NeoFluar40x/1.30 oil objective, a light source with excitation filter switching device (Oligochrome, TILL Photonics GmbH), a Dual-View beam splitter (Photometrics) with 516 nm dichroic mirror and emission filters for CFP (480/30 nm) and YFP (535/40 nm), and a charge-coupled device camera (Retiga 2000R; QImaging).

cGMP imaging was performed with VSMCs or CGNs isolated from R26-cGi500-L1 mice expressing the cGi500 sensor. For simultaneous imaging of cGMP and Ca<sup>2+</sup>, coverslips with cGMP sensor cells were incubated with 2.5 μM Fura-2AM (Calbiochem; 1 mM stock solution in DMSO) in Tyrode buffer (140 mM NaCl, 5 mM KCl, 1.2 mM MgSO<sub>4</sub>, 2.5 mM CaCl<sub>2</sub>, 5 mM D-glucose, 5 mM HEPES, pH 7.4) for 35 min at 37 °C in the dark before measurement. During cGMP only measurements, coverslips were briefly washed in Tyrode buffer to remove cell medium. All coverslips were mounted into a Warner Instrument SA-20LZ superfusion imaging chamber (Harvard Bioscience) and superfused at 37 °C at a flow rate of 1 mL/min with Tyrode buffer or Tyrode buffer supplemented with drugs. Test compounds were applied via Pharmacia IV-7 injection valves (GE Healthcare) with either 7.0 mL, 2.0 mL or 0.16 mL sample loops. CGNs were imaged at 40x magnification, VSMCs were imaged at 10x magnification, and both were imaged with 4x4 binning. Signals were recorded at a frequency of 5 Hz or 1 Hz for cGMP imaging alone or simultaneous cGMP/Ca<sup>2+</sup> imaging, respectively. For Fura-2-based Ca<sup>2+</sup> imaging in CGNs, fluorescence was excited at 340/26 nm and 387/11 nm (15% lamp intensity each) and emission was recorded in the 535/40 nm channel (65 ms and 20 ms exposure time with the respective excitation wavelength). For cGMP imaging with CGNs, excitation was performed at 445/20 nm (45% lamp intensity) and emission recorded simultaneously at 480/30 nm and 535/40 nm (40 ms exposure). For cGMP imaging with VSMCs, excitation was performed at 445/20 nm (100% lamp intensity) and emission was recorded simultaneously at 480/30 nm and 535/40 nm (300 ms exposure).

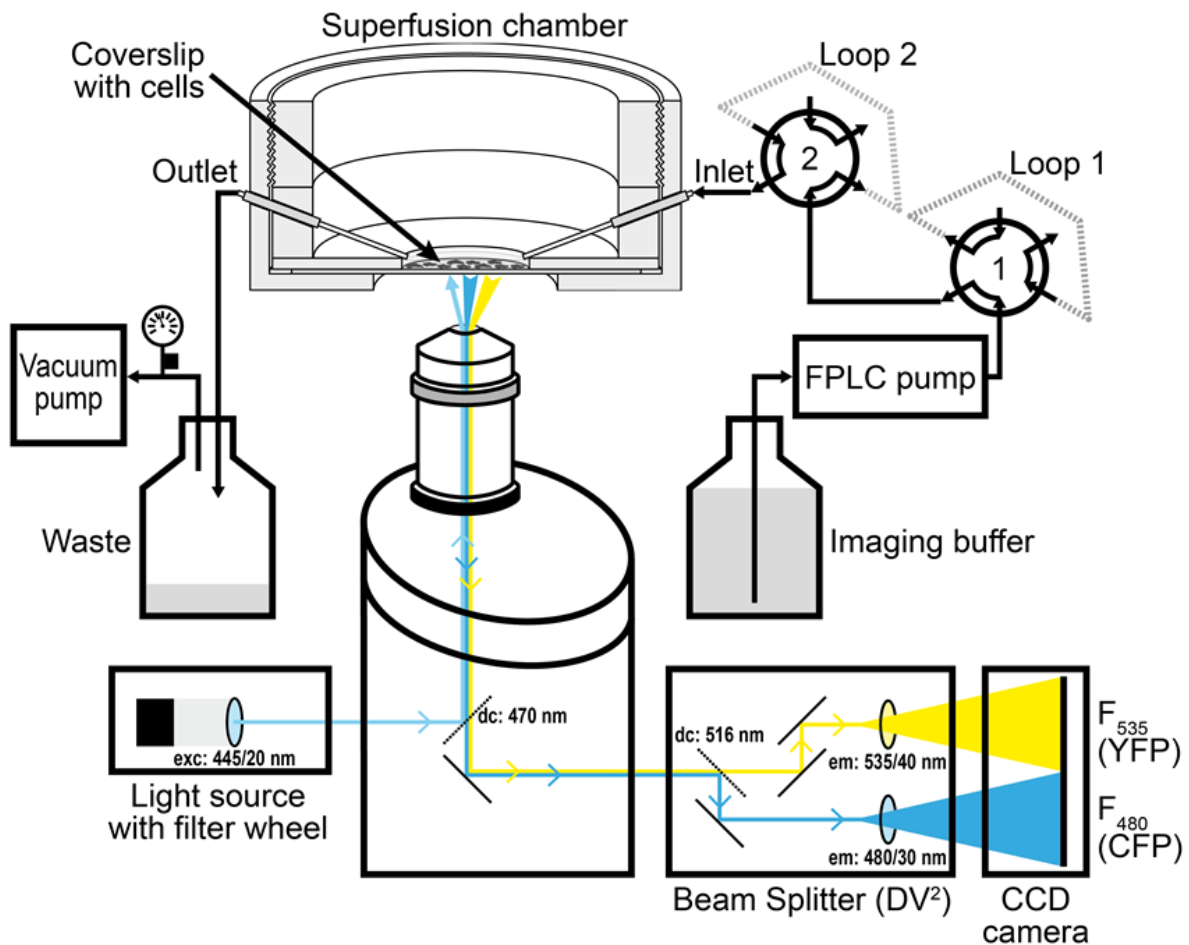


**Figure 8. Schematic representation of the cGi500 FRET imaging system.**

A schematic representation of the above described imaging setup to measure cGMP with the cGi500 FRET-based sensor. Adapted from [122].

### 2.8.2. Fluorescence microscopy with Examiner.Z1 spinning disc microscope

The spinning disk microscope setup consisted of an upright Examiner.Z1 microscope (Zeiss), a Yokogawa CSU-X1 spinning disk confocal scanner, three diode lasers (445 nm, 488 nm and 561 nm), three water immersion objectives [W N-ACHROMAT 10x/0.3, W Plan-APOCHROMAT 20x/1.0 DIC (UV) VIS-IR, W Plan-APOCHROMAT 40x/1.0 DIC VIS-IR; all from Zeiss] and one air objective [EC Plan-NEOFLUAR 2.5x/0.085; Zeiss]. For FRET-based cGMP imaging, the donor fluorophore CFP was excited with the 445 nm laser, and a Dual-View beam splitter (Photometrics) with 505 nm dichroic mirror, and 470/24 nm and 535/30 nm emission filters was used for simultaneous acquisition of CFP and YFP. Signals were recorded with an electron-multiplying charged-coupled device (EM-CCD) camera (QuantEM 512SC, Photometrics) at a frame rate of 0.2 Hz and an exposure time of 300 ms. The

system was controlled by VisiView software (Visitron Systems). A CoolLED pE-2 LED system was used for epifluorescence illumination at 400 nm, 450 nm, 500 nm, and 561 nm. During real-time imaging, the tissue was continuously superfused with carbogen-gassed Ringer buffer (126 mM NaCl, 2.5 mM KCl, 1 mM MgCl<sub>2</sub>, 1 mM CaCl<sub>2</sub>, 1.25 mM NaH<sub>2</sub>PO<sub>4</sub>, 26 mM NaHCO<sub>3</sub>, 20 mM D-glucose) or Ringer buffer containing drugs of interest at a flow rate of 1 mL/min at 37 °C. A custom-built superfusion system was used consisting of a FPLC pump (Pharmacia P-500, GE Healthcare), FPLC injection valves (Pharmacia V-7, GE Healthcare), a magnetic platform (Warner instruments), a superfusion chamber (RC-26, Warner Instruments), a Slice Hold-Down (SHD-26H/10, Warner Instruments) and a sample loop (2 mL). To remove the buffer from the system, a vacuum pump with adjustable vacuum (Laboport N86, KNF Neuberger) was connected to the system [118,122].

### *2.8.3. Fluorescence microscopy with a 2-photon microscope*

Martin Thunemann (Department of Neurosciences, University of California, San Diego) assisted with data collection and analysis. Images were obtained using an Ultima 2-photon laser scanning microscopy system (Bruker Fluorescence Microscopy) equipped with an Ultra II femtosecond Ti:Sapphire laser (Coherent) tuned between 800–1000 nm and cooled GaAsP PMT tube detectors (H7422P-40, Hamamatsu) and a multialkali PMT (R3896, Hamamatsu). The setup was equipped with two filters (ET480/40m, Chroma and T505lpxr, Chroma). Olympus 20x (XLUMPlanFLNXW, NA=1.0) and Zeiss 40x (IR-ACHROPLAN, NA = 0.8) water-immersion objectives were used for high-resolution imaging. In experiments involving manipulation of a micropipette under the coverslip, we used a combination of Zeiss 5x (Plan-NEOFLUAR, NA=0.16) and Olympus 20x (UMPlanFI, NA=0.5) objectives for a coarse approach and fine manipulation under the glass coverslip, respectively. The laser beam diameter was adjusted to overfill the back aperture. Arteriolar diameter measurements were performed in a frame-scan mode at 10–20 Hz, or in a 'free-hand' line-scan mode with a scan rate of 25–50 Hz. The scan resolution was 0.5 μm or less.

## 2.9. Imaging protocols

Below is the detailed work flow for the cGMP FRET measurement of cells expressing cGi500. This is true for both the Axiovert 200 microscope and Examiner.Z1 spinning disc microscope.

Note: VSMCs were serum starved 24 hours before measurement. This procedure should better imitate the in vivo situation where VSMCs are mitotically inactive.

1. Before measurement, perform a solvent change (injection valves in load mode) with buffer and check the beam splitter for CFP and YFP alignment. Also ensure that the appropriate sample loops are assembled and that all other materials needed for the measurement are prepared (drugs, drug application sheets, pipettes etc.)
2. Assemble the superfusion chamber with a coverslip: Use a paint brush to apply silicon to the chamber and ensure that the border of the chamber is free of silicon where the coverslip will be placed. The silicon may influence measurement quality. Place the coverslip in the chamber and cover the cells with buffer (gently pipet about 700  $\mu$ L onto the coverslip). If working with tissue slices, then use the harp to immobilize the tissue slice and ensure the chamber is full of buffer (about 1 mL).
3. Clean the bottom side of the coverslip (where no cells should be) with a kimwipe and, if necessary, ethanol.
4. Place the chamber on the microscope and connect it to the superfusion system, both in and out valves.
5. Start the superfusion system with a rate of 60 mL/hour and ensure injection valves are in the load mode. Make sure that the buffer is correctly aspirated, just enough volume to ensure the cells or tissues are always wet. Large volumes tend to produce weaker signals. Ensure that the chamber is not leaky.
6. Use the YFP filter set to identify a representative region of interest (ROI). Acquire a fine-grained image of this region (1x1 binning and ~2 sec exposure time). This image makes it easier to map the cells for analysis.
7. Adjust the imaging settings as necessary for your specific measurement.
8. Start the measurement and first record a stable baseline for about 3 min. This is important for the baseline correction used in the analysis.

9. For drug application, prepare the appropriate concentrations by diluting them in buffer. Then load the solution into the loop ensuring no air bubbles enter the system. Initiate drug release into the perfusion system by switching the injection valves from load into inject mode. Natriuretic peptides and glutamate are rather stable and dilutions can be prepared in large scale. DEA/NO is only stable in an alkaline environment, dilutions should be prepared shortly before administration.
10. Observe FRET changes and wait until the baseline is reached before initiating the next drug administration. After the baseline is reached, flush Tyrode buffer through the sample loop to remove potential drug residues which could influence the next application.
11. After completing the measurement clean the superfusion system by flushing it 2x with 20% ethanol (run solvent change, injection valves once in load mode and once in injection mode). Remove the sample and any remaining silicon from the superfusion chamber. Clean up any spills. Save data ASAP to an external hard drive.

### **2.10. PDE inhibitor experiments**

Stefanie Peters (Interfaculty Institute of Biochemistry, University of Tübingen) collected and analysed the data. cGMP measurements with various PDE inhibitors were performed on the Axiovert 200 microscope setup described previously. A baseline of 3 mins was collected. Then primary CGNs were stimulated for 2 min with DEA/NO (50 nM) alone and then superfused for 5 min with PDE inhibitor followed by 2 min with DEA/NO (50 nM) and PDE inhibitor in combination, and a final 2-min stimulation with DEA/NO (50 nM) alone. All drug applications were performed after the preceding FRET signal had returned to baseline.

### **2.11. Protein isolation and western blotting**

Andrea Schramm (Department of Pharmacology and Toxicology, University of Regensburg) performed some of the Western blots and analysis. Either tissues or CGNs in culture were treated with lysis buffer (0.67% SDS (w/v), 21 mM Tris/HCl (pH 8.3), 0.2 mM phenylmethylsulfonylfluoride, and one tablet of PhosSTOP™ phosphatase inhibitor cocktail (Roche) per 10 mL). Protein concentrations of the

lysates were measured with the Total Protein Kit, Micro Lowry, Peterson's modification (Sigma). Protein lysates were subjected to sodium dodecyl sulfate polyacrylamide gel electrophoresis (SDS-PAGE) and Western blot analysis on polyvinylidene fluoride membranes. Membranes were stained with the following antibodies: rabbit polyclonal anti-VASP (1:1000, Cell Signaling, 3112); rabbit polyclonal anti-cGKI (1:5000, [142]); rabbit monoclonal anti-GAPDH (1:1000, Cell Signaling, 2118); rabbit polyclonal anti-cGKII (1:100, [143]); and rabbit polyclonal anti- $\beta$ -actin (1:2000, Abcam, 8227). Antibody binding was detected using HRP-conjugated secondary antibodies (goat anti-rabbit IgG, 1:2000, Cell Signaling, 7074; or 1:7500, Dianova, 111-035-003) and a chemiluminescent substrate (Advansta WesternBright ECL, Biozym; or Clarity<sup>TM</sup> Western ECL Substrate, Bio-Rad Laboratories). Signals were recorded with a CCD camera (Alpha-Imager, Bio-Rad Laboratories; or ChemiDoc system, Bio-Rad Laboratories). Further analysis was performed with Fiji (NIH) [154] or ImageLab software (Bio-Rad Laboratories). Control tissues were obtained from 8- to 25-week-old wild-type mice on a C57BL/6 or mixed C57BL/6 x 129/Sv genetic background. Tissues were dissected in PBS and then homogenized in lysis buffer using a FastPrep homogenizer (MP Biomedicals) or ultra-turrax (IKA).

VASP phosphorylation can be visualized via Western blot. VASP has three phosphorylation sites: Ser157, Ser239 and Thr278, which can be phosphorylated via interaction with cGKs or cAMP dependent protein kinases (cAKs). cAKs phosphorylate VASP preferentially at Ser157, whereas cGKs at Ser239. VASP and phosphorylated VASP at Ser157 migrate differently in a SDS/PAGE with unphosphorylated VASP at 46 kDa and phosphorylated VASP at 50 kDa [156]. VASP-phosphorylation is used as a measurement of cAK or cGK activity and thus indirectly cGMP or cAMP levels.

## **2.12. Detailed working protocol for Lowry, SDS-Page and Western blotting**

### *2.12.1. Lowry protein assay*

#### Protein extraction from cells

1. Aspirate culture medium and wash the cells 2x with room temperature PBS.
2. Add the appropriate volume of SDS lysis buffer (for example 1 well out of a 6 well plate can be lysed with 100  $\mu$ L but 2 wells can be pooled with 150  $\mu$ L) and

lyse the cells by scratching the culture dish with a pipette tip. If possible, pool the wells to increase protein concentration.

3. Tilt the culture dish and use a cell scratcher to pull the lysate to the bottom of the dish (this will increase the protein concentration). Store samples on ice.
4. Denature cell lysates at 95°C for 10 minutes.
5. Centrifuge for 5 min at 18,000 rcf and transfer the supernatant into a new tube.
6. Store the samples at -20°C.

#### Protein extraction from tissue

1. Isolate the desired tissue and transfer it into an Eppendorf tube.
2. Storage is possible by shock freezing the samples with liquid nitrogen and storing at -80°C.
3. Alternatively, transfer the tissues into prepared lysis cups with a ceramic ball and a spatula of sand.
4. Add SDS lysis buffer. The amount of lysis buffer depends on the tissue (**Table 3**) but no less than 200 µL should be used.
5. Place the tubes in the FastPrep homogenizer (MP Biomedicals) and run the device for 20 seconds at 6.5 M/s.
6. Centrifuge the samples for 2 minutes at 10,600 rcf and check if they are lysed. If not add some additional lysis buffer and go back to step number six.
7. Denature the lysates at 95°C for 10 minutes.
8. Store at -20°C.

**Table 3. Recommended amount of SDS lysis buffer**

<b>Tissue</b>	<b>SDS lysis buffer (min. 200 µL)</b>
Brain, Liver, Colon	4 µL/mg
Lunge	9 µL/mg
Heart, Spleen, Kidney	10 µL/mg

#### Determination of protein concentration with Lowry assay

To determine protein concentration, we used the Total Protein Kit from Sigma. This assay is based on the Peterson modification of the Lowry method. In a first reaction step, alkaline copper tartrate forms complexes with protein peptide bonds (Biuret reaction). In the second colorimetric reaction step, Folin-Ciocalteu is reduced by copper whereby a blue product is formed. The intensity of the color correlates with the protein concentration. The Lowry assay is performed within a 96 well plate and the samples are quantified by the Thermo Multiskan EX plate reader. A concentration series of bovine serum albumin (BSA) is used to generate the standard curve.

1. Transfer 200 µL of each sample from the BSA standard series into a new Eppendorf tube. As a blank reference use 200 µL H<sub>2</sub>O.
2. Pipette 15–30 µL of the protein lysate into a new Eppendorf tube and fill up to 200 µL with H<sub>2</sub>O. As a second reference, use 15-30 µL lysis buffer filled to 200 µL with H<sub>2</sub>O.

3. Add 200  $\mu\text{L}$  Lowry Reagent Solution (total volume 400  $\mu\text{L}$ ), lightly vortex the sample and incubate for 20 minutes at rt.
4. Add 100  $\mu\text{L}$  Folin-Ciocalteu (total volume 500  $\mu\text{L}$ ), vortex the sample and incubate for 30 minutes at room temperature in the dark. This step is when the colorimetric reaction occurs.
5. Transfer 200  $\mu\text{L}$  of this reaction into a 96 well plate giving a total volume of 500  $\mu\text{L}$ . Prepare duplicates or triplicates for each sample. Remove air bubbles either with a lighter flame or carefully with a pipette.
6. Read absorption at 620 nm with the Thermo Multiskan EX plate reader.
7. Prepare a calibration curve of the BSA concentration series and use it to calculate the protein concentration of the samples.

Materials:

- Total Protein Kit (Sigma): This kit supplies the Lowry Reagent Solution and Folin-Ciocalteu.
- Bovine serum albumin (BSA): Prepare a BSA (Roth) concentration series (200, 100, 50, 25, 12.5  $\mu\text{g}/\text{mL}$ ) in  $\text{H}_2\text{O}$  and store it at  $-20^\circ\text{C}$ .

*2.12.2. SDS-Page and Western blotting*

To identify the expression of specific protein in target samples, the samples must first be separated according to their molecular weight by SDS-Page. Subsequent Western blot analysis is then performed where the proteins separated by SDS-Page are transferred to a PVDF (poly-vinylidene fluoride) membrane. Protein specific primary antibodies are used to bind the desired target and horseradish peroxidase (HRP) linked secondary antibodies are used to visualize the immobilized proteins on the PVDF membrane. For the detection of the secondary antibody we used a commercially available ECL (enhanced chemiluminescence) reagent which reacts with HRP under light emission and can be detected by a CCD-camera.

Depending on the molecular weight from the protein of interest, SDS-gels with the appropriate percent acrylamide have been prepared (using Mini Protean 3 system from BioRad). For larger proteins ( $> 30$  kDa), gels with lower acrylamide content (8%) were prepared (**Table 4**) and gels with greater acrylamide content were used for the separation of smaller proteins ( $< 30$  kDa). Depending on the amount of protein loaded it was possible to choose between 0.75 mm or 1.5 mm thick gels. The standard gel used in this thesis was 1.5 mm thick and had an acrylamide content of 10%. The 10-slot comb was used to produce ten wells. This allows one to load  $\sim 30$   $\mu\text{L}$  of protein sample without any problems.

**Table 4. Composition of polyacrylamide gel**

Components	Separating gel (1 gel 0.75 mm)			Stacking gel (max. 3 gels 0.75 mm)
	8%	10%	12%	4%
Rotiophorese®	1.4 mL	1.7 mL	2 mL	0.65 mL
4x Tris/SDS pH (8.8)	1.3 mL	1.3 mL	1.3 mL	///
4x Tris/SDS pH (6.8)	///	///	///	1.3 mL
H <sub>2</sub> O	2.4 mL	2.1 mL	1.7 mL	3.1 mL
TEMED	5 µL	5 µL	5 µL	10 µL
APS	25 µL	25 µL	25 µL	25 µL

**Note:** Double the amount for the preparation of 1.5 mm thick gels.

#### SDS gel preparation

1. Clean spacer and glass plates with 70% ethanol.
2. Assemble the glass plates in the BioRad system.
3. Prepare the separating gel and pour it between the glass plates up to the lower edge of the green boarder. To get rid of bubbles, overlay the gel with a thin ethanol layer. The polymerization reaction takes about 20-30 minutes.
4. Tilt the gel und use a paper towel to remove the ethanol.
5. Prepare the stacking gel and pour it up to the top edge of the glass plates.
6. Insert the comb and ensure no bubbles form in the solution. Allow polymerization to occur for about 20-30 minutes.
7. If the gel is not used immediately then wrap it in a wet paper towel, pack it with fresh wrap and store at 4°C.

#### Materials

- 4x Tris-Cl/SDS pH 8.8: Tris-Cl 1.5 M (182 g/L), SDS 0.4% (4 g/L), H<sub>2</sub>O to 1 L, adjust pH to 8.8 with HCl, store at 4°C
- 4x Tris-Cl/SDS pH 6.8: Tris-Cl 0.5 M (60.4 g/L), SDS 0.4% (4 g/L), H<sub>2</sub>O to 1 L, adjust pH to 6.8 with HCl, store at 4°C
- 10x SDS running buffer: Tris-Cl 0.25 M (30.2 g/L), Glycine 1.9 M (144 g/L), SDS 0.1% (1 g/L), H<sub>2</sub>O to 1 L
- 5x SDS loading dye: Tris-Cl (3.2 mL/10 mL Tris-CL pH 6.8), Glycerol 40% (4 mL/10mL), SDS 15% (1.5 g/10 mL), 2-mercaptoethanol 3.6 M (2.5 mL/10 mL), Bromphenol blue 0.1% (10 mg/10 mL), H<sub>2</sub>O to 10 mL, store 1 mL aliquots at -20°C
- 20% APS: Dissolve 2 g ammonium persulfate (APS) in 10 mL H<sub>2</sub>O, prepare 1 mL aliquots and store at -20°C

### SDS-Page and Western Blot analysis

1. Pull out the comb from the SDS gel
2. Carefully use deionized water to wash the gel pockets free of any remaining acrylamide.
3. Place the gel into the running chamber. The short side has to be faced inward.
4. Fill up the inner and outer part of the chamber with 1x SDS running buffer.
5. Denature the protein sample (lysate in 1x SDS loading dye) for 10 minutes at 95°C.
6. Load the sample and 3  $\mu$ L protein marker (PageRuler™ Plus Prestained Protein Ladder, Fermentas).
7. Run the gel with 100 V until the stacking gel is passed and then apply up to 150 V for the separating gel.
8. In the meantime, prepare the Whatman filter papers (16 per gel) and PVDF membrane for Western blot analysis.
9. Around 5 minutes before the SDS gel is ready immerse the Whatman papers in the proper buffers and rinse the PVDF membrane in methanol. This methanol procedure is crucial to “hydrate” the PVDF. Otherwise protein transfer and binding would be impaired.
10. Assemble the Whatman papers, PVDF membrane and SDS gel in the semi dry blotting device (Roth). After every layer of filter papers use a plastic pipette and roll over the stack to remove potential air bubbles (**Figure 9**).

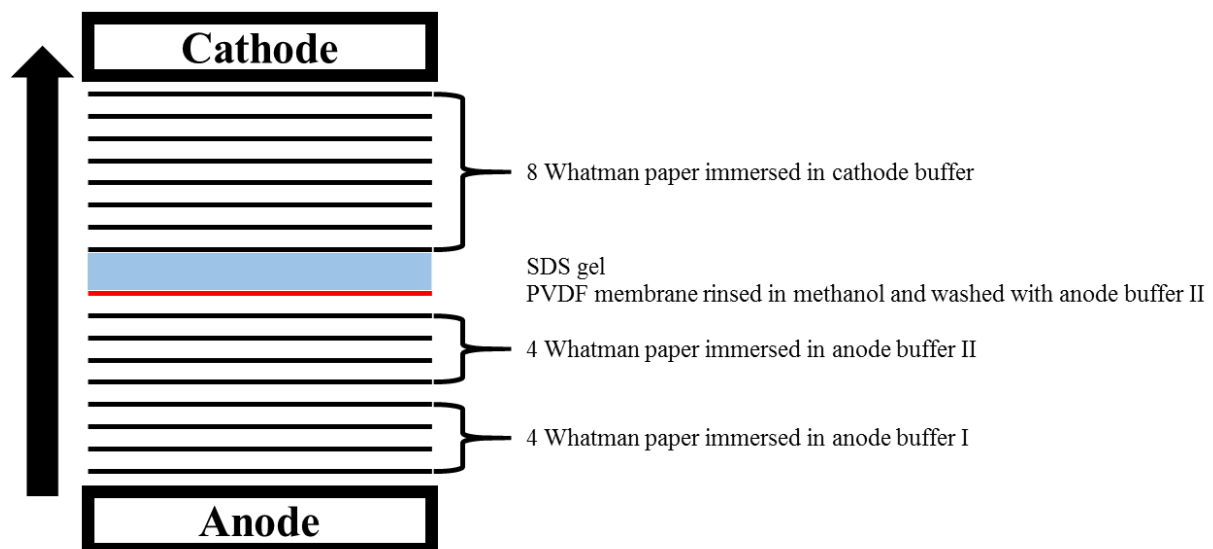


**Figure 9. How to set up the Western blot with Whatman papers.**

Image credit: Jacek Dobrowinski.

11. Blot the membrane for 80 minutes with 55 mA per stack. In the meantime, prepare 5% and 1% milk powder in 1x Tris-buffered saline with Tween-20 (TBS-T).

12. Cut the membrane and label it with a pencil.
13. Block the membrane for 1 hour with 5% milk powder solution at rt.
14. Wash the membrane 2x 3 min with 1x TBS-T.
15. Put the membrane into the primary antibody and incubate it overnight at 4°C on a rolling shaker. Alternatively incubate for 2 hours at rt (This depends on the experience with the desired antibody).
16. Wash the membrane 3x 3 minutes with 1% milk powder solution. In the meantime, prepare the HRP-linked secondary antibody (5 mL in a 50 mL Falcon tube are suitable).
17. Put the membrane into the secondary antibody and incubate it for at least 1 hour at rt on a rolling shaker.

It is recommended to seal the primary and secondary antibody tubes with Parafilm to prevent leaking.

18. Wash the membrane 1x 3 minutes in 1% milk powder and 2x 3 minutes in 1x TBS-T.
19. Prepare undiluted or diluted (1:2 up to 1:10) ECL reagent by mixing solution A and solution B. For the preparation of the dilution use 1x TBS-T. Pipette the ECL reagent on the membrane and acquire chemiluminescence images after appropriate acquisition times (3 seconds up to 10 minutes).
20. After developing the blot, also acquire a bright field image of the marker.
21. The Western blot can be evaluated with ImageJ [157].

#### Materials

- Anode buffer I (pH 10.4): Tris-Cl 0.3 M (36.3 g/L), Methanol 20% (200 mL/L), H<sub>2</sub>O to 1 L
- Anode buffer II (pH 10.4): Tris-Cl 0.025 M (3.03 g/L), Methanol 20% (200 mL/L), H<sub>2</sub>O to 1 L
- Cathode buffer (pH 7.6): Aminocaproic acid 0.04 M (5.2 g/L), Tris-Cl 0.025 M (3.03 g/L), Methanol 20% (200 mL/L), H<sub>2</sub>O to 1 L
- 1x TBS-T: 1x TBS (100 mL/L 10x TBS-T) with 0.1% Tween-20 (1 mL/L)
- Milk powder solution: Dissolve 5 g (5%) or 1 g (1%) milk powder in 100 mL 1x TBS-T
- Primary antibody diluent: TBS-T with 5% BSA and 0.05% NaN<sub>3</sub>. Primary antibodies are prepared in a 50 mL Falcon Tube (5-10 mL per antibody). The antibodies are stored at 4°C and used multiple times
- Secondary antibody diluent: Secondary antibodies are prepared freshly in 1% milk powder solution

### 2.13. Immunostaining

CGNs on coverslips were washed two times with PBS and then treated with ice-cold immuno-fix (3.7% formaldehyde in PBS) for 10 min. The cells were then washed three times with 0.5% BSA (in PBS) and incubated in 5% Normal Goat Serum (in 0.5% BSA solution) for 1 hour at room temperature. The cells were then washed two times with 0.5% BSA and incubated with mouse monoclonal antibody against  $\beta$ III-tubulin (Cell Signaling, 4466, 1:1000 in 0.5% BSA with 0.01% Triton X-100) for 1 h at room temperature. The cells were then washed two times with 0.5% BSA and then incubated with secondary antibody conjugated with Alexa 488 (goat anti-mouse IgG, Cell Signaling, A-11029, 1:100 in 0.5% BSA with 0.01% Triton X-100) and 1  $\mu$ g/mL Hoechst 33258 (Sigma) for 30 min in the dark at room temperature. The cells were then washed three times with 0.5% BSA and mounted on glass slides with mounting medium (Shandon Immu-Mount, Thermo Scientific). The cells were photographed with the Axiovert 200 microscope setup.

### 2.14. X-gal staining

For cells: Transfer cells on coverslips into 6-well plate. Wash twice with 3 ml PBS. Fix cells with 2 ml pre-chilled Cell fix solution for 10 min at rt. (Important: work under chemical hood). Wash cells twice gently with 3 ml PBS. Incubate cells in 2 ml X-Gal staining solution for 3-12 h at 37 °C in the dark. Wash twice with 3 ml PBS.

For tissues: Isolate tissue and then wash in a dish of PBS. Fix tissue with pre-chilled Cell fix solution for 30 min at rt and inverted gently every 5 min. (Important: work under chemical hood). Wash tissue twice with ~3 ml PBS. Incubate tissues in X-Gal staining solution for 3-12 h at 37 °C in the dark. Wash twice with 3 ml PBS.

#### Materials

- Cell fix: 2% Formaldehyde, 0.2% Glutaraldehyde in PBS, store at 4 °C.
- X-Gal stock solution: X-Gal (in DMSO, 40 mg/mL), store in 1 mL aliquots at -20 °C.
- X-Gal staining solution: MgCl<sub>2</sub> (2.0 mM), K<sub>3</sub>Fe(CN)<sub>6</sub> (2.5 mM), K<sub>4</sub>Fe(CN)<sub>6</sub> (2.5 mM) in PBS, store at rt in the dark. X-Gal (1 mg/mL, always add fresh).

### 2.15. $\beta$ -gal-NONOate activity in vivo as determined by VASP phosphorylation

Susanne Feil (Interfaculty Institute of Biochemistry, University of Tübingen) assisted with data collection. To investigate  $\beta$ -gal-NONOate's activity in vivo, wild type and SM-

CreER<sup>T2</sup> x R26-lacZ mice were used. SM-CreER<sup>T2</sup> mice express the tamoxifen-inducible CreERT2 recombinase under control of the smooth muscle-specific SM22 promotor. To activate lacZ expression specifically in smooth muscle-specific SM22 positive cells, 12-week-old and SM-CreER<sup>T2</sup> mice were treated injected with 1 mg of tamoxifen once a day for five days via intraperitoneal injection. Mice were put under narcosis by Dr. Susanne Feil and then 50  $\mu$ L of saline (0.9% NaCl in H<sub>2</sub>O) or 50  $\mu$ L of  $\beta$ -gal-NONOate (3.5 mM in saline) was injected via the tail vein. 8.5  $\mu$ L of  $\beta$ -gal-NONOate (100 mM) was diluted in 241.5  $\mu$ L saline for an end concentration of 3.5 mM. Mice received a 50  $\mu$ L injection resulting in a blood concentration of about 100  $\mu$ M assuming 2 mL of blood volume for the mouse. Then, 20 min after injection the mouse was sacrificed and the organs were isolated (heart, aorta, colon, bladder, skeletal muscle from the torso, and lungs). Tissues were halved with scissors. Half of all tissues were immediately transferred to lysis buffer solution (0.67% SDS (w/v), 21 mM Tris/HCl (pH 8.3), 0.2 mM phenylmethylsulfonylfluoride, and one tablet of PhosSTOP<sup>TM</sup> phosphatase inhibitor cocktail (Roche) per 10 mL) and further prepped for protein extraction. Samples were stored at -20 °C before performing further analysis. Western blot was performed at a later date. The other halves were fixed and stained with x-gal overnight.

### **2.16. Synthesis of $\beta$ -gal-NONOate**

The synthesis was performed in the laboratories of Prof. Dr. Stafforst (Interfaculty Institute of Biochemistry, University of Tübingen) and Prof. Dr. Ziegler (Institute of Organic Chemistry, University of Tübingen) with help from Anne Stroppel (Interfaculty Institute of Biochemistry, University of Tübingen) and Gregor Lemanski (Institute of Organic Chemistry, University of Tübingen). Synthesis was conducted in a similar manner to the methodology reported previously [141]. The synthesis was a five-step reaction completed with an overall yield of 6%. The synthesis involved acetylation of the reactive alcohol groups, bromination of galactose at the anomeric carbon. The NONOate (diazoniumdiolate) was prepared under a high-pressure reaction with NO gas and pyrrolidine. Then the NONOate compound and the brominated, acetylated galactose were combined in a coupling reaction that produced only the  $\beta$ -anomer of the sugar due to inversion of stereochemistry via the S<sub>N</sub>2 reaction. The coupling reaction could be nicely followed because the galactose sugar

stains brown upon treatment with sulfuric acid and heat, while the NONOate is visible under UV light, as described below. Subsequent deprotection via hydrolysis and purification via column chromatography produced the final  $\beta$ -gal-NONOate compound.

#### *Galactose protection via peracetylation*

1 g of peracetylated galactose were suspended in 2 ml of an ice-cold mixture of acetic acid and acetic anhydride (ratio 2:3). While stirring, 4 ml of 33% HBr-acetic acid were added dropwise within 30 min. Then the mixture is stirred for 30 minutes as it warms to rt. The mixture is stirred at rt for 2 h, then 20 ml of dichloromethane are added. The organic phase is washed with about 13 ml of ice-cold water and then three times with 13 ml of ice-cold saturated sodium carbonate solution, then dried over sodium sulphate. The solvent was stripped off on a rotary evaporator and the brominated product is crystallized from diethyl ether. The resulting white solid (1,2,3,4,5-penta-O-acetyl- $\beta$ -D-galactopyranoside) was dried in vacuo and stored at -20 °C. Percent yield 73%.

#### *Bromination of the galactose anomeric carbon*

62.5 ml of 33% HBr in glacial acetic acid (1079 mmol, 1.1 eq) were carefully added dropwise to a solution of 25.0 g (64.4 mmol, 1 eq) of 1,2,3,4,5-penta-O-acetyl- $\beta$ -D-galactopyranoside in 250 ml DCM at 0 ° C. After complete addition, the reaction solution was stirred for 2 hours at rt. The reaction progress was tracked (TLC control: PE / EA 1: 1). Note: to visualize the sugar, spray the TLC plate with 5% sulfuric acid in methanol and then heat with a heat gun to produce a brown spot. Once the reaction was complete it was diluted with 200 ml of ice-water. The organic phase was washed with 100 ml of saturated NaHCO<sub>3</sub> solution and once with 150 ml of water. Finally, the organic phase was dried over sodium sulfate and the solvent removed under vacuum. The product was a slightly brown colored oil. Percent yield 91%.

#### *Synthesis of the diazeniumdiolate*

Anne Stroppe (Interfaculty Institute of Biochemistry, University of Tübingen) and Gregor Lemanski (Institute of Organic Chemistry, University of Tübingen) performed the synthesis of the diazeniumdiolate.

**Note:** This reaction uses the toxic gas NO under high pressures with a danger of

explosion. For more information see previous work [158].

1 ml of pyrrolidine was combined with 2.4 ml of sodium methoxide in methanol (5 M) in 20 ml of anhydrous methanol under a nitrogen atmosphere. Then the reaction mixture is placed under vacuum for a short time to remove all dissolved gases from the liquid solution. The reaction is then set to a pressure of 4 bar with NO and stirred vigorously for 3-4 h at rt. The reaction mixture is concentrated into a syrup and then taken up in diethyl ether in which the product precipitates as a white powder. It is filtered with diethyl ether and then dried under vacuum. The resulting diazeniumdiolate is stored under nitrogen and protected from light. Percent yield 28%.

#### *Glycosylation of the diazeniumdiolate*

1 g of diazeniumdiolate and 2 g of brominated, acetylated galactose are dissolved in 30 ml of anhydrous acetonitrile and stirred for 24 h. The reaction mixture is protected from light in order to prevent radical side reactions of the liberated hydrogen bromide. The reaction progress was tracked (TLC control: PE / EA 1: 1). Note: the diazeniumdiolate product fluoresces under UV light while the sugar can be visualized with sulfuric acid as stated previously. The reaction mixture was concentrated on a rotary evaporator and taken up in 50 ml of ethyl acetate. The reaction was then shaken out three times with 50 ml of water and dried over sodium sulfate. The product was purified on a silica gel column with a 1: 1 mixture of ethyl acetate and petroleum ether. Percent yield 38%.

#### *Deacetylation of the $\beta$ -D-Galactopyranosyl 1-(pyrrolidine-1-yl)-diazenium-1,2-diolate (acetylated $\beta$ -gal-NONOate)*

1 g of  $\beta$ -D-Galactopyranosyl 1-(pyrrolidine-1-yl)-diazenium-1,2-diolate is dissolved in 50 ml of anhydrous methanol. Sodium methoxide is added until the pH is at least 8-9; a higher pH does not appear to disrupt the reaction. The mixture was stirred for 2 h at rt and then purified on a silica gel column using a 1:10 mixture of methanol and chloroform as eluent. The product was then set under vacuum and the final product collected as a white solid. The resulting  $\beta$ -gal-NONOate was protected from light and moisture and stored at 4 °C. Percent yield 86%. Nuclear magnetic resonance (NMR) spectra were produced by BrukerAvance III HDX 400 spectrometer at 400.16 MHz for proton NMR spectra. The  $^1\text{H}$  NMR was collected at the NMR facility (Institute of

Organic Chemistry, University of Tübingen) with help from the Stafforst Laboratory (Interfaculty Institute of Biochemistry, University of Tübingen). The complete five-step synthesis was completed with an overall yield of 6% resulting in 110 mg of  $\beta$ -gal-NONOate.

### **2.17. Data analysis and statistics**

Imaging data were analysed as previously described [118]. For image acquisition and online analysis, VisiView (Visitron) was used, and for offline analysis Fiji software (NIH) [154]. For further analysis, Microsoft Excel (Microsoft Corp.) and Origin (OriginLab Corp.) were used.  $F_{480}$  signals (CFP emission at 480 nm, cyan traces in respective graphs) and  $F_{535}$  signals (YFP emission at 535 nm, orange traces in respective graphs) were background-corrected and used to calculate the  $F_{480}/F_{535}$  ratio R (green traces in respective graphs).  $F_{340}$  signals (intensity of emission at 535 nm after excitation at 340 nm) and  $F_{387}$  signals (intensity of emission at 535 nm after excitation at 387 nm) were background-corrected and used to calculate the  $F_{340}/F_{387}$  ratio R (black traces in respective graphs).  $\Delta F_{480}/F_{480}$ ,  $\Delta F_{535}/F_{535}$ ,  $\Delta F_{340}/F_{340}$ ,  $\Delta F_{387}/F_{387}$  and corresponding  $\Delta R/R$  traces were obtained by normalization to the baseline recorded for ~3 min at the beginning of each experiment. For  $\Delta R/R$  peak area and peak height calculation, Peak Area/Height Analyzer of Origin was used. Peak borders were defined manually. Statistical analysis was performed using Origin software. Statistical differences between more than two groups were analyzed by one-way ANOVA followed by Bonferroni's test.  $p$  values < 0.05 were considered to be significant.

## 3 Results

### 3.1. NO-cGMP signaling in CGNs

As discussed in the introduction, the cGMP signaling pathway has proven itself highly drugable (**Table 1**). However, information about this pathway in the nervous system is limited and in need of further investigation. To this end, we have investigated the cGMP signaling components in CGNs.

#### 3.1.1. cGMP imaging in CGNs reveals a NO-induced cGMP response

Primary CGN cultures were prepared from 7-day-old R26-cGi500-L1 mice [118], which express the cGi500 sensor ubiquitously. As shown in Figure 10, CGNs expressed the cGMP sensor protein (**Figure 10A**, green fluorescence). It is important to note that the green fluorescence shown in Figure 10A shows the YFP emission of the sensor and not the cGMP concentration, which is reflected by the CFP/YFP emission ratio. To determine which substances can induce a reliable elevation of cGMP in CGNs, the cells were exposed to ANP (100 nM), CNP (100 nM), or the NO-releasing compound diethylamine NONOate (DEA/NO) (100 nM) during real-time imaging under continuous flow (**Figures 10A and B**). Application of DEA/NO induced a robust cGMP elevation as indicated by a simultaneous increase in CFP emission (cyan trace) and decrease in YFP emission (orange trace) resulting in an increased CFP/YFP ratio (black trace) (**Figure 10B**). Application of ANP or CNP did not result in a cGMP increase. To determine the sensitivity of the cGMP response of CGNs to DEA/NO, a concentration-response curve experiment was performed and revealed an  $EC_{50}$  of  $\approx 32$  nM (**Figure 10C**). CGN primary cultures were immunostained with  $\beta$ III-tubulin (neuronal marker, green) and nuclei with Hoechst dye (blue) to confirm they are neurons (**Figure 10D**). We then wanted to compare the results in tissue slices.

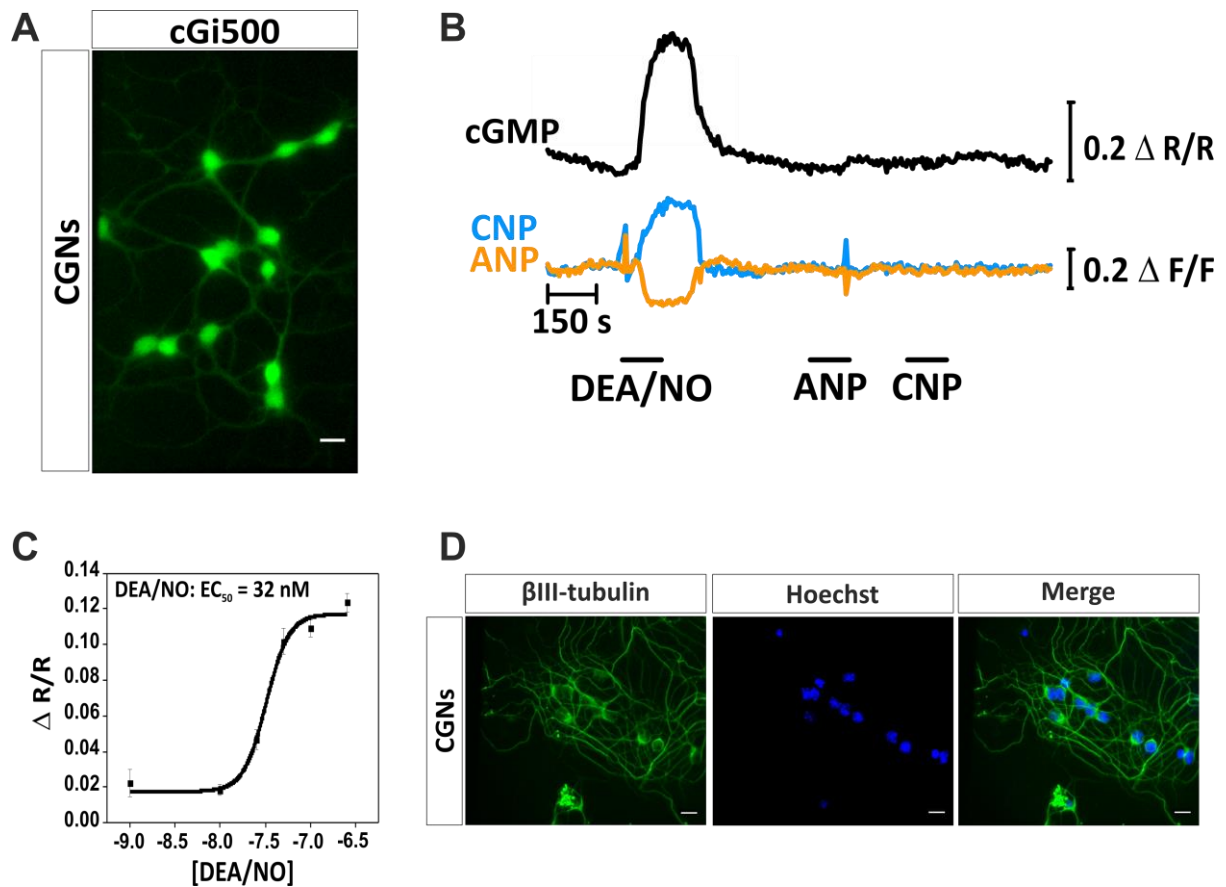


**Figure 10. Visualization of cGMP in CGNs reveals a NO-induced cGMP response.**

(A) CGNs isolated from 7-day-old R26-cGi500-L1 mice express the cGi500 sensor (green). The green color represents the YFP fluorescence of cGi500. Scale bar 10  $\mu$ m. (B) cGMP measurement in CGNs upon stimulation with DEA/NO (100 nM), ANP (100 nM), and CNP (100 nM). Black, cyan, and orange traces represent CFP/YFP ratio, CFP emission, and YFP emission, respectively. Scale bars represent the change in fluorescence of the single fluorophores CFP or YFP ( $\Delta F/F$ ) or their ratio (CFP/YFP;  $\Delta R/R$  reflecting [cGMP]<sub>i</sub>). The signals are from a single cell representative of the data set ( $n = 57$  cells measured on six coverslips obtained from three independent cultures). (C) Increasing concentrations of DEA/NO were applied to CGNs to establish a concentration-response curve. The  $EC_{50}$  of CGNs for DEA/NO is  $\approx 32$  nM. Data are presented as mean  $\pm$  SEM ( $n = 12$  cells per data point; cells from one culture were measured on one coverslip). (D) Representative picture of a CGN primary culture stained for  $\beta$ III-tubulin (neuronal marker, green) and nuclei with Hoechst dye (blue); an overlay of both channels is also shown (Merge). Scale bar 10  $\mu$ m.

### 3.1.2. cGMP imaging in acute cerebellar slices reveals a NO-induced cGMP response

cGMP was also visualized in freshly prepared cerebellar slices isolated from R26-cGi500-L1 mice, which express the cGi500 sensor ubiquitously. The cerebellar tissue slices fluoresce green, which is the expressed cGMP sensor protein (**Figure 11A**, green fluorescence). It is important to note that the green fluorescence shown in Figure 11A is the YFP emission of the sensor and not the cGMP concentration, which is reflected by the CFP/YFP emission ratio. To determine which substances can induce a reliable elevation of cGMP in cerebellar slices, the tissue was exposed to ANP (250 nM), CNP (250 nM) and DEA/NO (5  $\mu$ M) during real-time imaging under continuous flow. As in the CGN cultures, cGMP was elevated in acute cerebellar slices upon DEA/NO application, but not ANP nor CNP (**Figure 11B**, black trace). We then wanted to investigate the relationship between NO-induced cGMP and  $\text{Ca}^{2+}$  responses in CGNs.

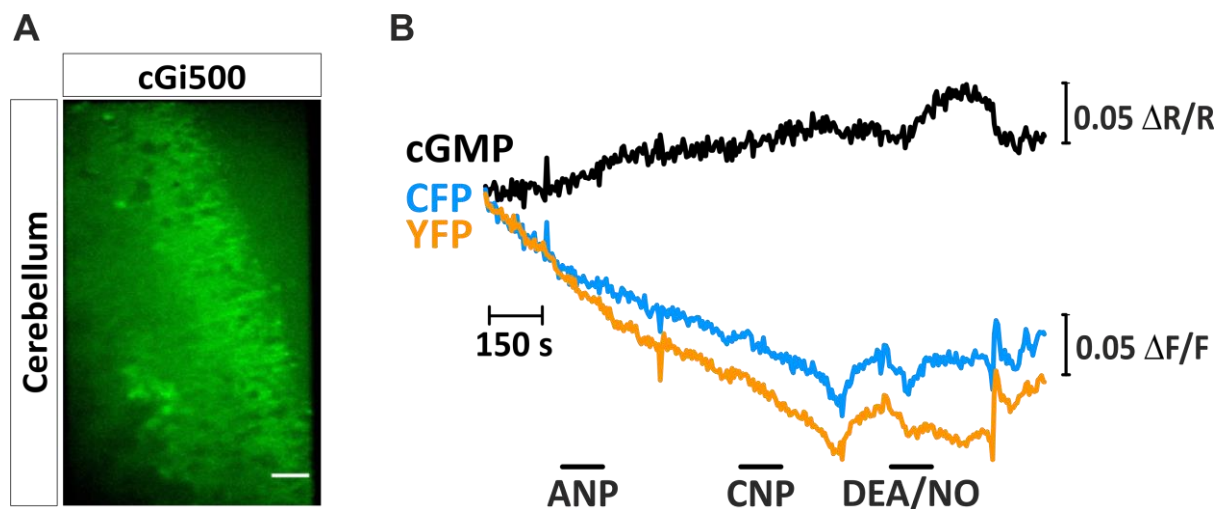


**Figure 11. Visualization of cGMP in acute cerebellar slices reveals a NO-induced cGMP response.**

(A) Acute cerebellar slice isolated from a 7-week-old R26-cGi500-L1 mouse. The green color represents the YFP fluorescence of cGi500. Scale bar 20  $\mu$ m. (B) cGMP measurement in the granule cell layer of a cerebellar slice upon stimulation with ANP (250 nM), CNP (250 nM), and DEA/NO (5  $\mu$ M). Black, cyan, and orange traces represent CFP/YFP ratio, CFP emission, and YFP emission, respectively. Scale bars represent the change in fluorescence of the single fluorophores CFP or YFP ( $\Delta F/F$ ) or their ratio (CFP/YFP;  $\Delta R/R$  reflecting  $[\text{cGMP}]_i$ ). The signals are from a single region of interest representative of the data set ( $n = 3$  acute cerebellar slices analyzed in three independent experiments).

### 3.1.3. Simultaneous imaging of Ca<sup>2+</sup> and cGMP reveals NO potentiation of glutamate-induced Ca<sup>2+</sup> transients in CGNs

To investigate the potential crosstalk between NO-cGMP signaling and Ca<sup>2+</sup> signaling, cGMP and Ca<sup>2+</sup> were simultaneously measured under flow in real-time in CGNs isolated from sensor mice (R26-cGi500-L1). The CGNs were loaded with the fluorescent Ca<sup>2+</sup> indicator Fura-2 and then stimulated with glutamate to induce a Ca<sup>2+</sup> response and DEA/NO to induce a cGMP response (**Figure 12**). Figure 12A depicts the control stimulation without the addition of DEA/NO. CGNs were exposed to glutamate (100  $\mu$ M, 9.6 s) to evoke Ca<sup>2+</sup> transients (black trace) twice per measurement. There were no observed changes in cGMP concentration (green trace) during glutamate-induced Ca<sup>2+</sup> transients (black trace). Figure 12B shows a representative trace during stimulation with both glutamate and DEA/NO (100 nM). Glutamate addition during NO-induced elevated cGMP levels resulted in augmented glutamate-induced Ca<sup>2+</sup> transients compared to control Ca<sup>2+</sup> transients in the absence of DEA/NO (**Figures 12A-C**). The evaluation was performed by taking the ratio of the peak height of the second Ca<sup>2+</sup> transient (in the presence of Tyrode buffer or DEA/NO) and the peak height of the first Ca<sup>2+</sup> transient (in the absence of DEA/NO) (2<sup>nd</sup> peak height : 1<sup>st</sup> peak height). Analysis revealed a second peak to first peak height ratio of  $\approx 1.2$  vs.  $\approx 0.7$  (**Figure 12C**;  $p < 0.001$ ). These data depicted a NO-induced augmentation of glutamate-induced Ca<sup>2+</sup> transients in primary mouse CGNs.

To determine if the observed augmented Ca<sup>2+</sup> transients is cGMP dependent and not an NO-induced cGMP-independent effect, CGN cultures were prepared from cGMP sensor mice lacking the  $\beta_1$  subunit of NO-GC (NO-GC KO) [144] that therefore expressed no functional NO-GC. These CGNs showed normal glutamate-induced Ca<sup>2+</sup> transients (**Figure 12D**, black trace; **Figure 3F**, Tyrode). As expected, NO-GC KO CGNs showed no increase in the cGMP concentration upon addition of DEA/NO (100 nM) (**Figure 12E**, green trace), confirming the absence of functional NO-GC in these cells. In contrast to wild type CGNs (**Figures 12A-C**), NO-GC KO cells showed similar glutamate-induced Ca<sup>2+</sup> transients in the absence and presence of DEA/NO, supporting the notion that the NO-induced augmentation of Ca<sup>2+</sup> transients is indeed cGMP-dependent (**Figures 12D-F**). After confirming our hypothesis with the NO-GC KO CGNs, we wanted to use pharmacological tools to further test the importance of cGMP in the observed crosstalk.

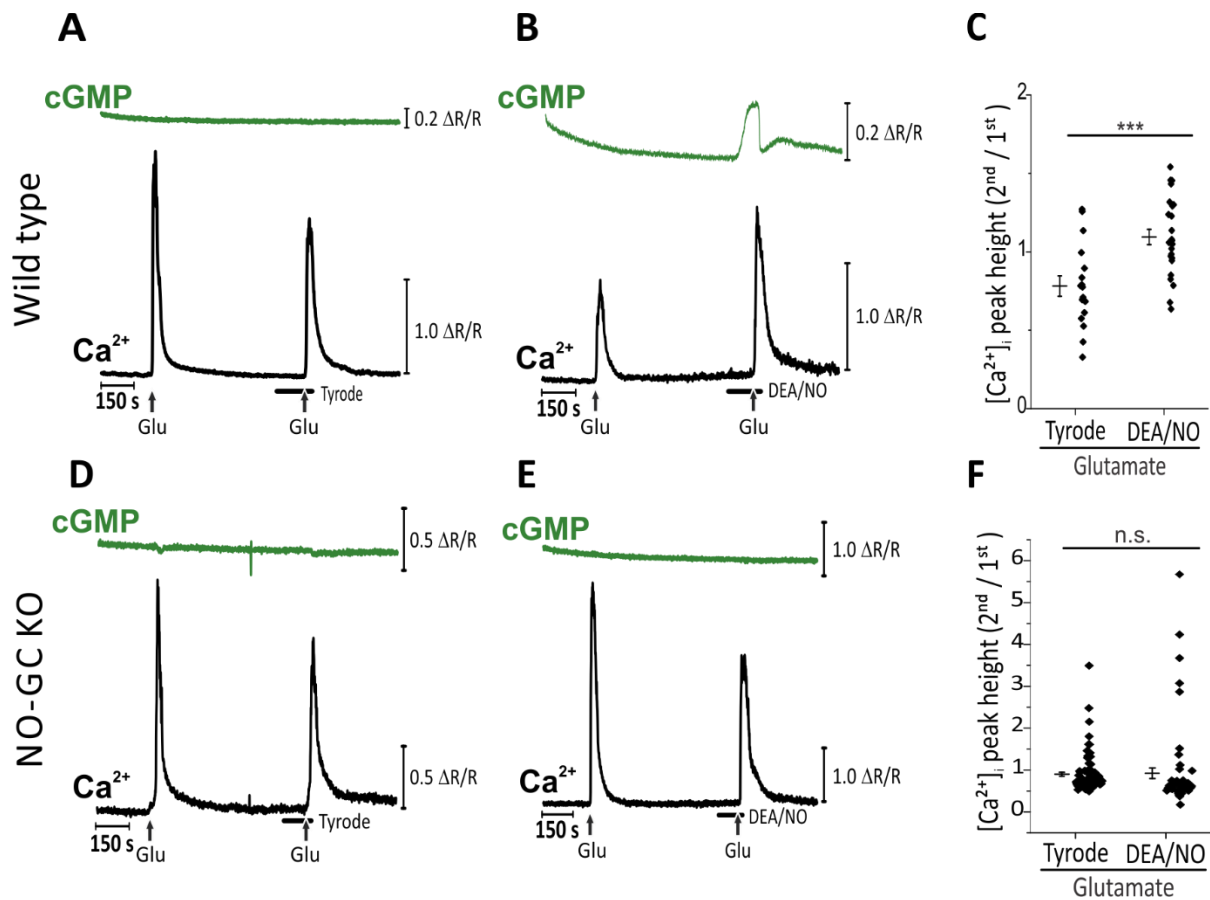


**Figure 12. Simultaneous measurement of cGMP and  $\text{Ca}^{2+}$  reveals cGMP- $\text{Ca}^{2+}$  crosstalk in CGNs.**

Traces depict cGMP (green) visualized with the cGi500 sensor, and  $[\text{Ca}^{2+}]_i$  (black) visualized with Fura-2. CGNs were exposed to glutamate (100  $\mu\text{M}$ ) (for 9.6 s, represented by vertical arrows) to elevate  $[\text{Ca}^{2+}]_i$ , and to DEA/NO (100 nM) (represented by horizontal bars) to increase the cGMP concentration. Tyrode buffer was used as a control in the absence of DEA/NO. Traces depict representative measurements of individual cells. Scale bars represent the change in fluorophore ratio ( $\Delta\text{R}/\text{R}$  reflecting  $[\text{cGMP}]_i$  or  $[\text{Ca}^{2+}]_i$ ). (A-C) Imaging of cGi500-expressing CGNs with NO-GC wild type alleles (wild type). (A) Brief repetitive stimulation with glutamate under control conditions. (B) CGNs were exposed to glutamate alone and then to DEA/NO followed by a second stimulation with glutamate in the presence of DEA/NO. (C) Quantification of the results obtained under conditions shown in (A) and (B). Depicted is the ratio of the  $[\text{Ca}^{2+}]_i$  peak heights (2<sup>nd</sup> over 1<sup>st</sup> peak) of individual cells. Data are presented as mean  $\pm$  SEM;  $p < 0.001$ \*\*\* (n = 17 cells for Tyrode, n = 25 cells for DEA/NO, measured on six coverslips obtained from three independent cultures). (D-F) Imaging of cGi500-expressing CGNs with a genetic deletion of NO-GC (NO-GC KO). (D) Brief repetitive stimulation with glutamate under control conditions. (E) CGNs were exposed to glutamate alone and then to DEA/NO followed by a second stimulation with glutamate in the presence of DEA/NO. (F) Quantification of the results obtained under conditions shown in (D) and (E). Depicted is the ratio of the  $[\text{Ca}^{2+}]_i$  peak heights (2<sup>nd</sup> over 1<sup>st</sup> peak) of individual cells. Data are presented as mean  $\pm$  SEM; n.s., not significant (n = 90 cells for Tyrode, n = 60 cells for DEA/NO, measured on twelve coverslips obtained from two independent cultures). The NO-GC KO mouse lines were originally developed by the Friebe laboratory (Institute of Physiology, Julius-Maximilians-University).

### 3.1.4. cGMP analogues support a cGMP-dependent increase of glutamate-induced $\text{Ca}^{2+}$ transients

To further investigate the importance of cGMP in augmented glutamate-induced  $\text{Ca}^{2+}$  responses, the membrane-permeable cGMP analogue 8-Br-cGMP (100  $\mu\text{M}$ ) or 8-pCPT-cGMP (100  $\mu\text{M}$ ) was applied in place of DEA/NO during glutamate-induced  $\text{Ca}^{2+}$  transients. In the presence of 8-Br-cGMP or 8-pCPT-cGMP, glutamate-induced  $\text{Ca}^{2+}$  transients were significantly augmented compared to controls without cGMP analogues (**Figure 13A**,  $p < 0.05$ ; **Figure 13B**,  $p < 0.01$ ). The results with cGMP analogues further support a cGMP- $\text{Ca}^{2+}$  crosstalk in CGNs, which could be mediated via cGKs, CNG channels, or other cGMP effector proteins. Our next experiment aimed to identify the cGMP-effector proteins that were possibly involved in this crosstalk.

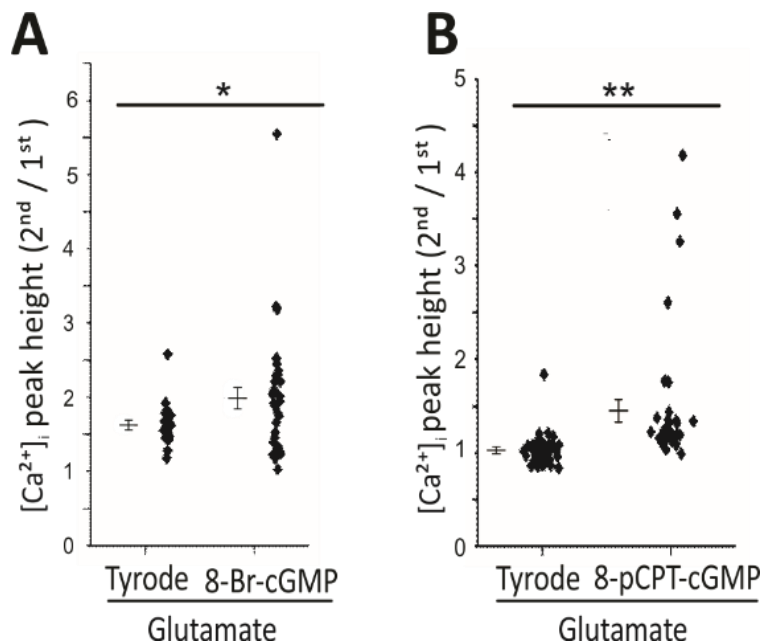


**Figure 13. The addition of cGMP analogues confirms cGMP- $\text{Ca}^{2+}$  crosstalk in CGNs.**

(A) Quantification of glutamate (100  $\mu\text{M}$ , 9.6 s)-induced elevation of  $[\text{Ca}^{2+}]_i$  in the absence of cGMP analogue (Tyrode) or after pre-incubation of cells with 8-Br-cGMP (100  $\mu\text{M}$ , 5.5 min). Data are depicted as the ratio of the  $[\text{Ca}^{2+}]_i$  peak heights of individual cells (2<sup>nd</sup> over 1<sup>st</sup> peak, where the 2<sup>nd</sup> peak was induced by glutamate in the presence of Tyrode or 8-Br-cGMP) and presented as mean  $\pm$  SEM;  $p < 0.05^*$  ( $n = 15$  cells for Tyrode,  $n = 34$  cells for 8-Br-cGMP, measured on seven coverslips obtained from three independent cultures). (B) Quantification of glutamate (100  $\mu\text{M}$ , 10 s)-induced elevation of  $[\text{Ca}^{2+}]_i$  in the absence of cGMP analogue (Tyrode) or after pre-incubation of cells with 100  $\mu\text{M}$  8-pCPT-cGMP for 5.5 min. Data are depicted as the ratio of the  $[\text{Ca}^{2+}]_i$  peak heights of individual cells (2<sup>nd</sup> over 1<sup>st</sup> peak, where the 2<sup>nd</sup> peak was induced by glutamate in the presence of Tyrode or 8-pCPT-cGMP) and

presented as mean  $\pm$  SEM;  $p < 0.01^{**}$  (n = 29 cells for Tyrode, n = 22 cells for 8-pCPT-cGMP, measured on six coverslips obtained from two independent cultures).

### **3.1.5. CGN primary cultures do not express cGKI nor cGKII as determined by Western blot analysis**

To determine if cGKs could be downstream targets of cGMP, protein lysates from CGN primary cultures were analyzed via Western blot with cGKI and cGKII antibodies (**Figures 14 and 15**). All antibodies were validated with respective knockout tissues to confirm their specificity. While the cGKI protein was readily detected in lysates from colon and cerebellum isolated from wild type mice, it was not detected in our primary CGNs (**Figure 14**). Using a highly specific antibody made in the laboratory of Prof. Dr. Jens Schlossmann (Department of Pharmacology and Toxicology, University of Regensburg) , the cGKII protein was detected in lysates from jejunum of wild type mice as well as in cerebellum isolated from wild type or cGKI knockout mice, but it was not detected in our CGN lysates (**Figure 15A**). Another cGKII antibody from Proteintech proved to be of limited use to detect cGKII, but rather stained several unknown protein bands including one in CGNs with a molecular weight of about 72 kDa (**Figure 15B**). These data indicate that neither cGKI nor cGKII are expressed in our primary cultured CGNs and thus do not play a role in cGMP/Ca<sup>2+</sup> crosstalk. These data also highlight the importance of antibody validation with positive and knock-out controls. We next wanted use real-time imaging to investigate the specific PDEs involved in cGMP degradation in CGNs.

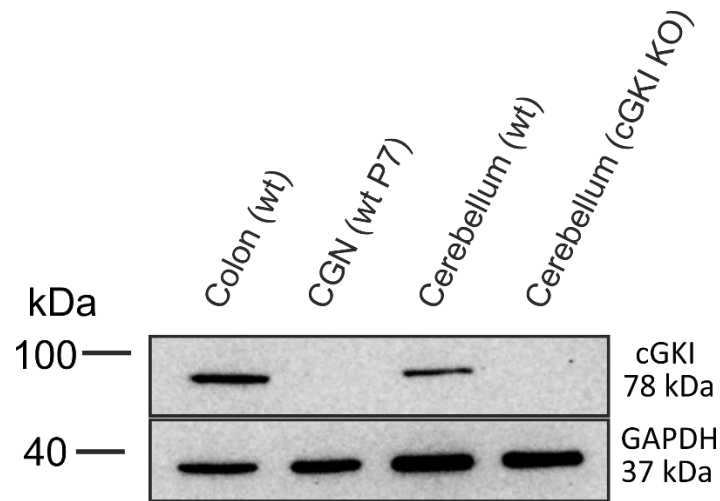


**Figure 14. Western blot analysis reveals no cGKI expression in primary CGN cultures.**

Lysates prepared from CGN cultures grown for 5 days *in vitro* (10  $\mu$ g), colon (10  $\mu$ g) and cerebellum of a wild type mouse (wt) (10  $\mu$ g) as well as cerebellum of a cGKI knockout mouse (cGKI KO) (10  $\mu$ g) were stained with a highly specific cGKI antibody. GAPDH was used as a loading control. Representative data from three independent CGN primary cultures are shown. Expected molecular weights of respective proteins are indicated on the right. CGN cultures were established from 7-day-old wild type mice (wt P7) and extracts of the cerebellum and internal organs were prepared from 8- to 25-week-old mice.

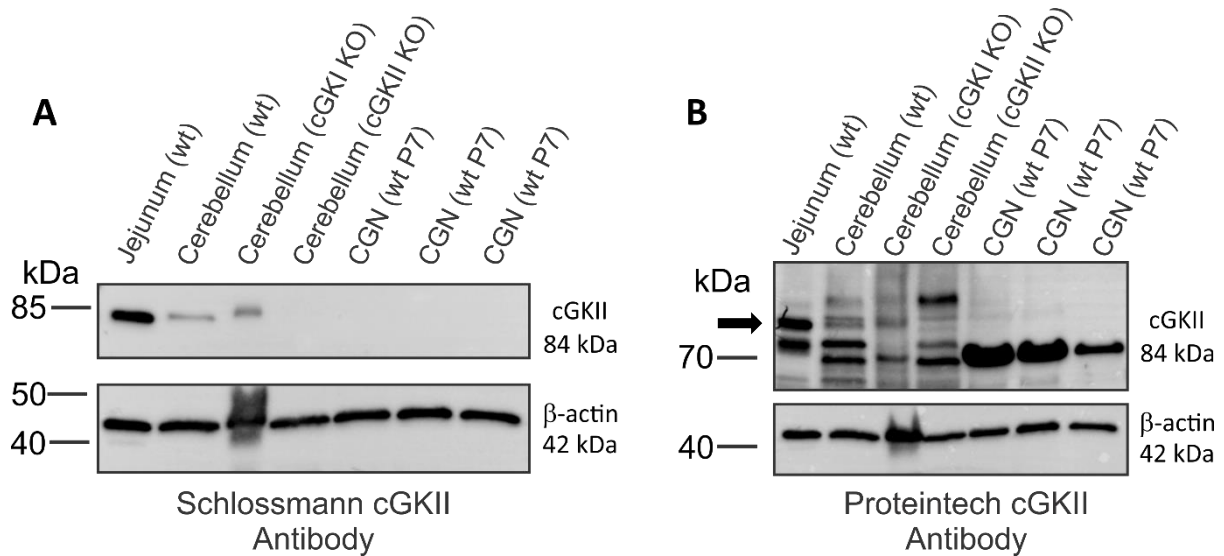


**Figure 15. Western blot analysis reveals no cGKII expression in primary CGN cultures.**

(A) Lysates prepared from three CGN cultures grown for 5 days *in vitro* (30  $\mu$ g), jejunum (20  $\mu$ g) and cerebellum of a wild type mouse (wt) (70  $\mu$ g) as well as cerebellum of a cGKI knockout mouse (cGKI KO) (70  $\mu$ g) and of a cGKII knockout mouse (cGKII KO) (70  $\mu$ g) were stained with a highly specific cGKII antibody.  $\beta$ -actin was used as a loading control. Expected molecular weights of respective proteins are indicated on the right. CGN cultures were established from 7-day-old wild type mice (wt P7) and extracts of the cerebellum and internal

organs were prepared from 8- to 25-week-old mice. **(B)** Lysates prepared from three CGN cultures grown for 5 days *in vitro* (30 µg), jejunum (20 µg) and cerebellum of a wild type mouse (wt) (70 µg) as well as cerebellum of a cGKI knockout mouse (cGKI KO) (70 µg) and of a cGKII knockout mouse (cGKII KO) (70 µg) were stained with a cGKII antibody from Proteintech. The black arrow represents the band that is potentially cGKII. β-actin was used as a loading control. Representative data from two independent Western blots are shown. Expected molecular weights of respective proteins are indicated on the right. CGN cultures were established from 7-day-old wild type mice (wt P7) and extracts of the cerebellum and internal organs were prepared from 8- to 25-week-old mice. The Western blots were performed with help from Prof. Dr. Jens Schlossmann and Andrea Schramm (Department of Pharmacology and Toxicology, University of Regensburg).

### 3.1.6. Real-time cGMP imaging in CGNs reveals cGMP degradation via Zaprinast-sensitive PDEs

To evaluate which PDE(s) degrade cGMP in murine CGNs, the cells were exposed to various PDE inhibitors. CGNs from cGMP sensor mice were first superfused with DEA/NO (50 nM) alone (**Figure 16A**, first peak), and then with the general PDE inhibitor IBMX (100 µM) followed by DEA/NO (50 nM) in the presence of IBMX (**Figure 16A**, second peak) and a final application of DEA/NO (50 nM) alone (**Figure 16A**, third peak). IBMX alone had no influence on the basal cGMP level in cultured CGNs, however, it strongly potentiated the cGMP increase elicited by DEA/NO compared to DEA/NO alone (**Figure 16A**). To identify the PDEs that play a role in cGMP degradation in CGNs, specific PDE inhibitors [69] were applied in the same manner as shown for IBMX in Figure 16A. These PDE inhibitors were Vinpocetine (5 µM) for PDE1, Bay 60-7550 (10 nM) for PDE2, EHNA (10 µM) for PDE2, Milrinone (10 µM) for PDE3, Sildenafil (20 µM) for PDE5, and Zaprinast (20 µM) for PDE5, 6, 9, 10, and 11. These measurements (**Figure 16B**) revealed a weak but significant effect of Sildenafil ( $p < 0.05$ ) and a strong effect of Zaprinast ( $p < 0.05$ ). The other tested PDE inhibitors did not show statistically significant effects on NO-induced cGMP elevation. These data implicated PDE5, 6, 9, 10, and 11 as possible cGMP-degrading PDEs in murine CGNs.

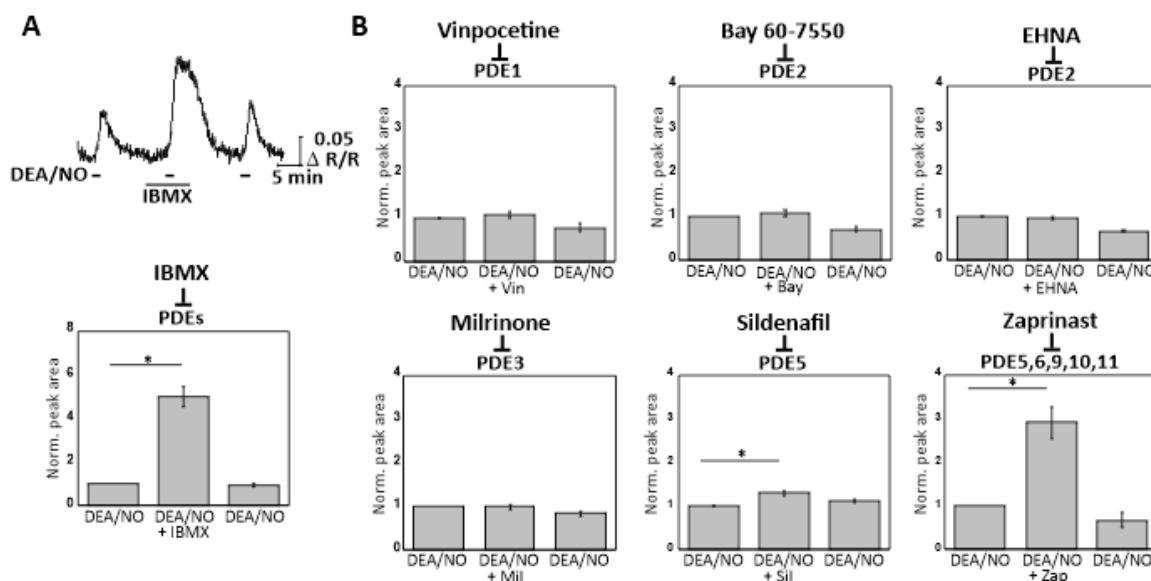


**Figure 16. Real-time cGMP imaging in CGNs reveals degradation of cGMP by Zaprinast-sensitive PDEs.**

(A) cGi500-expressing CGNs isolated from R26-cGi500-L1 mice were stimulated three times with DEA/NO (50 nM), first with DEA/NO alone, then in the presence of IBMX (100  $\mu$ M), and finally again with DEA/NO alone. The bar graph shows the statistical evaluation of DEA/NO-induced cGMP peak areas before (1<sup>st</sup> peak), during (2<sup>nd</sup> peak) and after (3<sup>rd</sup> peak) incubation with IBMX. Peak areas were normalized to the 1<sup>st</sup> peak of each experiment. Data are presented as mean  $\pm$  SEM;  $p < 0.05^*$  1<sup>st</sup> versus 2<sup>nd</sup> peak ( $n = 6$  cells measured on three coverslips obtained from three CGN cultures). (B) As described for (A), CGNs were superfused with DEA/NO (50 nM) in the absence and presence of indicated PDE inhibitors. The following PDE inhibitors were tested: 5  $\mu$ M Vinpocetine (Vin); 10 nM Bay 60-7550 (Bay); 10  $\mu$ M EHNA; 10  $\mu$ M Milrinone (Mil); 20  $\mu$ M Sildenafil (Sil); 20  $\mu$ M Zaprinast (Zap). Data are presented as mean  $\pm$  SEM;  $p < 0.05^*$  1<sup>st</sup> versus 2<sup>nd</sup> peak ( $n = 6-12$  cells per condition; cells were measured on two coverslips obtained from two CGN cultures). Data were collected and evaluated by Stefanie Peters (Interfaculty Institute of Biochemistry, University of Tübingen).

### 3.2. Cell type specific NO release with $\beta$ -gal-NONOate

As mentioned previously, traditional NO releasing compounds act ubiquitously on all cell types [140]. It was our aim to enable cell type specific NO release to facilitate more accurate investigation of NO signaling. To this end, we planned to use  $\beta$ -gal-NONOate, which only releases NO in the presence of  $\beta$ -galactosidase, in combination with lacZ under the control of cell-specific Cre/loxP mouse lines. We investigated the viability of this methodology to enable cell type specific NO generation in cell cultures, acute tissue slices, and in vivo.

### 3.2.1. Synthesis of $\beta$ -gal-NONOate

Due to limited availability and high costs from commercial sources, we synthesized  $\beta$ -gal-NONOate ourselves in collaboration with the laboratories of Prof. Dr. Stafforst (Interfaculty Institute of Biochemistry, University of Tübingen) and Prof. Dr. Ziegler (Institute of Organic Chemistry, University of Tübingen). The overall yield for the five-step synthesis was ~6% resulting in 110 mg of  $\beta$ -gal-NONOate. Proton nuclear magnetic resonance ( $^1\text{H}$  NMR) analysis was performed and chemical shifts are in ppm (**Figure 17**). The  $^1\text{H}$  NMR shows us the chemical shifts of the unique protons in the synthesized compound and helps to confirm the molecule's structure [159]. The integration of the  $^1\text{H}$  NMR signals is proportional to the ratio of the protons in the molecule [159].

The synthesis of  $\beta$ -gal-NONOate was performed in five steps (**Figure 18**). The first reaction was an acetylation protection reaction of the alcohol groups on the galactose ring. This was then followed by bromination to facilitate the subsequent coupling reaction. The NONOate salt (diazoniumdiolate) was synthesized under high pressure with NO gas (~4 bar) and pyrrolidine. The diazeniumdiolate was then combined with the brominated, galactose to produce acetylated  $\beta$ -gal-NONOate. Deprotection and subsequent purification via column chromatography were performed to produce the final product  $\beta$ -gal-NONOate. For more information refer to section 2.16. After successful synthesis of  $\beta$ -gal-NONOate, we wanted to test its ability to induce NO-cGMP signalling in living cells and tissues.

## Results

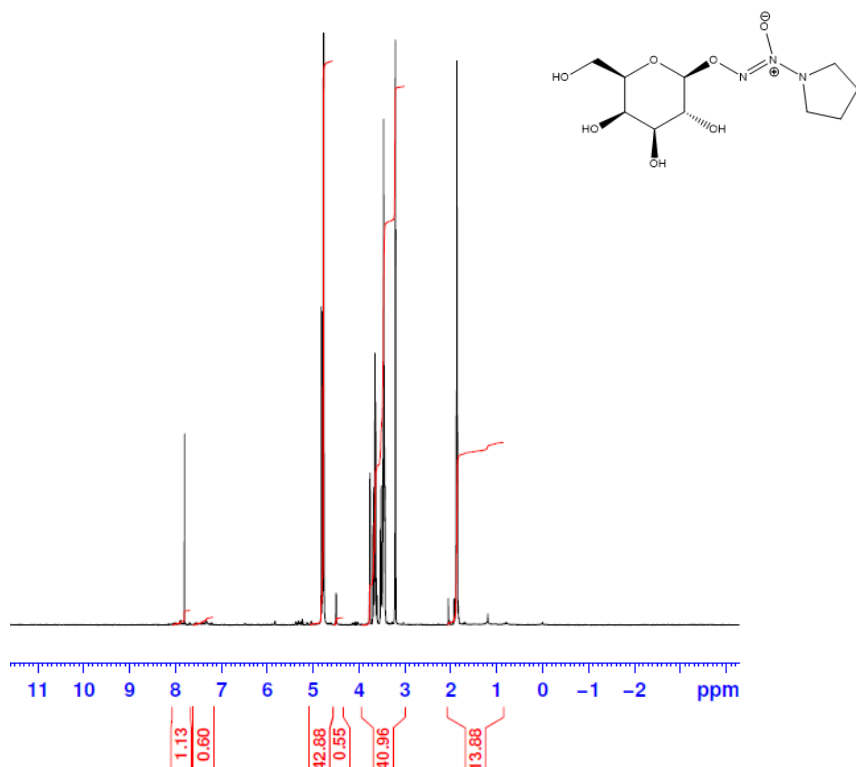


**Figure 17.** <sup>1</sup>H NMR spectrum of the end product.

Proton NMR spectra were produced by BrukerAvance III HDX 400 spectrometer at 400.16 MHz. <sup>1</sup>H NMR (400 MHz, CD<sub>3</sub>OD):  $\delta$  7.88 (s, 1H), 4.83–4.77 (m, 4H), 4.50 (dd, 2H), 3.77–3.47 (m, 4H), 3.22 (s, 2H), 2.06–1.93 (m, 4H). The <sup>1</sup>H NMR was collected with help from the NMR facility (Institute of Organic Chemistry, University of Tübingen) and the Stafforst Laboratory (Interfaculty Institute of Biochemistry, University of Tübingen).

## Results

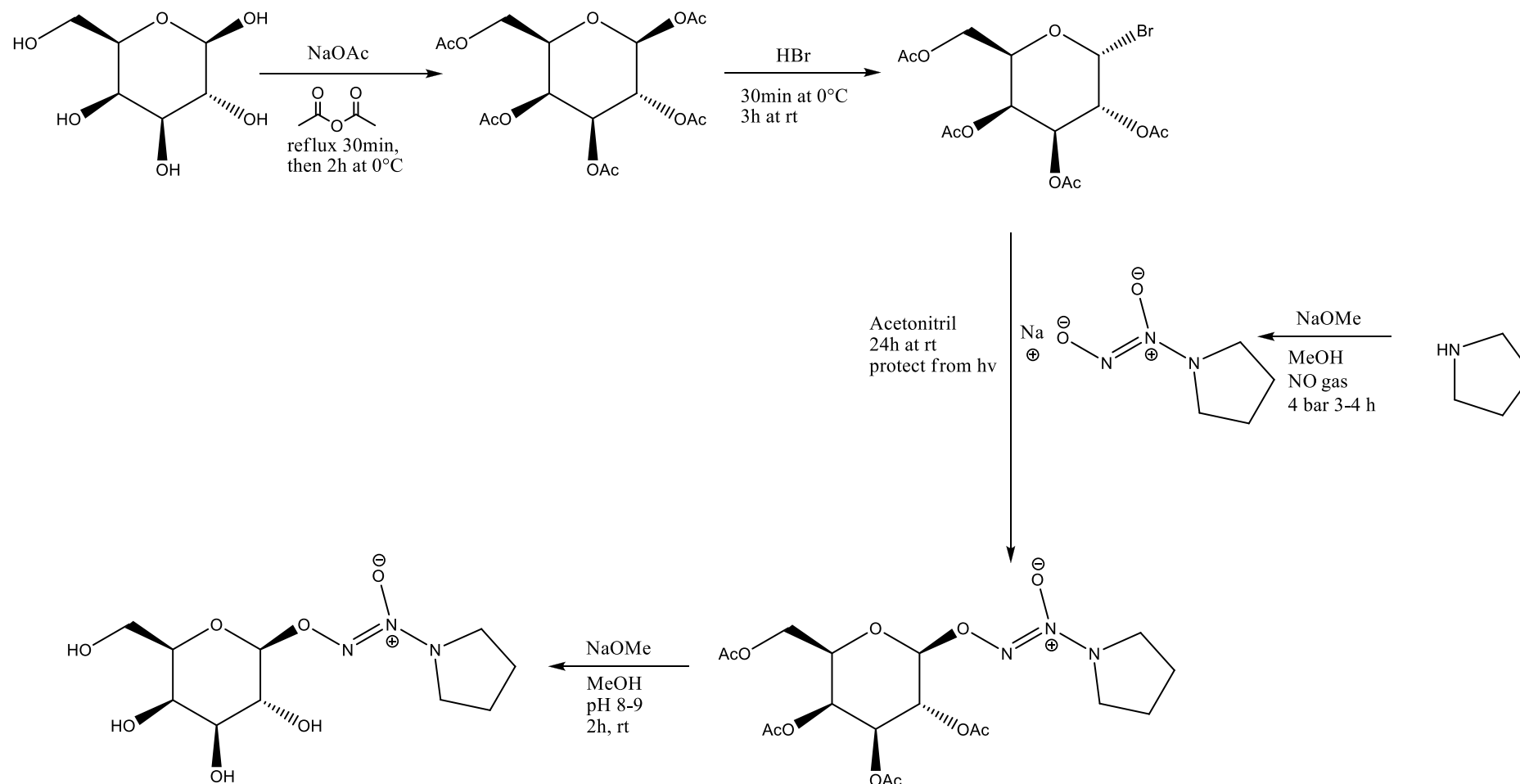


**Figure 18. Synthesis of  $\beta$ -gal-NONOate.**

The synthesis was completed in five reaction steps.  $\beta$ -galactose was protected via acetylation. Then HBr was used to prime the sugar for  $S_N2$  addition of the NONOate salt. In a separate reaction, pyrrolidine was mixed with sodium methoxide and NO gas under high pressure (4 bar) to produce the NONOate salt. The NONOate was then combined with the brominated galactose in a coupling reaction. The acetylated  $\beta$ -gal-NONOate was deprotected to yield the final product. The  $\beta$ -gal-NONOate compound was synthesized with help from the lab of Prof. Dr. Stafforst (Interfaculty Institute of Biochemistry, University of

## Results

---

Tübingen), Anne Stroppel (Interfaculty Institute of Biochemistry, University of Tübingen), the lab of Prof. Dr. Ziegler (Institute of Organic Chemistry, University of Tübingen) and Gregor Lemanski (Institute of Organic Chemistry, University of Tübingen).

### 3.2.2. Real-time cGMP imaging in VSMCs with $\beta$ -gal-NONOate

We then wanted to determine if our synthesized  $\beta$ -gal-NONOate could elevate cGMP in biological models. For this, VSMCs were isolated from 8-12-week-old R26-cGi500-L1 mice (**Figures 19A and 20A**), which express the cGi500 sensor ubiquitously. The VSMCs fluoresce green because of the expressed cGMP sensor protein (**Figures 19A and 20A**, green fluorescence). It is important to note that the green fluorescence is the YFP emission of the sensor and not the cGMP concentration, which is reflected by the CFP/YFP emission ratio. To achieve expression of  $\beta$ -galactosidase, VSMCs were transfected with the  $\beta$ -galactosidase encoding plasmid pFRT $\beta$ -gal and then stained with x-gal, where  $\beta$ -galactosidase positive VSMCs appear dark blue (**Figure 19B**). Other VSMCs were not transfected and used as a negative control (**Figure 20B**). To determine if  $\beta$ -gal-NONOate can reliably induce an elevation of cGMP in  $\beta$ -galactosidase expressing VSMC cultures, the cells were exposed to  $\beta$ -gal-NONOate (50  $\mu$ M) and the positive control DEA/NO (100  $\mu$ M) during continuous superfusion (**Figures 19C-E**). The addition of  $\beta$ -gal-NONOate resulted in an elevation in cGMP levels in  $\approx$ 62% of VSMCs and the addition of the positive control DEA/NO resulted in a response in all VSMCs (**Figures 19C-E**). Some VSMCs displayed a strong elevation in cGMP upon the addition of  $\beta$ -gal-NONOate (**Figure 19C**), others showed weak cGMP elevation upon the addition of  $\beta$ -gal-NONOate (**Figure 19D**), while another subset of VSMCs revealed no cGMP elevation upon the addition of  $\beta$ -gal-NONOate (**Figure 19E**). Control cells (no  $\beta$ -galactosidase expression) were exposed to  $\beta$ -gal-NONOate (50  $\mu$ M, 100  $\mu$ M) and the positive control DEA/NO (100  $\mu$ M) during continuous superfusion (**Figures 20C and D**). The addition of  $\beta$ -gal-NONOate did not elevate cGMP levels, whereas the positive control DEA/NO did (**Figures 20C and D**). Some VSMCs displayed a strong elevation in cGMP upon the addition of DEA/NO (**Figure 20C**), while others showed weak cGMP elevation upon the addition of DEA/NO (**Figure 20D**). These data demonstrate that  $\beta$ -gal-NONOate induces cGMP synthesis only in  $\beta$ -galactosidase expressing cultures and does not spontaneously release NO. Therefore,  $\beta$ -gal-NONOate appeared to be a suitable tool for cell-type targeted NO generation and intracellular cGMP elevation. To further investigate this, we next tested  $\beta$ -gal-NONOate in acute cerebellar brain slices.

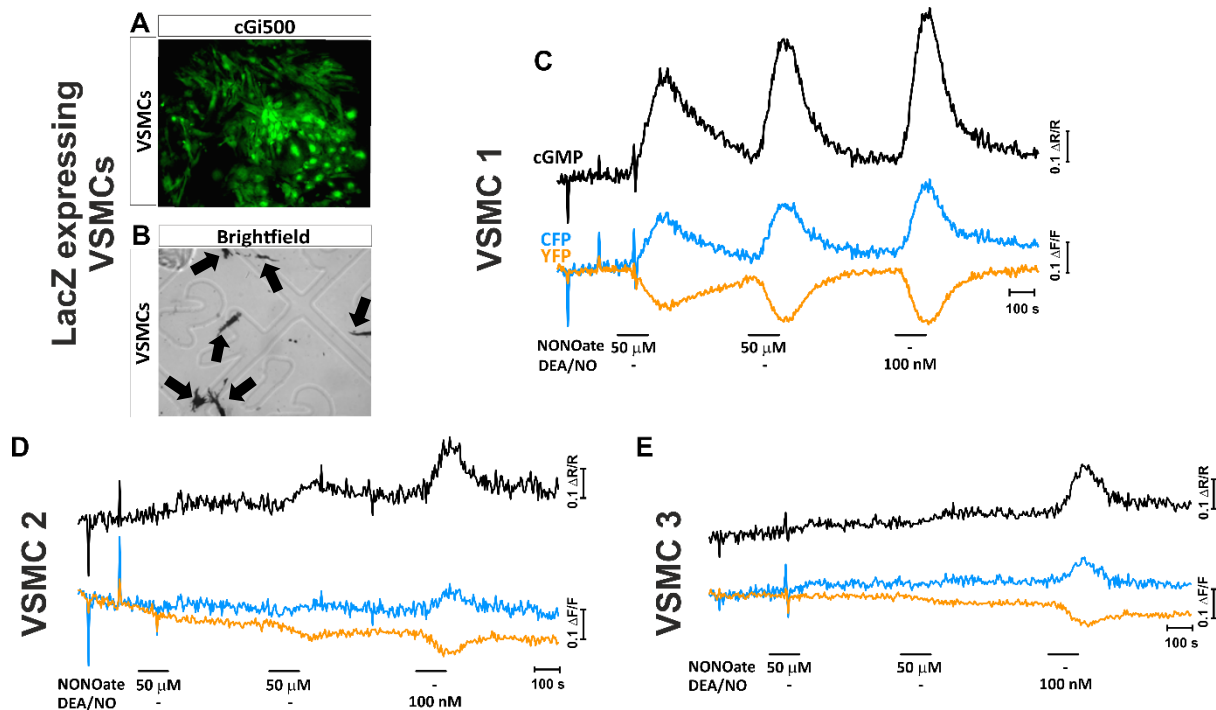


**Figure 19.  $\beta$ -gal-NONOate elevates cGMP in VSMC cultures expressing  $\beta$ -galactosidase.**

(A) VSMCs isolated from 8-12-week-old R26-cGi500-L1 mice expressing the cGi500 sensor (green) were transfected with the  $\beta$ -galactosidase encoding plasmid pFRT $\beta$ -gal. The green color represents the YFP fluorescence of cGi500. (B) A bright field view of the same VSMCs to show the  $\beta$ -galactosidase positive cells ( $\approx 7\%$ ) that are indicated with black arrows. (C-E) VSMCs expressing  $\beta$ -galactosidase were exposed twice to  $\beta$ -gal-NONOate (NONOate) ( $50 \mu\text{M}$ ) during continuous superfusion. DEA/NO ( $100 \text{ nM}$ ) was applied as a positive control. Black, cyan, and orange traces represent CFP/YFP ratio, CFP emission, and YFP emission, respectively. Scale bars represent the change in fluorescence of the single fluorophores CFP or YFP ( $\Delta F/F$ ) or their ratio (CFP/YFP;  $\Delta R/R$  reflecting  $[\text{cGMP}]_i$ ). (C) VSMC 1 is a representative cell that showed a strong cGMP elevation upon  $\beta$ -gal-NONOate addition. cGMP was elevated upon exposure to DEA/NO (VSMC 1,  $n = 15/74$  cells, measured on three coverslips obtained from one culture). (D) VSMC 2 is a representative cell that showed weak cGMP elevation upon  $\beta$ -gal-NONOate addition. cGMP was elevated upon exposure to DEA/NO (VSMC 2,  $n = 31/74$  cells, measured on three coverslips obtained from one culture). (E) VSMC 3 is a representative cell that did not show cGMP elevation upon  $\beta$ -gal-NONOate addition. cGMP was elevated upon exposure to DEA/NO (VSMC 3,  $n = 28/74$  cells, measured on three coverslips obtained from one culture).

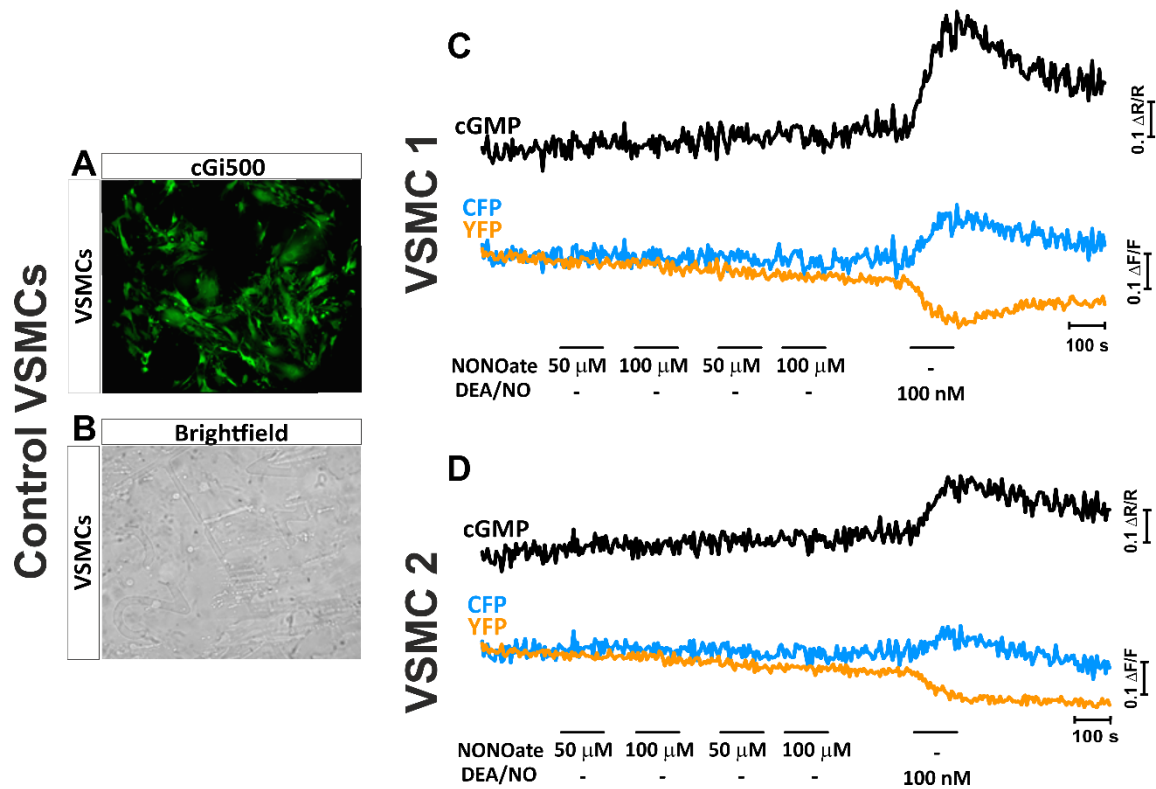


**Figure 20.  $\beta$ -gal-NONOate does not elevate cGMP in VSMC cultures lacking  $\beta$ -galactosidase.**

(A) VSMCs isolated from 8-12-week-old R26-cGi500-L1 mice expressing the cGi500 sensor (green). The green color represents the YFP fluorescence of cGi500. (B) A bright field view of the same VSMCs to show the absence of lacZ positive cells. (C, D) VSMCs were exposed to  $\beta$ -gal-NONOate (NONOate) (50  $\mu$ M, 100  $\mu$ M) during continuous superfusion. DEA/NO (100 nM) was applied at the end as a positive control. Black, cyan, and orange traces represent CFP/YFP ratio, CFP emission, and YFP emission, respectively. Scale bars represent the change in fluorescence of the single fluorophores CFP or YFP ( $\Delta F/F$ ) or their ratio (CFP/YFP;  $\Delta R/R$  reflecting [cGMP]). (C) VSMC 1 is a representative cell that showed no cGMP elevation upon the addition NONOate and a strong cGMP elevation in response to DEA/NO ( $n = 61/93$  cells, measured on two coverslips obtained from one culture). (D) VSMC 2 is a representative cell that showed no cGMP elevation upon the addition NONOate and a weak cGMP elevation in response to DEA/NO ( $n = 32/93$  cells, measured on two coverslips obtained from one culture).

### 3.2.3. Real-time cGMP imaging in Purkinje cells in acute cerebellar slices with $\beta$ -gal-NONOate

After demonstrating the efficacy of  $\beta$ -gal-NONOate to elevate cGMP in cell culture, we wanted to test it in tissue slices. To this end, we measured cGMP in Purkinje cells in acute cerebellar slices prepared from mice with the lacZ gene and cGi500 sensor expression under the control of a Purkinje cell specific promoter (L7-Cre (tg/+) x R26-lacZ (L2/lacZ) x R26-cGi500-L2 (L2/lacZ)), where '+' denotes the wild-type allele, 'tg' denotes the transgene. (Figure 21A). Control mice expressed only the cGi500 sensor

under the control of a Purkinje cell specific promoter without lacZ (L7-Cre (tg/+) x R26-lacZ (+/L2) x R26-cGi500-L2 (+/L2)) (**Figure 21D**). The presence and absence of  $\beta$ -galactosidase expression was confirmed by x-gal staining (**Figures 21B and E**).  $\beta$ -gal-NONOate was applied to acute cerebellar slices via superfusion to determine if the compound is able to release NO and induce an elevation of cGMP in Purkinje cells. Indeed, mice expressing the cGi500 sensor and lacZ in Purkinje cells showed an elevation of cGMP upon the addition of  $\beta$ -gal-NONOate (25  $\mu$ M) or the positive control, DEA/NO (5  $\mu$ M) (**Figure 21C**). No increase in cGMP was observed in mice expressing the cGi500 sensor without lacZ in Purkinje cells upon the addition of  $\beta$ -gal-NONOate (5  $\mu$ M), but the positive control DEA/NO (5  $\mu$ M) did increase cGMP as expected (**Figure 21F**). These data supported the ability of  $\beta$ -gal-NONOate to release NO in a lacZ-controlled manner in specific cell types of acute tissue slices. However, the question remained if  $\beta$ -gal-NONOate was able to influence downstream cGMP effectors. To investigate this, we injected mice with  $\beta$ -gal-NONOate and then investigated phosphorylation of the downstream molecule VASP via Western blot analysis.

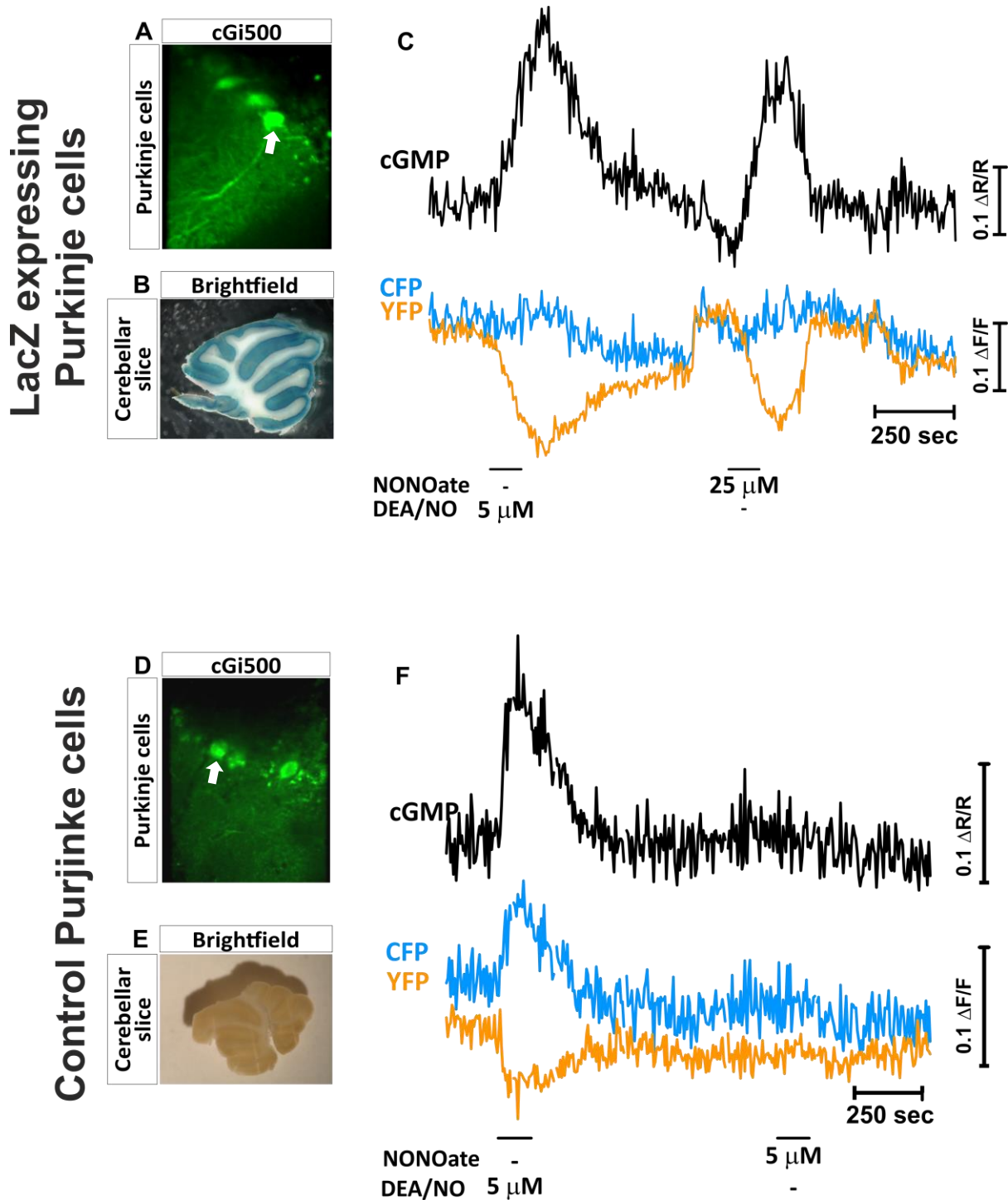


**Figure 21.  $\beta$ -gal-NONOate elevates cGMP in Purkinje cells in the presence of  $\beta$ -galactosidase.**

(A) Acute cerebellar slices isolated from 2-8-month-old (L7-Cre (tg/+)  $\times$  lacZ (lacZ/L2)  $\times$  R26-cGi500-L2 (lacZ/L2)) mice expressing lacZ and the cGi500 sensor only in Purkinje cells (green). The green color represents the YFP fluorescence of cGi500. The white arrow shows the cell that is depicted in Figure 21C. (B) A bright field view of x-gal stained cerebellar slice to show the  $\beta$ -galactosidase positive cells. The Purkinje layer is clearly positive. (C) Acute cerebellar slices expressing the cGi500 sensor and  $\beta$ -galactosidase only in Purkinje cells were exposed to DEA/NO (5  $\mu$ M) as a positive control and to  $\beta$ -gal-NONOate (NONOate) (25  $\mu$ M) during continuous superfusion. Black, cyan, and orange traces represent CFP/YFP ratio, CFP

emission, and YFP emission, respectively. Scale bars represent the change in fluorescence of the single fluorophores CFP or YFP ( $\Delta F/F$ ) or their ratio (CFP/YFP;  $\Delta R/R$  reflecting [cGMP]<sub>i</sub>). The signals are from a single representative cell indicated in panel A (n = 9 cells, measured in three acute cerebellar slices obtained from three independent mice). (D) Acute cerebellar slices isolated from 2-8-month-old (L7-Cre (tg/+) x lacZ (+/L2) x R26-cGi500-L2 (+/L2)) mice expressing the cGi500 sensor only in Purkinje cells (green) without lacZ expression. The green color represents the YFP fluorescence of cGi500. The white arrow shows the cell that is depicted in Figure 21F. (E) A bright field view of x-gal stained cerebellar slice to show the absence of lacZ positive cells. (F) Acute cerebellar slices expressing the cGi500 sensor only in Purkinje cells were exposed to DEA/NO (5  $\mu$ M) as a positive control and to  $\beta$ -gal-NONOate (NONOate) (5  $\mu$ M) during continuous superfusion. Black, cyan, and orange traces represent CFP/YFP ratio, CFP emission, and YFP emission, respectively. Scale bars represent the change in fluorescence of the single fluorophores CFP or YFP ( $\Delta F/F$ ) or their ratio (CFP/YFP;  $\Delta R/R$  reflecting [cGMP]<sub>i</sub>). The signals are from a single representative cell indicated in panel D (n = four cells, measured in one acute cerebellar slice obtained from one mouse).

### 3.2.4. $\beta$ -gal-NONOate-induced VASP phosphorylation in vivo

After demonstrating the efficacy of  $\beta$ -gal-NONOate in cell culture and tissue slices, we wanted to test it in the in vivo situation. Mice expressing  $\beta$ -galactosidase specifically in smooth muscle cells (SM-CreER<sup>T2</sup> (tg/+) x R26-lacZ (+/lacZ) x ApoE (+/-)) and control mice without  $\beta$ -galactosidase expression (SM-CreER<sup>T2</sup> (tg/+) x R26-lacZ (+/+) x ApoE (+/-)) were injected with  $\beta$ -gal-NONOate to determine if the compound induces VASP-phosphorylation via NO release and cGMP elevation as investigated via Western blot. VASP phosphorylation can be visualized via Western blot by using an antibody that detects both unphosphorylated and phosphorylated VASP, which migrate at 46 kDa and 50 kDa, respectively [156]. VASP-phosphorylation is used as a measurement of cAK or cGK activity and thus indirectly cGMP or cAMP levels.

Mouse 1, 3, and 4 were anesthetized and injected with  $\beta$ -gal-NONOate (50  $\mu$ L, 3.5 mM) via tail vein injection, which should result in blood concentration of about 100  $\mu$ M assuming 2 mL of blood volume for the mouse. Mouse 2 was anesthetized and injected with saline solution (50  $\mu$ L) via tail vein injection. After 20 min, the organs (bladder, colon, aorta, lung, skeletal muscle, heart) were isolated and placed into x-gal staining solution to determine  $\beta$ -galactosidase expression (**Figure 22**) or lysis buffer for protein isolation and subsequent detection of VASP-phosphorylation by Western blotting (**Figure 23**). Mice expressing  $\beta$ -galactosidase (Mouse 1 and 3;

**Figures 22 and 23**) revealed increased VASP-phosphorylation in tissues with smooth muscle cells (bladder, colon, aorta, and lung) compared to control tissues lacking smooth muscle cells (skeletal muscle and heart) and control mice completely lacking  $\beta$ -galactosidase (Mouse 2 and 4; **Figures 22 and 23**). Mouse 1 and 3 (SM-CreER<sup>T2</sup> (tg/+) x R26-lacZ (+/lacZ) x ApoE (+/-)) show x-gal positive staining in the bladder and colon and negative x-gal staining in the skeletal muscle and heart (**Figures 22A and C**). Mouse 1 showed some weak positive x-gal staining in the lung and no visible x-gal staining in the aorta (**Figures 22A**). Mouse 3 showed no visible x-gal staining in the aorta and lung (**Figures 22C**). Mouse 2 (C57BL/6) and mouse 4 (SM-CreER<sup>T2</sup> (tg/+) x R26-lacZ (++) x ApoE (+/-)) were x-gal negative in all tissues, as expected (**Figures 22B and D**). Phosphorylated VASP is visible in the Western blot as the upper band at 50 kDa and unphosphorylated VASP is visible at 46 kDa. Mouse 1 was injected with  $\beta$ -gal-NONOate and showed phosphorylated VASP in the lung and colon, it was difficult to detect and evaluate VASP phosphorylation due to low protein concentrations in the aorta and bladder, there was no visible VASP in the skeletal muscle and heart (**Figure 23A left**). Mouse 2 was injected with saline and served as a negative control and shows no to low levels of phosphorylated VASP, as expected (**Figure 23A right**). Mouse 3 was injected with  $\beta$ -gal-NONOate and showed increased phosphorylated VASP in the lung and colon, it was difficult to detect and evaluate VASP phosphorylation due to low protein concentrations in the aorta and bladder, there was no visible VASP in the skeletal muscle and heart (**Figure 23B left**). Mouse 4 was injected with saline and served as a negative control and shows no to low levels of phosphorylated VASP as expected (**Figure 23B right**). **Note:** the ApoE gene is not interesting for this experiment and should not influence the results. The mice available at the time all were heterozygous knock-outs for ApoE. After collecting some positive indications that  $\beta$ -gal-NONOate can indeed induce VASP phosphorylation, we aimed to determine if  $\beta$ -gal-NONOate can induce vasodilation in mice in vivo.

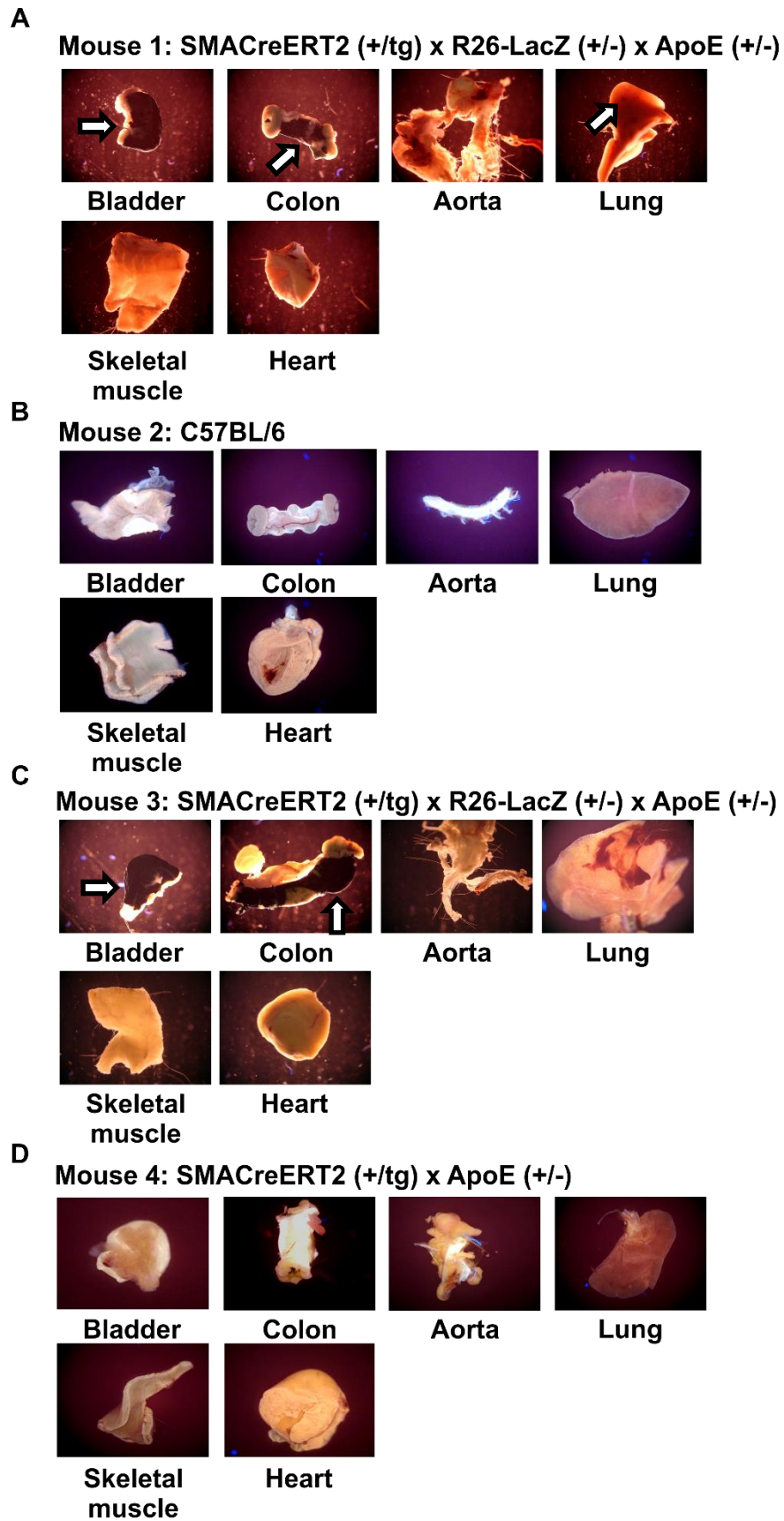


Figure 22. X-gal staining of isolated tissues from SM-CreER<sup>T2</sup> mice and controls.

(A) Mouse 1 (SM-CreER<sup>T2</sup> (tg/+) x R26-lacZ (+/lacZ) x ApoE (+/-)) was treated at 12-weeks-old

## Results

---

with 1 mg of tamoxifen once a day for five days via intraperitoneal injection. Mouse 1 showed positive x-gal staining in the bladder and colon, weak positive staining in the lungs, and no obvious x-gal staining in the aorta, skeletal muscle, and heart. Positive x-gal staining is shown with the white arrows. **(B)** Mouse 2 (C57BL/6; Wild type) was x-gal negative for all tissues. **(C)** Mouse 3 (SM-CreER<sup>T2</sup> (tg/+) x R26-lacZ (+/lacZ) x ApoE (+/-)) was treated at 12-weeks-old with 1 mg of tamoxifen once a day for five days via intraperitoneal injection. Mouse 3 showed positive x-gal staining in the bladder and colon and no obvious x-gal staining in the aorta, lung, skeletal muscle and heart. Positive x-gal staining is shown with the white arrows. **(D)** Mouse 4 (SM-CreER<sup>T2</sup> (tg/+) x R26-lacZ (+/+)) x ApoE (+/-)) was treated at 12-weeks-old with 1 mg of tamoxifen once a day for five days via intraperitoneal injection. Mouse 4 was x-gal negative for all tissues. All x-gal stainings were performed immediately after tissue isolation overnight.  $\beta$ -gal-NONoate was injected when mice 1, 3, and 4 were 15-weeks old and mouse 2 was 14-weeks old.

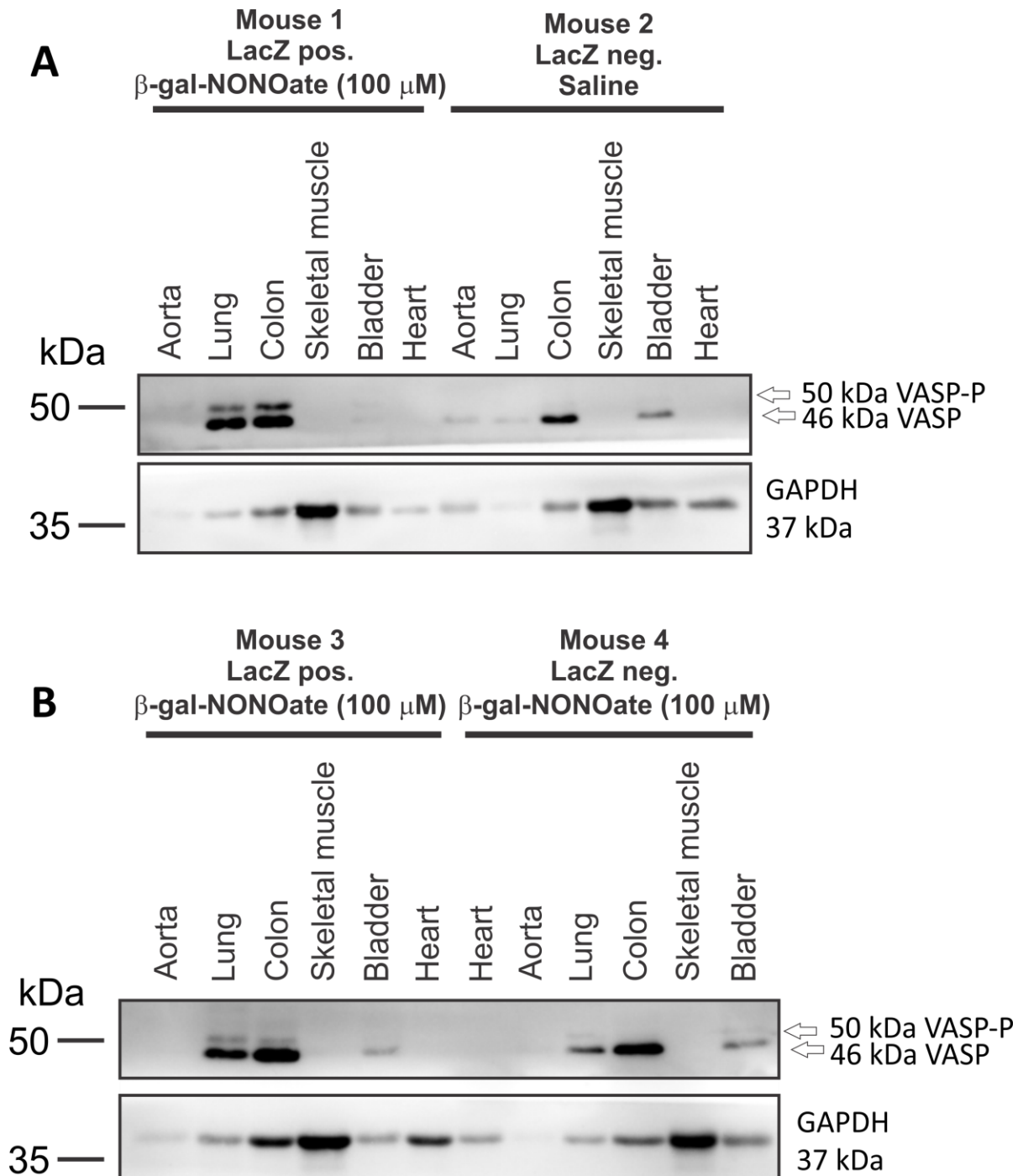


**Figure 23.  $\beta$ -gal-NONOate-induced VASP phosphorylation.**

(A)  $\beta$ -gal-NONOate was injected via the tail vein into a mouse expressing  $\beta$ -galactosidase in cells under the control of the smooth muscle-specific SM22 promoter (SM-CreER<sup>T2</sup> (tg/+) x R26-lacZ (+/lacZ) x ApoE (+/-)). Saline was injected into a control mouse, mouse 2 (Wild type; C57BL/6). Tissue lysates from aorta (5  $\mu$ g), lung (20  $\mu$ g), colon (20  $\mu$ g), skeletal muscle (20  $\mu$ g), bladder (10  $\mu$ g), and heart (20  $\mu$ g) were stained with a VASP antibody where phosphorylated VASP (VASP-P, 50 kDa) and unphosphorylated VASP (VASP, 46 kDa) bands are shown with white arrows. GAPDH was used as a loading control. (B)  $\beta$ -gal-NONOate was injected via the tail vein into a mouse expressing  $\beta$ -galactosidase, mouse 3 (SM-CreER<sup>T2</sup> (tg/+) x R26-lacZ (+/lacZ) x ApoE (+/-)) and a control mouse, mouse 4 (SM-CreER<sup>T2</sup> (tg/+) x R26-lacZ (+/+) x ApoE (+/-)). Tissue lysates from aorta (5  $\mu$ g), lung (20  $\mu$ g), colon (20  $\mu$ g), skeletal muscle (20

$\mu\text{g}$ ), bladder (10  $\mu\text{g}$ ), and heart (20  $\mu\text{g}$ ) were stained with a VASP antibody where phosphorylated VASP (VASP-P, 50 kDa) and unphosphorylated VASP (VASP, 46 kDa) bands are shown with white arrows. GAPDH was used as a loading control. Mice 1, 3, and 4 were treated at 12-weeks-old with 1 mg of tamoxifen once a day for five days via intraperitoneal injection.  $\beta$ -gal-NONOate was injected when mice 1, 3, and 4 were 15-weeks old and mouse 2 was 14-weeks old. Organs were isolated 20 minutes after  $\beta$ -gal-NONOate injection. See section 2.15 for further information.

### 3.2.5. $\beta$ -gal-NONOate-induced vasodilation in the cerebral cortex

A window was surgically implanted above the cerebral cortex to allow for real-time imaging and parallel addition of substances to determine if  $\beta$ -gal-NONOate could induce vasodilation in vivo. To determine if  $\beta$ -gal-NONOate-generated NO can induce vasodilation in nearby vessels, real-time two-photon measurements of the cerebral vasculature were performed with mice expressing  $\beta$ -galactosidase under the control of a neuron specific promotor (Camk2 $\alpha$ -CreBAC (tg/+) x R26-lacZ (+/lacZ)) and control mice without  $\beta$ -galactosidase expression (Wnt1-Cre (tg/+) x R26-lacZ (+/+)). Indeed, vasodilation was observed upon the addition of  $\beta$ -gal-NONOate (50 mM, local injection  $\approx$  5  $\mu\text{L}$ , see section 2.7.2 for further information) in mice expressing  $\beta$ -galactosidase in neurons (**Figures 24D and E**), while no increase in vasodilation was observed upon the addition of  $\beta$ -gal-NONOate (50 mM, local injection  $\approx$  5  $\mu\text{L}$ , see section 2.7.2 for further information) in mice without  $\beta$ -galactosidase expression (**Figures 24H and I**). The positive control DEA/NO (5 mM, local injection  $\approx$  5  $\mu\text{L}$ , see section 2.7.2 for further information) induced vasodilation independent of  $\beta$ -galactosidase expression (**Figures 24F,G,J,K**). These data support the hypothesis of neuronal NO as an effector in neurovascular coupling. The data here demonstrate  $\beta$ -galactosidase-controlled,  $\beta$ -gal-NONOate-induced neuronal NO generation, which diffuses to nearby vessels and causes a physiological response, namely vasodilation of the cortical arteries.

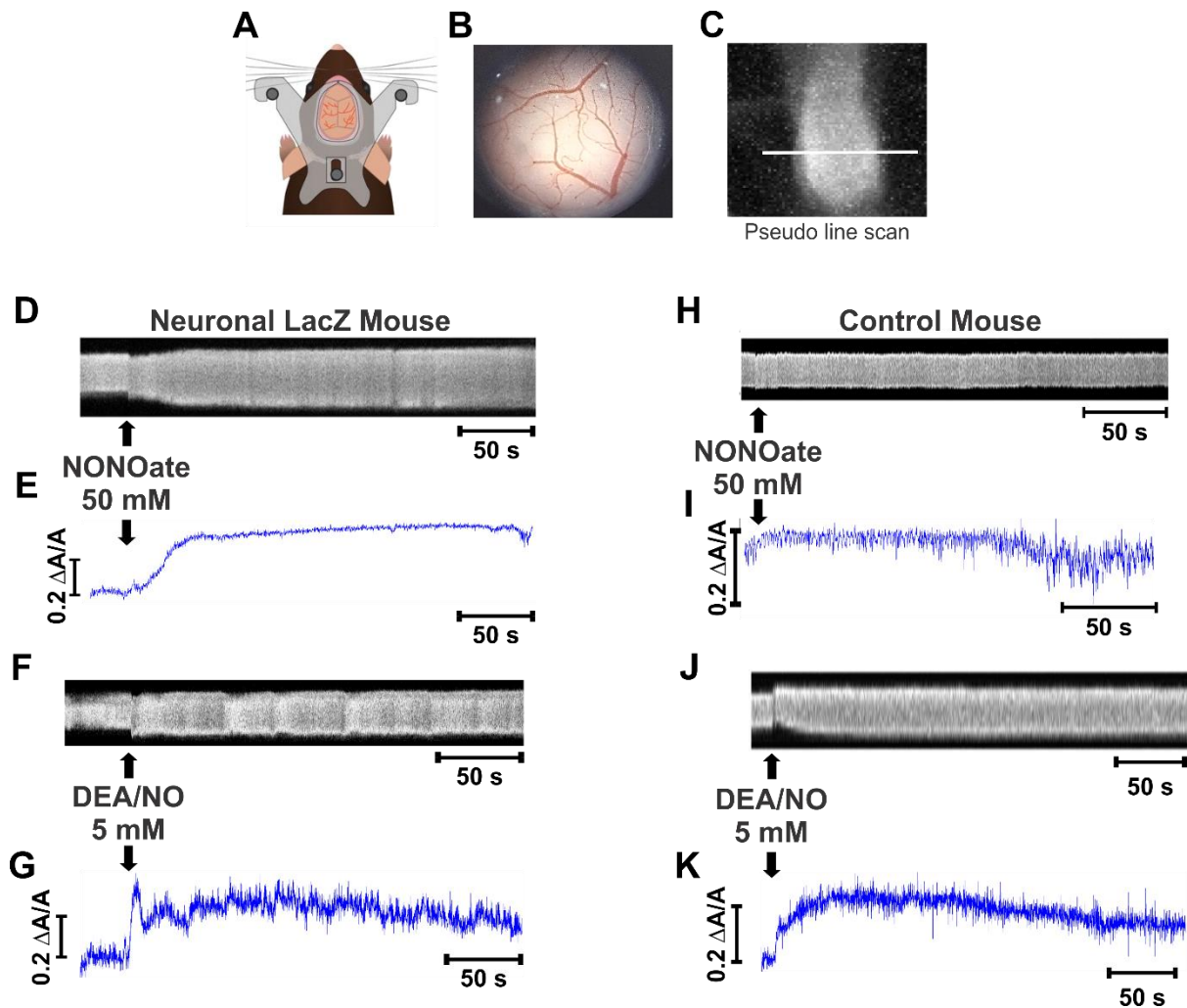


**Figure 24.  $\beta$ -gal-NONOate-induced vasodilation in the cerebral cortex.**

(A) A window was surgically implanted in the cerebral cortex to measure the neurovasculature in real-time. (B) An image of the prepared surgery allowing for imaging of the cortical neurovasculature. (C) A vessel analyzed with pseudo line scan to track the vessel diameter over time. (D) A mouse with neuronal-specific lacZ expression (*Camk2 $\alpha$ -CreBAC (tg/+)* x *R26-lacZ (+/lacZ)*) showed vasodilation upon the addition of  $\beta$ -gal-NONOate (50 mM local injection  $\approx 5 \mu\text{L}$ , see section 2.7.2 for further information). (E) Analysis of total vessel area for the same vessel in the same mouse (*Camk2 $\alpha$ -CreBAC (tg/+)* x *R26-lacZ (+/lacZ)*). Scale bars represent the change in vessel area ( $\Delta A/A$ ). The measurement is from a single representative vessel ( $n =$  three vessels, obtained from one mouse). (F) The same mouse (*Camk2 $\alpha$ -CreBAC (tg/+)* x *R26-lacZ (+/lacZ)*) showed vasodilation upon the addition of DEA/NO (5 mM, local injection  $\approx 5 \mu\text{L}$ , see section 2.7.2 for further information). (G) Analysis of total vessel area for the same vessel in the same mouse (*Camk2 $\alpha$ -CreBAC (tg/+)* x *R26-lacZ (+/lacZ)*). Scale bars represent the change in vessel area ( $\Delta A/A$ ). The measurement is from a single representative vessel ( $n =$  two vessels, obtained from one mouse). (H) A mouse with no lacZ expression (*Wnt1-Cre (tg/+)* x *R26-lacZ (+/+)*) showed no vasodilation upon the addition of  $\beta$ -gal-NONOate (50 mM, local injection  $\approx 5 \mu\text{L}$ , see section 2.7.2 for further information). (I) Analysis of total vessel area for the same vessel in the same mouse (*Wnt1-Cre (tg/+)* x *R26-lacZ (+/+)*). Scale bars represent the change in vessel area ( $\Delta A/A$ ). The measurement is from a single representative vessel ( $n =$  four vessels, obtained from one mouse). (J) The same mouse (*Wnt1-Cre (tg/+)* x *R26-lacZ (+/+)*) showed vasodilation upon the addition of DEA/NO (5 mM, local injection  $\approx 5 \mu\text{L}$ , see section 2.7.2 for further information). (K) Analysis of total vessel area for the same vessel in the same mouse (*Wnt1-Cre (tg/+)* x *R26-lacZ (+/+)*). Scale bars represent the change in vessel area ( $\Delta A/A$ ). The measurement is from a single representative vessel ( $n =$  four vessels, obtained from one mouse). All vessels were imaged with two-photon microscopy. For

## Results

---

further information see section 2.7. Martin Thunemann (Department of Neurosciences, University of California, San Diego) helped with the data collection and vessel area analysis.

## 4 Discussion

### 4.1. cGMP elevation in CGNs

The cGMP signaling cascade influences numerous physiological processes across the body, such as vasodilation [2], hormone secretion [5], neurotransmission [6], learning and memory [10,11], sensory axon bifurcation [7], among others. This thesis focuses on NO-cGMP signaling in nervous systems models and how to study the influence of NO signaling in a cell type specific manner. By combining the FRET-based cGMP sensor cGi500 and the fluorescent calcium indicator Fura-2AM, we were able to simultaneously measure cGMP and Ca<sup>2+</sup> signals in real-time. With this method we revealed a crosstalk between both signaling molecules in primary CGN cultures. Furthermore, we successfully synthesized the compound  $\beta$ -gal-NONOate and developed a strategy that allows us to generate NO in specific cell types to analyze NO signaling in a cell type specific manner.

#### 4.1.1. cGMP elevation in CGNs

Previous work has shown a relationship between cGMP and Ca<sup>2+</sup> signaling, specifically a dampening of Ca<sup>2+</sup> transients during cGMP elevation in VSMCs, platelets, dorsal root ganglion, olfactory bulb, endothelial cells, and other cell types [54,61,160-162]. Our aim was to investigate whether this crosstalk also exists in primary CGN cultures. CGNs are glutamatergic interneurons that provide an excitatory input to the molecular layer of the cerebellum. They constitute the largest neuronal population in the cerebellum and the largest homogeneous neuronal population in the entire brain [111]. CGNs serve as a model to investigate neuronal signal transduction in various labs across the world [111]. CGNs have been shown to express Ca<sup>2+</sup>-permeable NMDA receptors for glutamate [111,163,164], which are essential for neuronal survival, and previous research has reported that upon NMDA receptor stimulation, NOS is activated leading to NO synthesis [164,165]. In this work, NO-cGMP signal transduction in CGNs, as investigated via simultaneous imaging of cGMP and Ca<sup>2+</sup>, revealed cGK-independent cGMP/Ca<sup>2+</sup> crosstalk in primary CGNs.

The CGNs showed robust elevation of cGMP upon exposure to DEA/NO, but not during application of ANP or CNP (**Figures 10A and B**). These results indicated

that the cGMP synthesizing enzyme NO-GC is present in primary CGN cultures, while pGCs stimulated by ANP or CNP (GC-A and GC-B) are not. The failure to detect ANP- or CNP-induced cGMP increases (**Figure 10B**) could have been related to technical issues, such as an inability of the cytosolic cGi500 sensor to detect presumably membrane-associated cGMP pools that are generated in response to natriuretic peptides. However, this possibility is highly unlikely, because the cytosolic cGi500 sensor has been successfully used to detect ANP- and CNP-induced cGMP signals in various other cell types including smooth muscle cells [122] and dorsal root ganglion neurons [155]. The concentration-response curve revealed an EC<sub>50</sub> of 32 nM for primary CGNs (**Figure 10C**) and a DEA/NO concentration of 100 nM was used for further experiments to ensure a cGMP response in the CGNs.

To verify that our cultured cells were indeed neurons, cells were stained for the neuronal marker  $\beta$ III-tubulin (**Figure 10D**). Over 95% of cells (detected by nuclear staining with Hoechst dye) were positive for  $\beta$ III-tubulin indicating a nearly pure neuronal cell culture. Since there is no widely accepted marker for CGNs, the general neuronal marker protein  $\beta$ III-tubulin was used to confirm neuronal identity. Furthermore, the cell's morphology (small size  $\approx$ 5-10  $\mu$ m, with about four axonal extensions) is in agreement with previously reported CGN cultures [111,113], making it highly likely that the cultured cells are indeed CGNs (**Figure 10D**).

We also measured DEA/NO-induced cGMP elevation in acute cerebellar slices (**Figure 11**). These results demonstrated the presence of NO-cGMP signaling in cerebellar cells are in line with previous work [113,166]. Recently published work has also employed the same cGMP imaging system in acute brain slices of cGMP sensor mice to demonstrate NO-induced cGMP elevations in the cerebellum, striatum and hippocampus [40]. In this approach, they also found robust NO-induced cGMP signals in the granule cell layer of the cerebellum [40], further supporting the presence of a NO-cGMP signaling cascade in CGNs in vivo.

#### 4.1.2. cGMP-Ca<sup>2+</sup> crosstalk in CGNs

With the knowledge that NO is able to induce a robust cGMP response in CGNs, we investigated a potential crosstalk between the NO-cGMP pathway and glutamate-induced Ca<sup>2+</sup> signaling via simultaneous imaging of cGMP and Ca<sup>2+</sup> in individual CGNs in primary cultures. As revealed with Fura-2AM and cGi500

measurements,  $\text{Ca}^{2+}$  transients in CGNs were induced by glutamate and cGMP generation via DEA/NO. A NO-cGMP-dependent augmentation of glutamate-induced  $\text{Ca}^{2+}$  transients in CGNs was observed during real-time simultaneous cGMP and  $\text{Ca}^{2+}$  imaging (**Figure 12**). Separate analysis of  $\text{Ca}^{2+}$  responses in the neuronal extensions (axons) and the cell soma (perikaryon) revealed no differences (data not shown). For this reason, data analysis focused on signaling in the soma due to the higher signal to noise ratio and greater overall analyzable area compared to the thin neuronal extensions.

The glutamate-induced  $\text{Ca}^{2+}$  elevations were likely mediated by the NMDA receptor [167], but we cannot absolutely exclude other types of glutamate receptors as sources of  $\text{Ca}^{2+}$  entry. It has been reported that upon activation of  $\text{Ca}^{2+}$ -permeable NMDA-type glutamate receptors in the brain nNOS is activated and NO synthesized, leading to cGMP generation through the activation of NO-GC [164,165]. However, in our FRET experiments we never observed a change in cGMP upon addition of glutamate (**Figures 12A and B**). One reason for that distinction might be that here the CGNs were only stimulated for a short duration (~10 s) in contrast to the other studies where CGNs had been exposed to NMDA agonists for minutes [164,165].

As mentioned previously, glutamate-induced  $\text{Ca}^{2+}$  transients were augmented by DEA/NO. However, given that NO can also induce effects independent of cGMP [98], it was important to clarify whether the observed NO-induced  $[\text{Ca}^{2+}]_i$  augmentation was indeed cGMP-dependent. For that reason, we analyzed CGNs from knockout mice lacking functional NO-GC. In line with our hypothesis, exposure of NO-GC KO CGNs to DEA/NO did not increase  $[\text{cGMP}]_i$  and did not augment glutamate-induced  $[\text{Ca}^{2+}]_i$  transients (**Figures 12C-E**). These results strongly supported the notion that NO augmentation of glutamate-induced  $\text{Ca}^{2+}$  responses in CGNs is cGMP dependent and specifically mediated via NO-GC.

#### 4.1.3. cGMP analogues to investigate cGMP- $\text{Ca}^{2+}$ crosstalk in CGNs

To further determine the importance of cGMP in the potentiation of glutamate-induced elevation of  $[\text{Ca}^{2+}]_i$ , we exposed CGNs to the membrane-permeable cGMP analogues 8-Br-cGMP and 8-pCPT-cGMP. Both analogues are able to activate cGMP downstream targets [168,169]. Indeed, both cGMP analogues enhanced glutamate-induced elevation of  $[\text{Ca}^{2+}]_i$  (**Figure 13**). These results support the notion that NO

potentiates glutamate-induced  $\text{Ca}^{2+}$  transients in murine CGNs via activation of NO-GC and synthesis of cGMP. Interestingly, a recent study reported that the slow alcohol-induced increase of  $[\text{Ca}^{2+}]_i$  in CGNs was suppressed by pre-incubation of the cells with 8-Br-cGMP [170]. This would suggest that activation of cGMP signaling in CGNs can both increase and decrease  $[\text{Ca}^{2+}]_i$  depending on the type of  $\text{Ca}^{2+}$  signal.

It has to be mentioned that in the experiments with 8-Br-cGMP, the peak height ratio of the 2<sup>nd</sup> over the 1<sup>st</sup>  $\text{Ca}^{2+}$  transient under control conditions (Tyrode, no cGMP stimulation) was  $\approx 1.6$  (**Figure 13A**). This value was higher than the control ratios obtained in the other experiments, which were  $\approx 0.8-1.0$  (**Figures 12C and F; Figure 13B**). The variability of control transients might be related to different growth states of different CGN cultures. However, it is important to note that control cells (treated with Tyrode) and experimental cells (treated with DEA/NO or cGMP analogues) were always measured side-by-side with the same batch of cells. Therefore, the variability in the control ratio between different CGN cultures is not a confounding factor in these experiments.

While 8-Br-cGMP and 8-pCPT-cGMP are commonly used to activate cGKs, it is important to note that these cGMP analogues also bind to and modulate the activity of other cGMP downstream targets such as PDEs and CNG channels [171,172]. Indeed, previous work has reported a slow increase in resting  $[\text{Ca}^{2+}]_i$  in Fura-2 loaded rat CGNs upon the addition of 8-Br-cGMP, suggesting the presence of functional CNG channels [115]. However, under our experimental conditions, resting  $[\text{Ca}^{2+}]_i$  was not affected by NO-induced endogenous cGMP (**Figure 12B**) or two cGMP analogues, 8-Br-cGMP and 8-pCPT-cGMP. Thus, it is unlikely that the augmentation of glutamate-induced  $[\text{Ca}^{2+}]_i$  by these cGMP analogues was related to activation of CNG channels. Also, while cultured rat CGNs have been documented to express hyperpolarization-activated cyclic nucleotide-gated channels as determined by mRNA analysis [114], these ion channels are principally activated by cAMP and not cGMP. For this reason, it is unlikely that they were directly influenced by our test compounds.

#### 4.1.4. The role of cGKs in cGMP- $\text{Ca}^{2+}$ crosstalk in CGNs

A possible cGMP downstream target influencing cGMP/ $\text{Ca}^{2+}$  crosstalk could be cGKI or cGKII. Previous work with genetically modified mice has demonstrated important roles of cGKI in the brain, from modulation of synaptic plasticity in

hippocampal neurons [173] and cerebellar Purkinje cells [100] to the regulation of sleep-wake activity [174]. Moreover as mentioned previously, cGKI mediates cGMP- $\text{Ca}^{2+}$  crosstalk, specifically by dampening of  $\text{Ca}^{2+}$  transients during cGMP elevation, in VSMCs, platelets, dorsal root ganglion, olfactory bulb, endothelial cells, and other cell types [54,61,160-162,175]. Since activation of cGKI in these cells has been reported to dampen  $\text{Ca}^{2+}$  transients [176-178], cGKI is likely not the effector of the NO-cGMP-mediated augmentation of  $[\text{Ca}^{2+}]_i$  observed in CGNs. Indeed, Western blot analysis did not detect cGKI protein expression in our primary mouse CGNs (**Figure 14**). More surprisingly, was that cGKII protein expression was also not found with Western blot analysis of our primary CGNs (**Figure 15**). These findings contrast with previous studies of the Torres lab where they reported cGKI mRNA and protein and cGKII mRNA in CGNs [113,179]. Moreover, these studies demonstrated a role of cGKI and cGKII in synaptic vesicle recycling in CGNs [166,180]. The discrepancy could be explained by methodological differences. For example, we did not analyze mRNA levels but rather used highly specific antibodies for cGKI and cGKII, which were validated with respective knockout tissues (**Figures 14 and 15**). Torres and colleagues used a different cGKI antibody, with presumably different specificity and sensitivity for Western blotting, and did not show data from the respective knockout control. They did not analyze cGKII expression at the protein level. Antibody quality has a large influence over conclusions and if this work has been conducted without proper antibody validation then we could have erroneously concluded cGKII expression in the CGN lysates (**Figure 15B**).

It is interesting to note that while we were not able to detect cGKI and cGKII in our CGN lysates, both proteins were readily detected in extracts of whole cerebellum (**Figures 14 and 15A**). This suggests that cell types other than CGNs express cGKI and/or cGKII in the cerebellum. Indeed, immunohistochemical staining of cerebellar sections showed strong expression of cGKI in cerebral vessels and Purkinje neurons, but no evidence for its expression in CGNs [57,100]. cGKII has been detected in low levels in Purkinje neurons and occasionally in the cerebellum's granular cell layer [181]. Another reason for discrepant results regarding the expression and functional relevance of cGKs and CNG channels could be that CGNs develop differential expression of these cGMP pathway components upon culturing over time. Indeed, the Torres lab has reported that both CNG channels and cGKs expression varies with

the number of days the CGNs have been in culture [113,115]. Another reason for the discrepancy between our results and the data obtained by the Torres lab might be the species used. Most of the previous studies of NO-cGMP signaling in CGNs as well those from the Torres lab were done in cells isolated from rats, while we prepared primary CGN cultures from mice. Our studies, as well as those by Torres et al., were performed with CGNs isolated from young (P7) mice or rats. In summary, differences in antibody selectivity and sensitivity, culture conditions/times as well as species differences might account for variances in protein expression observed in our studies and those by Torres and co-workers. Even with these discrepancies, it seems likely that cGKs have no role in the observed cGMP-dependent augmented  $\text{Ca}^{2+}$  transients in our CGN models. Since cGMP signaling in the brain appears to dramatically change with aging [182], one must be careful when extrapolating the findings to CGNs in the adult cerebellum.

#### **4.1.5. cGMP degradation in CGNs via PDEs**

cGMP degradation occurs via PDEs and many of the eleven PDE families have been reported in the CNS [69,79,80]. To our knowledge, the PDEs involved in cGMP degradation in CGNs have not been previously characterized. With our FRET-based cGi500 sensor it was possible to investigate the role of PDEs in cGMP degradation in primary CGNs in real time (**Figures 16A and B**). NO-induced cGMP levels were not affected by inhibitors of PDE1, 2, and 3, while they were strongly potentiated by Zaprinast, which inhibits PDE5, 6, 9, 10, and 11. PDE5 inhibition via sildenafil only resulted in a small cGMP increase (**Figure 16B**).

Previous work has proposed that  $\text{Ca}^{2+}$  entry might decrease NO donor-induced cGMP levels in CGNs via activation of  $\text{Ca}^{2+}$ /calmodulin-stimulated PDE1 [183], but we did not observe this (**Figures 13A and B**). Moreover, we did not detect functional PDE1 in our functional studies (**Figure 16B**). The presence of PDE1 could be masked by compensatory PDEs that are able to sufficiently degrade cGMP in CGNs even when PDE1 is rendered non-functional by a PDE inhibitor. For this reason, we cannot completely exclude the role of PDE1 as suggested by previous work [183]. Our findings are consistent with the reported expression of PDE9 in rat CGNs [184], but not PDE2, in CGNs of the human brain [185]. Previous research performed in rodents

and humans has suggested that PDE9, 10 and 11 play a role in neurological diseases. For example, PDE9 was shown to be involved in bipolar affective disorder [81], PDE10 in social interaction, schizophrenia, and bipolar disorder [82-84] and PDE11 in major depression [85]. However, neither PDE6 nor PDE11 are expressed in the cerebellum [69,79,186].

Since both NO-GCs and pGCs can generate cGMP, researchers have theorized that two separate pools of cellular cGMP exist. The NO-GC generated pool is believed to be more global, while the pGC-generated pool is thought to be localized to the membrane. For this reason, different PDEs might more readily influence one of the pools depending on their cellular localization. For example, PDE9 appears to be localized to the membrane and nuclear fractions of cerebellar tissue [187]. For this reason, PDE9 has been suggested to specifically regulate cGMP pools generated by pGCs, but not by cytosolic NO-GC in heart muscle cells [188]. Given this data, it could be that PDE9 regulates the local cGMP pool and because cGMP was only elevated in CGNs upon stimulation of NO-GC (the presumably global cGMP pool generator), PDE9 might not be the major actor of cGMP degradation in CGNs. Therefore, we propose that PDE5 and especially PDE10 are the most likely candidates that degrade NO-induced cGMP pools in murine CGNs. In the future, experiments with more specific PDE targeting molecules should be done (e.g. PDE10 inhibitor PQ-10 [189]). As stated previously, it is important to note that the application of specific PDE inhibitors (targeting only one PDE family) cannot exclude its existence in a given cell due to potential compensatory interactions of other cGMP-degrading PDEs that could effectively mask the single blocked PDE.

Analysis of the messenger RNA (mRNA) levels via quantitative polymerase chain reaction (qPCR) studies could reveal if other cGMP effectors are expressed in CGNs, but it is important to note that there is often a low correlation between cellular mRNA levels and actual protein expression, as determined by Western blot, which reduces the quality of qPCR data [190]. Excitingly, the data shown here are derived from real-time visualization of the cGMP signaling pathway in living cells and are a prime example of the need to investigate signaling pathways under dynamic conditions, such as in living cultures, tissues and animal models. This methodology contrasts with the majority of cGMP signaling research, which tends to investigate cGMP levels as an endpoint rather than the dynamic process that it clearly is.

#### 4.1.6. Outlook for cGMP signaling in CGNs

The above discussed data demonstrate the power of real-time, simultaneous imaging of cGMP and  $\text{Ca}^{2+}$  combined with traditional biochemical experiments. Here we identified the presence of a cGK-independent NO-cGMP signaling cascade that potentiates glutamate-induced  $\text{Ca}^{2+}$  transients in murine CGNs, and a Zaprinast-sensitive degradation of cGMP in these cells. Further research is required before the downstream cGMP target(s) is(are) identified. Inhibitor experiments during real-time imaging could help to elucidate further signaling components, for example ion channel inhibitors like MK-801 for NMDA receptors [191] or L-cis-diltiazem for CGN channels [192]. The findings reported here deepen our mechanistic understanding of NO-cGMP signaling in the CNS (**Figure 25**). The cGMP- $\text{Ca}^{2+}$  crosstalk reported here likely influences neurotransmitter-stimulated functions of CGNs and perhaps other neuronal cell types and might be targeted by cGMP-modulating medications to treat neurological disorders.

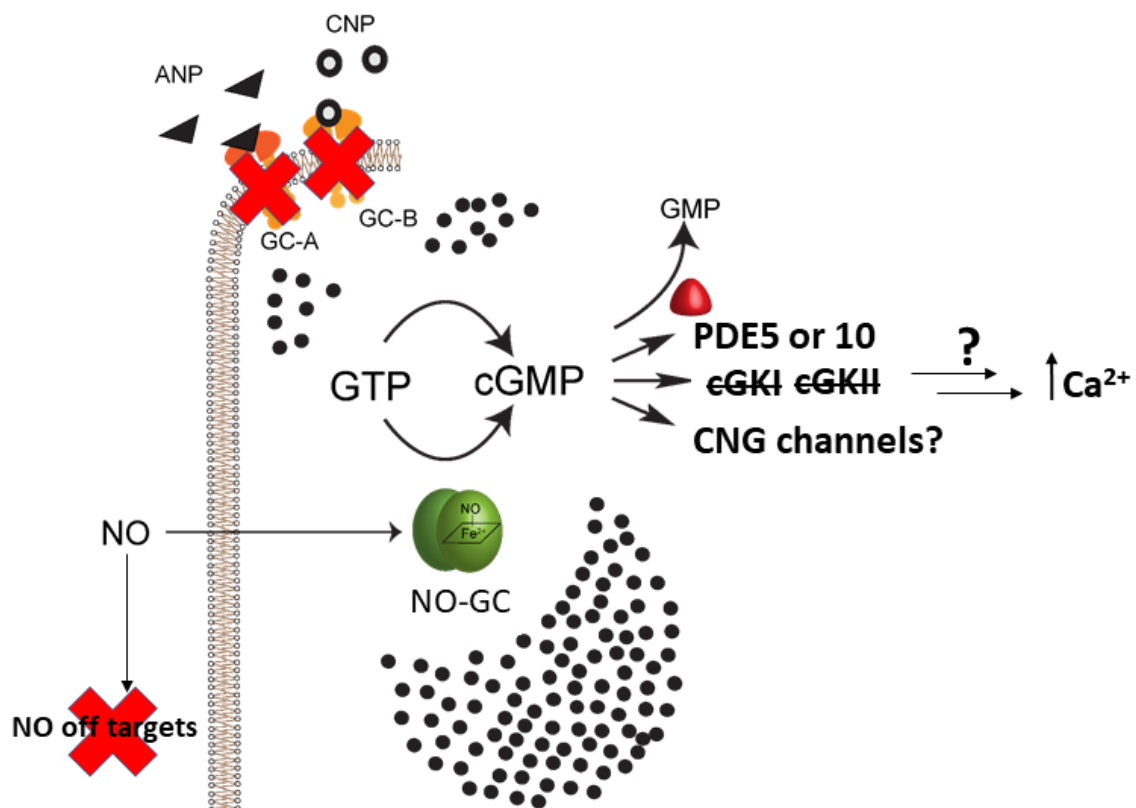


**Figure 25. Summary and outlook of the CGN findings.**

In CGNs, both ANP and CNP do not elevate cGMP levels in CGNs indicating that GC-A and GC-B are not expressed in CGNs (red crosses). Conversely, NO does activate NO-GCs resulting in conversion of GTP into cGMP. The observed cGMP/ $\text{Ca}^{2+}$  crosstalk is not a result of NO off targets (red cross), but

is rather cGMP-dependent. Said crosstalk is not modulated by cGKI or cGKII because neither were detected in our CGN cultures (both are crossed out). cGMP is most likely degraded to GMP by PDE5 or 10 in CGNs. Although CNG channels appear unlikely to mediate the observed cGMP/Ca<sup>2+</sup> crosstalk, their potential role should be investigated with real-time imaging and pharmacological tools. The cGMP-effector protein(s) that mediates the observed cGMP/Ca<sup>2+</sup> crosstalk has yet to be identified (two arrows with a question mark).

Furthermore, several imaging-based studies have identified important functions of cGMP, cAMP, and Ca<sup>2+</sup> in neuronal cells and, interestingly, complex relationships between the spatiotemporal dynamics of these signaling molecules. For instance, reciprocal regulation of cAMP and cGMP regulates axon/dendrite formation in hippocampal neurons [193]. In that study, FRET imaging showed that alterations in the amount of cAMP resulted in inversely proportional changes in the amount of cGMP, and vice versa, through the activation of PDEs and protein kinases. Another study showed that the NO-cGMP pathway inhibits transient cAMP signals through the activation of PDE2 in striatal neurons [74,194]. Recently, an interplay among cGMP, cAMP, and Ca<sup>2+</sup> was reported in olfactory sensory neurons [195] and dorsal root ganglion neurons [196,197] as well as a correlation of this signaling crosstalk with axonal pathfinding and neurotransmitter release. For these reasons, we postulate that the identified cGMP-Ca<sup>2+</sup> crosstalk in CGNs also involves cAMP. In the future, it will be interesting to monitor cGMP/cAMP and cAMP/Ca<sup>2+</sup> simultaneously in individual CGNs with the use of spectrally compatible fluorescent indicators that are currently under development. With such experiments, one could test the hypothesis that NO-cGMP signaling modulates cAMP levels, presumably via regulation of cAMP-degrading PDEs, and that cAMP in turn regulates glutamate-induced Ca<sup>2+</sup> transients in CGNs.

### **4.2. Cell type specific generation of NO with $\beta$ -gal-NONOate**

The results from the CGN experiments demonstrated the power of the tools that exist to investigate the role of signaling molecules in individual cells in culture. However, while it is relatively easy to prepare a pure cell culture with a specific cell type to investigate signaling cascades, it is more difficult to investigate said signaling cascades in specific cells in tissues or living animals. The cell type specific generation of NO is a possible solution to investigate the role of NO-cGMP in a more defined manner. The data reported in this thesis describe such a new method enabling cell-specific NO generation and subsequent cGMP elevation.

To our knowledge, this is the first report of cell type specific NO generation. We have developed this strategy by employing  $\beta$ -gal-NONOate. The closest experiments to those reported here involved the combination of  $\beta$ -gal-NONOate with implantable biomaterials to generate local NO release [198,199]. These grafts are designed to be inserted subcutaneously and, as such, the  $\beta$ -gal-NONOate generated NO is locally released, but not by specific endogenous cell types. Other researchers have demonstrated NO release with  $\beta$ -gal-NONOate in lacZ expressing cells. These authors utilized  $\beta$ -gal-NONOate to enable NO release in cultured tumor cells and suggested it could be combined with cisplatin treatment to increase tumor cell death [200]. The study used cell lines containing the lacZ gene and it is not clear how this would translate to a mammalian therapy where the lacZ gene is essentially entirely absent.

The research presented in this thesis focused on  $\beta$ -gal-NONOate as an ideal tool to enable cell type specific NO generation in vivo allowing for exquisite spatiotemporal investigation of the role of NO-cGMP signaling in biological systems. For example, it is possible to investigate the cell type specific role of NO in complex biological processes, such as learning and memory. As mentioned previously, cGMP signaling has been shown to play a role in LTP in the amygdala and hippocampus and in LTD in the cerebellum [10], but the detailed relevance of this signaling pathway in specific cell types has not been investigated. Another difficult to test hypothesis is that NO could act as a retrograde messenger and travel from the postsynapse across the synaptic cleft to the presynapse, or anterogradely, and increase presynaptic cGMP levels via NO-GC activation [201]. Numerous NO-releasing molecules have been developed [140], but they lack cell type specificity and, until now, none have been utilized to enable cell-specific NO generation in vivo. To perform these experiments, we first needed to synthesize the compound  $\beta$ -gal-NONOate.

#### 4.2.1. Synthesis of $\beta$ -gal-NONOate

Due to high costs and low availability from commercial sources,  $\beta$ -gal-NONOate was synthesized by the Feil lab in collaboration with the Stafforst Lab and Ziegler Lab. The synthesis of  $\beta$ -gal-NONOate was performed in 5-steps (**Figure 18**) and resulted in an overall yield of ~6% (**Figure 18**). The compound's molecular structure was investigated via  $^1\text{H}$  NMR (**Figure 17**). Due to the complex nature of the molecule, it

was not easily discernable from the  $^1\text{H}$  NMR structure alone, but the reported values are in general agreement with previously published values [141]. Investigation of the chemical's ability to release NO was ultimately validated in biological systems as discussed in the following sections.

#### 4.2.2. $\beta$ -gal-NONOate-induced cGMP responses in VSMCs

It was first crucial to determine that our newly synthesized compound released NO in a validated cell culture system.  $\beta$ -gal-NONOate was applied to primary VSMCs expressing the cGi500 sensor (**Figures 19A and 20A**) and shown to induce cGMP elevation in the presence of  $\beta$ -galactosidase (**Figures 19C-E**), but not under the same conditions in VSMCs lacking  $\beta$ -galactosidase (**Figures 20C and D**). X-gal staining was performed to determine  $\beta$ -galactosidase expression (**Figures 19B and 20B**). VSMC cultures were used as a cell model due to better rates of transfection when compared to neuronal cultures, which are notoriously resilient to transfection via traditional methods likely due to their post-mitotic nature [202]. Previous work with VSMCs revealed an increase in  $[\text{cGMP}]_i$  in nearly 100% of VSMCs upon the addition of DEA/NO (100 nM) [122], as observed in the experiments reported here (**Figures 19C-E; Figures 20C and D**). As expected, since only a portion of VSMCs ( $\approx 7\%$ ) expressed  $\beta$ -galactosidase (**Figure 19B**),  $[\text{cGMP}]_i$  elevation occurred in only some VSMCs ( $\approx 62\%$ ) upon the addition of  $\beta$ -gal-NONOate and with varying efficiency (**Figures 19C-E**). No elevation in  $[\text{cGMP}]_i$  was observed upon the addition of  $\beta$ -gal-NONOate in VSMC cultures lacking  $\beta$ -galactosidase indicating that there is no spontaneous release of NO from  $\beta$ -gal-NONOate (**Figures 20D and E**). As expected, the positive control DEA/NO produced clear cGMP elevations in both conditions (**Figures 19C,D, and E; Figures 20C and D**). The intensity of the cGMP response varied across VSMCs as observed upon exposure to the control stimulus DEA/NO (**Figures 19C-E; Figures 20C and D**). This might be caused by differential expression of NO-GCs, which could influence VSMC response-sensitivity to NO. Another possible explanation for variable cGMP responses is the differential expression of cGi500 across the cells, which can be inferred from the YFP intensity of the individual cells (**Figure 19A; Figure 20A**). This observation demonstrates the strength of real-time imaging in individual cells, which allows researchers to investigate the heterogeneity of phenotypes across cells

of the same type. Interestingly, previous work has suggested that cGMP is capable of moving across cells, perhaps via gap junctions, which could further influence cGMP response strengths in VSMCs [203].

Given that  $\beta$ -gal-NONOate did not induce cGMP elevation in control cultures (**Figure 20**), these results demonstrate  $\beta$ -gal-NONOate's ability to selectively release NO under the control of  $\beta$ -galactosidase. Similar research reported light-controlled release of NO using a photocaged NONOate substance in VSMCs [204]. Such a light-controlled methodology is powerful and allows for spatiotemporal release of NO. The here reported  $\beta$ -gal-NONOate methodology allows for NO generation under spatiotemporal control and in a cell-specific manner.

#### 4.2.3. $\beta$ -gal-NONOate-induced cGMP responses in cerebellar tissue slices

As mentioned previously, cGMP has been shown to play a role in LTP in the amygdala and hippocampus and in LTD in the cerebellum [10], but the role of specific cell types has remained elusive. By combining tissue-specific Cre mouse lines with cGi500 sensor mice and lacZ mice, it is possible to obtain cell type specific expression of both the cGi500 sensor and the lacZ gene. Here, we employed the L7-Cre mouse line that has been shown to induce recombination in Purkinje cells [100,145,205]. By combining these mouse lines and using  $\beta$ -gal-NONOate, it is possible to generate NO release only in Purkinje cells and verify this in real time with the cGi500 sensor by visualizing the cGMP dynamics in individual Purkinje neurons.

Here we measured cGMP in Purkinje cells expressing cGi500 (**Figures 21A and D**) under continuous superfusion. Indeed,  $\beta$ -gal-NONOate was shown to induce cGMP elevation in Purkinje neurons in  $\beta$ -galactosidase positive cerebellar slices (L7-Cre (tg/+) x R26-lacZ (lacZ/L2) x R26-cGi500-L2 (lacZ/L2)) (**Figure 21C**), but not under the same conditions in Purkinje neurons in  $\beta$ -galactosidase negative cerebellar slices (L7-Cre (tg/+) x R26-lacZ (L2/+) x R26-cGi500-L2 (L2/+)) (**Figure 21F**). However, because the control experiment (L7-Cre (tg/+) x R26-lacZ (L2/+) x R26-cGi500-L2 (L2/+)) used a lower concentration of  $\beta$ -gal-NONOate (5  $\mu$ M vs 25  $\mu$ M) (**Figure 21F**), spontaneous NO release from  $\beta$ -gal-NONOate in acute tissue slices cannot be excluded. DEA/NO produced clear cGMP elevations in both conditions (**Figures 21C and F**). X-gal staining was performed to determine  $\beta$ -galactosidase

expression (**Figures 21B and E**). These results are in line with other work that investigated NO-cGMP signaling and reported cGMP elevation in Purkinje cells [40]. Our data demonstrate the  $\beta$ -gal-NONOate strategy's capacity to induce cell-specific NO generation in tissue slices. After these results, we moved to determine if downstream cGMP effectors are influenced *in vivo* by injecting  $\beta$ -gal-NONOate into transgenic mice.

#### 4.2.4. $\beta$ -gal-NONOate-induced VASP phosphorylation *in vivo*

Due to the plethora of research done on NO-cGMP signaling in the smooth muscle cells [2], we first tested  $\beta$ -gal-NONOate's ability to phosphorylate VASP, a cGMP downstream target, in mice that express the lacZ gene under the control of smooth muscle-specific SM22 promotor (SM-CreER<sup>T2</sup> (tg/+) x R26-lacZ (+/lacZ)) [147]. In this model, if cGMP levels were successfully elevated upon addition of  $\beta$ -gal-NONOate then cGKI should be activated in VSMCs, which should induce VASP phosphorylation.

$\beta$ -gal-NONOate was injected via the tail vein of mice expressing  $\beta$ -galactosidase in smooth muscle cells (SM-CreER<sup>T2</sup> (tg/+) x R26-lacZ (+/lacZ) x ApoE (+/-)) and control mice without lacZ expression (SM-CreER<sup>T2</sup> (tg/+) x R26-lacZ (+/+) x ApoE (+/-) or C57BL/6). The mice were then sacrificed after 20 minutes and the organs (heart, aorta, colon, bladder, skeletal muscle from the torso, and lungs) were isolated for x-gal staining to determine  $\beta$ -galactosidase expression in the isolated tissues (**Figure 22**) as well as Western blotting to detect both VASP and phosphorylated VASP levels. Positive x-gal staining was observed in the bladder and colon of lacZ expressing mice (Mouse 2 and 4; **Figures 22B and D**), as well as the lung of one mouse to a lesser extent (Mouse 2; **Figures 22B**). Indeed, we observed increased VASP phosphorylation in the colon and lung isolated from  $\beta$ -galactosidase positive mice (Mouse 1 and 3; **Figures 23A and C**) compared to the control mice lacking lacZ, which showed no phosphorylated VASP (Mouse 2 and 4; **Figures 23B and D**). The bladder and aorta signals are weak due to low protein concentration making it difficult to draw conclusions from these data (all mice; **Figure 23**). Both skeletal muscle and heart were negative for x-gal staining in all mice and did not show a band for VASP suggesting the protein is not present in these tissues (all mice; **Figures 22 and 23**).

While these results should be repeated to improve the quality of the data, the increased VASP phosphorylation in the colon and lung isolated from  $\beta$ -galactosidase positive mice (Mouse 1 and 3; **Figures 23A and C**) compared to the control mice lacking lacZ (Mouse 2 and 4; **Figures 23B and D**) support the hypothesis that  $\beta$ -gal-NONOate is able to induce NO-cGMP signaling in vivo. We then investigated if  $\beta$ -gal-NONOate was able to induce a physiological response in vivo, namely vasodilation.

#### 4.2.5. $\beta$ -gal-NONOate-induced vasodilation in the cerebral cortex

Here, we demonstrated the ability of  $\beta$ -gal-NONOate to induce NO generation in neurons resulting in nearby vasodilation in living mice. Neuronal activity in the human brain can be measured noninvasively using Blood Oxygenation Level Dependent (BOLD) contrast in functional magnetic resonance imaging (fMRI). It has been hypothesized that BOLD signals reflect biochemical signaling processes which affect the cerebral vasculature through signaling cascades summarized as 'neurovascular coupling' [109,206]. However, the exact biochemical mechanisms which couple neuronal activity with vascular responses leading to regional changes in blood flow and oxygenation are far from understood. If elucidated, the molecular underpinnings of BOLD-fMRI would form an important framework to assess neuronal function in humans for both biochemical research and diagnostic purposes.

Previous research has demonstrated that NO increases cerebral blood flow, but this evidence lacks mechanistic understanding [109]. It has been postulated that NO released from neurons could diffuse to nearby vessels resulting in vasodilation and thus increase nutrient supply to the neural region [109]. Traditional methodology cannot easily investigate this hypothesis because conventional NO-releasing substances are not cell specific as previously stated [140]. Here, we surgically implanted a window in the cerebral cortex (**Figures 24A and B**) and conducted 2-photon imaging of blood vessels in the cerebral cortex of mice expressing lacZ under the control of a neuronal specific promoter (Camk2 $\alpha$ -CreBAC (tg/+) x R26-lacZ (+/lacZ)) to investigate the feasibility of NO as a modulator of neurovascular coupling (**Figure 24**). The vessels were analyzed with pseudo line scan or total area (**Figures 24C,E,G,I,K**)  $\beta$ -galactosidase was only expressed in neurons and not in the

vasculature in these mice [148]. Given the gaseous nature of NO, it can diffuse across cell membranes and enact physiological effects on nearby cells, such as blood vessels. Indeed, upon microinjection of  $\beta$ -gal-NONOate (50 mM) into the cerebral cortex we observed vasodilation of nearby vessels in mice expressing lacZ in neurons (**Figures 24D and E**), but not in mice lacking  $\beta$ -galactosidase expression (**Figures 24H and I**). The positive control DEA/NO (5 mM) induced vasodilation in both mice (Camk2 $\alpha$ -CreBAC (tg/+) x R26-lacZ (+/lacZ); and Wnt1-Cre (tg/+) x R26-lacZ (+/+)) (**Figures 24F,G,J,K**). These data provide the first in vivo evidence that  $\beta$ -gal-NONOate generated NO can induce a physiological effect, namely vasodilation, and support the notion of NO as an effector molecule in neurovascular coupling. These data demonstrate the power of cell type specific NO release and how we can use it to address previously difficult to investigate scientific questions.

#### **4.2.6. Outlook for $\beta$ -gal-NONOate as a tool to investigate the role of NO-cGMP signaling in behavior**

With  $\beta$ -gal-NONOate assisted cell-specific NO release, it is possible to more precisely elucidate the role of the NO-cGMP pathway in specific cell types during dynamic processes such as learning. The  $\beta$ -gal-NONOate methodology could also inform researchers about the diffusion area of NO by breeding R26-lacZ mice with Cre mice under the control of a cell specific promoter and R26-cGi500-L1 mice to produce global cGi500 sensor expression, but cell specific lacZ expression. Then NO would be released from specific cell types and cGMP could be visualized in neighboring cells that do not generate NO. A caveat to this type of study is that only cells expressing NO-GC would be expected to show elevated cGMP levels upon exposure to NO, thus limiting the strength of such an experiment.

As stated before, NO is believed to influence LTD in Purkinje neurons, but the exact role is still debated [100,166,179,207-211]. One could investigate this hypothesis based on the findings presented here using a mouse containing the cGi500 sensor and lacZ under the control of a Purkinje cell specific promoter (L7-Cre (tg/+) x R26-cGi500-L2 (L2/lacZ) x R26-lacZ (L2/lacZ)), the same mouse line as used in our cerebellar tissue slice experiments (**Figure 21**). The influence of NO-cGMP signaling in Purkinje cells on LTD can be investigated by motor learning paradigms, such as a

'balance beam test' [212]. Moreover,  $\beta$ -gal-NONOate could be remotely injected at time points defined by the researchers via a surgically implanted intracranial pump to investigate the role of NO-cGMP at different phases of learning (i.e. encoding, storage and recall) (**Figure 26**). An intracranial pump might be necessary because it is not clear if  $\beta$ -gal-NONOate crosses the blood brain barrier. A potential experiment to determine to what extent, if at all,  $\beta$ -gal-NONOate crosses the blood brain barrier would be injection into a mouse (i.e. tail vein injection) and then after some time (~20 min) isolate the cerebral spinal fluid and perform a mass spectrometry analysis. Western blot analysis of cGMP influenced neuronal markers (e.g. CREB) is also a possibility.

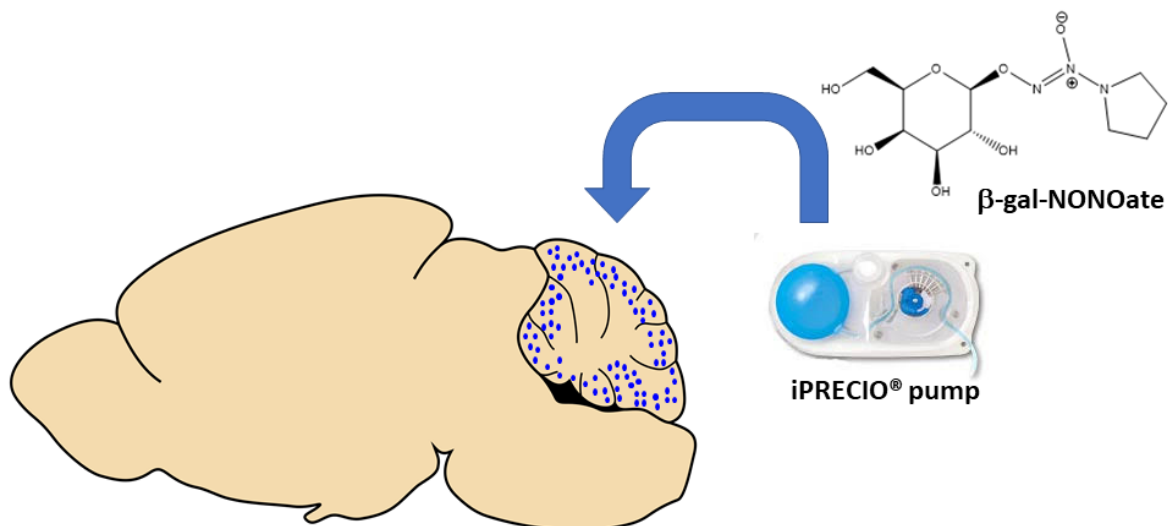


**Figure 26. Controlled intracranial injection of  $\beta$ -gal-NONOate to investigate the role of NO signaling in behavior paradigms.**

It is possible to inject  $\beta$ -gal-NONOate into the brain via a controllable pump (e.g. iPRECIO<sup>®</sup> pump) that the researcher can activate at specified time points. This could be done in a mouse line with cell-specific Cre expression to enable lacZ and thus  $\beta$ -galactosidase expression only in the desired cell type (e.g. Purkinje cells, the blue cells in mouse cerebellum). Behavioral paradigms could then be employed to investigate the cell-specific role of NO signaling in learning and memory.

If  $\beta$ -gal-NONOate influences motor learning when compared to control mice -- those without lacZ -- then tools can be employed to determine if NO works via a cGMP-dependent or independent manner, for example by inhibiting NO-GC either with a KO mouse line or pharmacologically (i.e. ODQ). However, it is important to note that ODQ

is not a perfect inhibitor of NO-GC as demonstrated by Friebe and colleagues who showed that cGMP elevation is possible to achieve with high NO concentrations even in the presence of ODQ [213]. As reported by Peters and colleagues, NO-cGMP signaling is present in various neuronal regions [40]. With the Cre/loxP system under the control of cell type specific promoters, it is possible to target specific brain cells, such as the Purkinje cells as described previously (**Figure 21**). With these the relevant Cre mouse lines, it is possible to investigate the role of NO-cGMP signaling in learning and memory (e.g. fear conditioning, motor learning, spatial learning, memory recall, and others) in different neuronal cell types.

The role of cGMP in neural plasticity suggests that future cGMP-modulating medications could be used to treat neurological disorders. For example, researchers have demonstrated that the PDE5 inhibitor sildenafil can improve learning in a rat model of hepatic encephalopathy which has dysfunctional cGMP signaling and neural deficits [214]. Similar research reported that PDE9 inhibition also results in memory enhancement in wild type rodents [215]. Indeed, a number of papers have implicated PDE inhibitors in cognitive enhancement in rats [216-220], mice [221-223] and even macaques [224]. More preclinical and clinical trials need to be done before these drugs make it into human use as it is important to completely understand the role of cGMP signaling in the CNS.

The dearth of information about cell type specific influences on cognitive processes highlights the importance and strength of our  $\beta$ -gal-NONOate method. With this new strategy it is now possible to investigate NO-cGMP signaling in specific cell types at the molecular and behavioral levels. However, it is important to note that the lacZ gene itself can confound results. For example, researchers have identified an influence of lacZ expression on hippocampus-dependent memory in [225]. In short, the study investigated the influence of lacZ expression on Cre reporter mouse lines in behavioral tests, such as acoustic startle response, fear-conditioning, and hippocampus-dependent spatial learning. The researchers reported decreased hippocampus dependent spatial learning in mice that showed lacZ expression in the cortex and hippocampus (R26-Nex-Cre (tg/+) x R26-lacZ (+/lacZ)) when compared to wild type controls. This study has important implications for mouse research given that many laboratories use lacZ as a reporter gene to determine the temporal and spatial expression of gene of interest [149,226,227]. LacZ has also been used as a reporter

to investigate to investigate addiction behavior and learning and memory by placing lacZ under the control of the neuronal activity-associated promoter Fos. The method has been applied in mouse, rat and monkey models [228-230]. Furthermore, the  $\beta$ -galactosidase protein is analogous to mammalian senescence-associated  $\beta$ -galactosidase and because protein accumulation is associated with neurodegeneration, constitutive expression of lacZ has been hypothesized to induce neuronal death. Indeed, the previously mentioned study did find reduced hippocampal volume in lacZ expressing mice [225]. Other research has also shown an association between YFP accumulation and neurodegenerative effects demonstrating the potential side effects of transgenic gene expression in the nervous system [231]. To control for the potential influence of genetic tools on results, it is important to compare the modified mice with wild type control mice.

Other strategies have been developed for cell type specific investigation of biological processes. One such strategy employed genetic mouse models and pharmacological agents to investigate the specific roles of dopamine receptor 1 (D1) or dopamine receptor 2 (D2) in neuronal culture, brain tissue slices and a mouse model of Parkinson's disease [232]. The researchers used DART (drugs acutely restricted by tethering), which is a technique capable of capturing and tethering drugs to the surface of specific cells. The cell specific ligands bind molecules and spatially restrict their action to that one cell providing researchers with the ability to make conclusions about the role of specific cell types in behavioral paradigms. This methodology has similarities to the  $\beta$ -gal-NONOate and lacZ cell specific NO generation strategy described here. For example, the cell specificity is also derived from a cell type specific promoter using the Cre/loxP system. It can be used as a reference paper for future behavioral work with  $\beta$ -gal-NONOate.

We have demonstrated the power of this method in cell culture, tissue slices and in vivo. While this work primarily emphasizes the use of  $\beta$ -gal-NONOate in the brain, with the various cell type specific mouse lines available, it is possible to conduct experiments to investigate the cell type specific role of NO-cGMP signaling in both the nervous system and other biological systems.

## 5 Appendix

### 5.1. Polymerase chain reaction protocols

**Table A1. Primer Sequences**

Primer	Sequence
BB01	CTCTGCTGCCTCCTGGCTTCT
BB02	CGAGGCGGATCACAAGCAATA
BB03	TCAATGGGCGGGGGTTCGTT
BB19	AAGATGCTGAAGGGAAGGATGC
BB20	CAGCCCAAAGAAACAAGAAGAAAG
BB21	GATGTGGGATTGTTTCTGAGGA
Cre800	GCTGCCACGACCAAGTGACAGCAATG
Cre1200	GTAGTTATTCGGATCATCAGCTACAC
RF127	GCGAAGAGTTTGTCTCAACC
Cam k1	GGTTCTCCGTTTGCCTCAGGA
Cam k2	CCTGTTGTTTCAGCTTGCACCAG
Cam k5	CTGCATGCACGGGACAGCTCT

**Table A2. Polymerase chain reaction conditions**

PCR	Primer	Conditions
L7-Cre; Wnt1-Cre; SM-CreER <sup>T2</sup>	Cre800 Cre1200	95 °C 5 min
		95 °C 10 sec
		58 °C 30 sec 35x
		72 °C 30 sec
		72 °C 5 min
R26-cGi500-L1 and R26-cGi500-L2	BB01 BB02 BB03	95 °C 5 min
		95 °C 10 sec
		61 °C 30 sec 35x
		72 °C 30 sec
		72 °C 5 min
lacZ	BB01 BB02 RF127	95 °C 5 min
		95 °C 10 sec
		61 °C 30 sec 35x
		72 °C 30 sec
		72 °C 5 min
NO-GC KO	BB 19 BB 20 BB 21	94 °C 3 min
		95 °C 60 sec
		60 °C 45 sec 30x
		72 °C 60 sec
		72 °C 7 min
Camk2 $\alpha$ -CreBAC	Cam k1 Camk2 Camk5	95 °C 2 min
		95 °C 30 sec
		66 °C 30 sec 45x
		72 °C 90 sec
		72 °C 10 min

## 5.2. Construct map of pFRTβ-gal

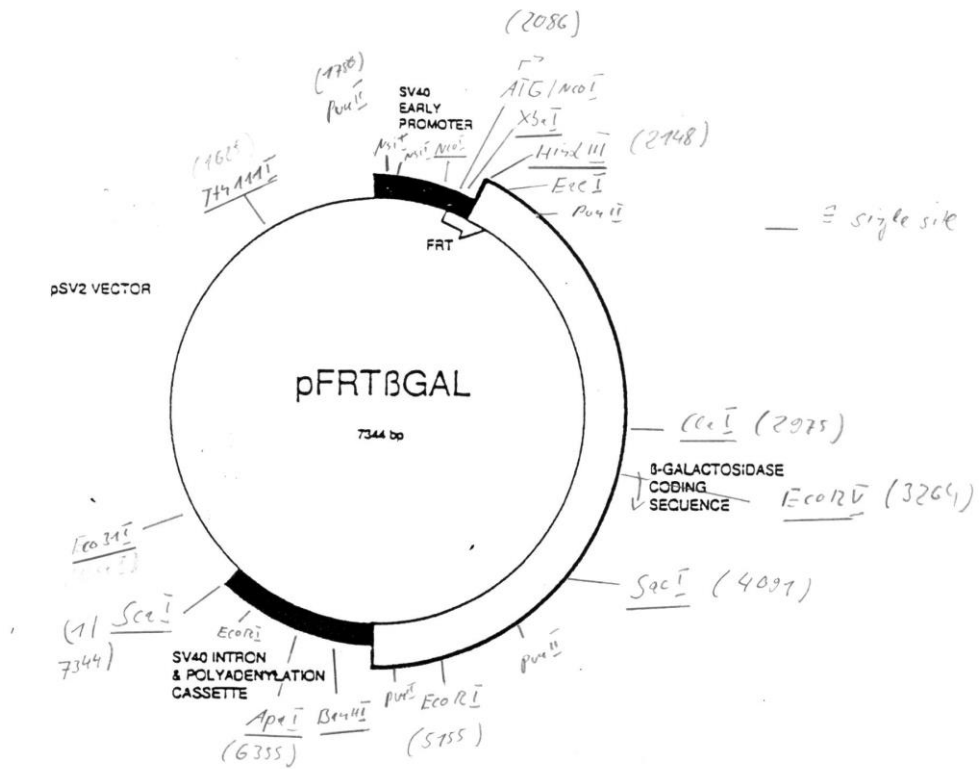


**Figure A1.** Construct map of pFRTβ-gal. Map provided by Prof. Dr. Robert Feil.

## 6 References

1. Rall, T. W.; Sutherland, E. W. Formation of a cyclic adenine ribonucleotide by tissue particles. *J Biol Chem.* 1958, 232, 1065-1076.
2. Lehnert, M.; Dobrowinski, H.; Feil, S.; Feil, R. cGMP signaling and vascular smooth muscle cell plasticity. *J Cardiovasc Dev Dis.* 2018, 5, pii: E20.
3. Kalyanaraman, H.; Schall, N.; Pilz, R. B. Nitric oxide and cyclic GMP functions in bone. *Nitric Oxide.* 2018, 76, 62-70.
4. Ziche, M.; Morbidelli, L. Nitric oxide and angiogenesis. *J Neurooncol.* 2000, 50, 139-148.
5. Fisker, S.; Nielsen, S.; Ebdrup, L.; Bech, J. N.; Christiansen, J. S.; Pedersen, E. B.; Jørgensen, J. O. The role of nitric oxide in L-arginine-stimulated growth hormone release. *J Endocrinol Invest.* 1999, 22, 89-93.
6. Vincent, S. R. Nitric oxide neurons and neurotransmission. *Prog Neurobiol.* 2010, 90, 246-255.
7. Dumoulin, A.; Ter-Avetisyan, G.; Schmidt, H.; Rathjen, F. G. Molecular analysis of sensory axon branching unraveled a cGMP-dependent signaling cascade. *Int J Mol Sci.* 2018, 19, pii: E1266.
8. Schmidtko, A.; Tegeder, I.; Geisslinger, G. No NO, no pain? The role of nitric oxide and cGMP in spinal pain processing. *Trends Neurosci.* 2009, 32, 339-346.
9. Schmidtko, A. Nitric oxide-mediated pain processing in the spinal cord. *Handb Exp Pharmacol.* 2015, 227, 103-117.
10. Kleppisch, T.; Feil, R. cGMP signalling in the mammalian brain: role in synaptic plasticity and behaviour. *Handb Exp Pharmacol.* 2009, 191, 549-579.
11. Paul, V.; Ekambaram, P. Involvement of nitric oxide in learning & memory processes. *Indian J Med Res.* 2011, 133, 471-478.
12. Beavo, J. A.; Brunton, L. L. Cyclic nucleotide research - still expanding after half a century. *Nat Rev Mol Cell Biol.* 2002 3, 710-718.
13. Sutherland, E. W.; Rall, T. W. Formation of adenosine-3,5-phosphate (cyclic adenylylate) and its relation to the action of several neurohormones or hormones. *Acta Endocrinol Suppl (Copenh).* 1960, 34(Suppl 50), 171-174.
14. Krebs, E. G.; Fischer, E. H. The phosphorylase b to a converting enzyme of rabbit skeletal muscle. *Biochim Biophys Acta.* 1956, 20, 150-157.
15. Gilman, A. G. A protein binding assay for adenosine 3':5'-cyclic monophosphate. *Proc Natl Acad Sci U S A.* 1970, 67, 305-312.
16. Rodbell, M.; Birnbaumer, L.; Pohl, S. L.; Krans, H. M. Properties of the adenylyl cyclase systems in liver and adipose cells: the mode of action of hormones. *Acta Diabetol Lat.* 1970, 7 Suppl 1, 9-63.
17. Murad, F. Nitric oxide signaling: would you believe that a simple free radical could be a second messenger, autacoid, paracrine substance, neurotransmitter, and hormone? *Recent Prog Horm Res.* 1998, 53, 43-60.
18. Furchgott, R. F.; Zawadzki, J. V. The obligatory role of endothelial cells in the relaxation of arterial smooth muscle by acetylcholine. *Nature.* 1980, 288, 373-376.
19. Ignarro, L. J.; Buga, G. M.; Wood, K. S.; Byrns, R. E.; Chaudhuri, G. Endothelium-derived relaxing factor produced and released from artery and vein is nitric oxide. *Proc Natl Acad Sci U S A.* 1987, 84, 9265-9269.
20. Ignarro, L. J.; Byrns, R. E.; Wood, K. S. Endothelium-dependent modulation of cGMP levels and intrinsic smooth muscle tone in isolated bovine intrapulmonary artery and vein. *Circ Res.* 1987, 60, 82-92.
21. Katsuki, S.; Arnold, W. P.; Murad, F. Effects of sodium nitroprusside, nitroglycerin, and sodium azide on levels of cyclic nucleotides and mechanical activity of various tissues. *J Cyclic Nucleotide Res.* 1977, 3, 239-247.
22. Frost, W. N.; Clark, G. A.; Kandel, E. R. Parallel processing of short-term memory for sensitization in *Aplysia*. *J Neurobiol.* 1988, 19, 297-334.

## References

23. Carlsson, A.; Lindqvist, M. Effect of chlorpromazine or haloperidol on formation of 3-methoxytyramine and normetanephrine in mouse brain. *Acta Pharmacol Toxicol (Copenh)*. 1963, 20, 140-144.
24. Beam, K. G.; Greengard, P. Cyclic nucleotides, protein phosphorylation and synaptic function. *Cold Spring Harb Symp Quant Biol*. 1976, 40, 157-168.
25. Marsh, N.; Marsh, A. A short history of nitroglycerine and nitric oxide in pharmacology and physiology. *Clin Exp Pharmacol Physiol*. 2000, 27, 313-319.
26. Furchgott, R. F.; Zawadzki, J. V. The obligatory role of endothelial cells in the relaxation of arterial smooth muscle by acetylcholine. *Nature*. 1980 288, 373-376.
27. Knowles, R. G.; Moncada, S. Nitric oxide synthases in mammals. *Biochem J*. 1994, 298, 249-258.
28. Marletta, M. A. Nitric oxide synthase: aspects concerning structure and catalysis. *Cell*. 1994, 78, 927-930.
29. Alderton, W. K.; Cooper, C. E.; Knowles, R. G. Nitric oxide synthases: structure, function and inhibition. *Biochem J*. 2001, 357, 593-615.
30. Garthwaite, J. Concepts of neural nitric oxide-mediated transmission. *Eur J Neurosci*. 2008, 27, 2783-2802.
31. Brenman, J. E.; Chao, D. S.; Gee, S. H.; McGee, A. W.; Craven, S. E.; Santillano, D. R.; Wu, Z.; Huang, F.; Xia, H.; Peters, M. F.; Froehner, S. C.; Bredt, D. S. Interaction of nitric oxide synthase with the postsynaptic density protein PSD-95 and alpha1-syntrophin mediated by PDZ domains. *Cell*. 1996, 84, 757-767.
32. Christopherson, K. S.; Hillier, B. J.; Lim, W. A.; Bredt, D. S. PSD-95 assembles a ternary complex with the N-methyl-D-aspartic acid receptor and a bivalent neuronal NO synthase PDZ domain. *J Biol Chem*. 1999, 274, 27467-27473.
33. Pyriochou, A.; Papapetropoulos, A. Soluble guanylyl cyclase: more secrets revealed. *Cell Signal*. 2005, 17, 407-413.
34. Friebe, A.; Koesling, D. The function of NO-sensitive guanylyl cyclase: what we can learn from genetic mouse models. *Nitric Oxide*. 2009, 21, 149-156.
35. Kuhn, M. Molecular physiology of membrane guanylyl cyclase receptors. *Physiol Rev*. 2016, 96, 751-804.
36. Potter, L. R.; Abbey-Hosch, S.; Dickey, D. M. Natriuretic peptides, their receptors, and cyclic guanosine monophosphate-dependent signaling functions. *Endocr Rev*. 2006, 27, 47-72.
37. Schmidt, H.; Stonkute, A.; Jüttner, R.; Koesling, D.; Friebe, A.; Rathjen, F. G. C-type natriuretic peptide (CNP) is a bifurcation factor for sensory neurons. *Proc Natl Acad Sci U S A*. 2009, 106, 16847-16852.
38. Russwurm, M.; Behrends, S.; Harteneck, C.; Koesling, D. Functional properties of a naturally occurring isoform of soluble guanylyl cyclase. *Biochem J*. 1998, 335 ( Pt 1), 125-130.
39. Derbyshire, E. R.; Marletta, M. A. Biochemistry of soluble guanylate cyclase. *Handb Exp Pharmacol*. 2009, 191, 17-31.
40. Peters, S.; Paolillo, M.; Mergia, E.; Koesling, D.; Kennel, L.; Schmidtko, A.; Russwurm, M.; Feil, R. cGMP imaging in brain slices reveals brain region-specific activity of NO-sensitive guanylyl cyclases (NO-GCs) and NO-GC stimulators. *Int J Mol Sci*. 2018, 19, pii: E2313.
41. Zabel, U.; Kleinschnitz, C.; Oh, P.; Nedvetsky, P.; Smolenski, A.; Muller, H.; Kronich, P.; Kugler, P.; Walter, U.; Schnitzer, J. E.; Schmidt, H. H. Calcium-dependent membrane association sensitizes soluble guanylyl cyclase to nitric oxide. *Nat Cell Biol*. 2002, 4, 307-311.
42. Agullo, L.; Garcia-Dorado, D.; Escalona, N.; Ruiz-Meana, M.; Mirabet, M.; Inserte, J.; Soler-Soler, J. Membrane association of nitric oxide-sensitive guanylyl cyclase in cardiomyocytes. *Cardiovasc Res*. 2005, 68, 65-74.
43. Castro, L. R.; Verde, I.; Cooper, D. M.; Fischmeister, R. Cyclic guanosine monophosphate compartmentation in rat cardiac myocytes. *Circulation*. 2006, 113, 2221-2228.
44. Russwurm, M.; Wittau, N.; Koesling, D. Guanylyl cyclase/PSD-95 interaction: targeting

## References

- of the nitric oxide-sensitive alpha2beta1 guanylyl cyclase to synaptic membranes. *J Biol Chem.* 2001, 276, 44647-44652.
45. Wedel, B.; Humbert, P.; Harteneck, C.; Foerster, J.; Malkewitz, J.; Böhme, E.; Schultz, G.; Koesling, D. Mutation of His-105 in the beta 1 subunit yields a nitric oxide-insensitive form of soluble guanylyl cyclase. *Proc Natl Acad Sci U S A.* 1994, 91, 2592-2596.
  46. Schmidt, P. M.; Schramm, M.; Schroder, H.; Wunder, F.; Stasch, J. P. Identification of residues crucially involved in the binding of the heme moiety of soluble guanylate cyclase. *J Biol Chem.* 2004, 279, 3025-3032.
  47. Wolin, M. S.; Wood, K. S.; Ignarro, L. J. Guanylate cyclase from bovine lung. A kinetic analysis of the regulation of the purified soluble enzyme by protoporphyrin IX, heme, and nitrosyl-heme. *J Biol Chem.* 1982, 257, 13312-13320.
  48. Cary, S. P.; Winger, J. A.; Marletta, M. A. Tonic and acute nitric oxide signaling through soluble guanylate cyclase is mediated by nonheme nitric oxide, ATP, and GTP. *Proc Natl Acad Sci U S A.* 2005, 102, 13064-13069.
  49. Russwurm, M.; Koesling, D. NO activation of guanylyl cyclase. *EMBO J.* 2004, 23, 4443-4450.
  50. Stone, J. R.; Marletta, M. A. Soluble guanylate cyclase from bovine lung: activation with nitric oxide and carbon monoxide and spectral characterization of the ferrous and ferric states. *Biochemistry.* 1994, 33, 5636-5640.
  51. Pacher, P.; Beckman, J. S.; Liaudet, L. Nitric oxide and peroxynitrite in health and disease. *Physiol Rev.* 2007, 87, 315-424.
  52. Feil, R.; Kemp-Harper, B. cGMP signalling: from bench to bedside. Conference on cGMP generators, effectors and therapeutic implications. *EMBO Rep.* 2006, 7, 149-153.
  53. Pfeifer, A.; Ruth, P.; Dostmann, W.; Sausbier, M.; Klatt, P.; Hofmann, F. Structure and function of cGMP-dependent protein kinases. *Rev Physiol Biochem Pharmacol.* 1999, 135, 105-149.
  54. Feil, R.; Lohmann, S. M.; de Jonge, H.; Walter, U.; Hofmann, F. Cyclic GMP-dependent protein kinases and the cardiovascular system: insights from genetically modified mice. *Circ Res.* 2003, 93, 907-916.
  55. Schlossmann, J.; Desch, M. cGK substrates. *Handb Exp Pharmacol.* 2009, 191, 163-193.
  56. Hofmann, F.; Bernhard, D.; Lukowski, R.; Weinmeister, P. cGMP regulated protein kinases (cGK). *Handb Exp Pharmacol.* 2009, 191, 137-162.
  57. Feil, S.; Zimmermann, P.; Knorn, A.; Brummer, S.; Schlossmann, J.; Hofmann, F.; Feil, R. Distribution of cGMP-dependent protein kinase type I and its isoforms in the mouse brain and retina. *Neuroscience.* 2005, 135, 863-868.
  58. Geiselhoringer, A.; Gaisa, M.; Hofmann, F.; Schlossmann, J. Distribution of IRAG and cGKI-isoforms in murine tissues. *FEBS Lett.* 2004, 575, 19-22.
  59. Vaandrager, A. B.; Ehlert, E. M.; Jarchau, T.; Lohmann, S. M.; de Jonge, H. R. N-terminal myristoylation is required for membrane localization of cGMP-dependent protein kinase type II. *J Biol Chem.* 1996, 271, 7025-7029.
  60. el-Husseini, A. E.; Bladen, C.; Vincent, S. R. Molecular characterization of a type II cyclic GMP-dependent protein kinase expressed in the rat brain. *J Neurochem.* 1995, 64, 2814-2817.
  61. Lohmann, S. M.; Vaandrager, A. B.; Smolenski, A.; Walter, U.; De Jonge, H. R. Distinct and specific functions of cGMP-dependent protein kinases. *Trends Biochem Sci.* 1997, 307-312.
  62. Surks, H. K. cGMP-dependent protein kinase I and smooth muscle relaxation: a tale of two isoforms. *Circ Res.* 2007, 101, 1078-1080.
  63. Weber, S.; Bernhard, D.; Lukowski, R.; Weinmeister, P.; Worner, R.; Wegener, J. W.; Valtcheva, N.; Feil, S.; Schlossmann, J.; Hofmann, F.; Feil, R. Rescue of cGMP kinase I knockout mice by smooth muscle specific expression of either isozyme. *Circ Res.* 2007, 101, 1096-1103.
  64. Wall, M. E.; Francis, S. H.; Corbin, J. D.; Grimes, K.; Richie-Jannetta, R.; Kotera, J.; Macdonald, B. A.; Gibson, R. R.; Trewhella, J. Mechanisms associated with cGMP

## References

- binding and activation of cGMP-dependent protein kinase. *Proc Natl Acad Sci U S A*. 2003, *100*, 2380-2385.
65. Biel, M.; Michalakis, S. Cyclic nucleotide-gated channels. *Handb Exp Pharmacol*. 2009, *191*, 111-136.
  66. Kaupp, U. B.; Seifert, R. Cyclic nucleotide-gated ion channels. *Physiol Rev*. 2002, *82*, 769-824.
  67. Zufall, F.; Shepherd, G. M.; Barnstable, C. J. Cyclic nucleotide gated channels as regulators of CNS development and plasticity. *Curr Opin Neurobiol*. 1997, *7*, 404-412.
  68. Barnstable, C. J.; Wei, J. Y.; Han, M. H. Modulation of synaptic function by cGMP and cGMP-gated cation channels. *Neurochem Int*. 2004, *45*, 875-884.
  69. Bender, A. T.; Beavo, J. A. Cyclic nucleotide phosphodiesterases: molecular regulation to clinical use. *Pharmacol Rev*. 2006, *58*, 488-520.
  70. Conti, M.; Beavo, J. Biochemistry and physiology of cyclic nucleotide phosphodiesterases: essential components in cyclic nucleotide signaling. *Annu Rev Biochem*. 2007, *76*, 481-511.
  71. Francis, S. H.; Corbin, J. D.; Bischoff, E. Cyclic GMP-hydrolyzing phosphodiesterases. *Handb Exp Pharmacol*. 2009, *191*, 367-408.
  72. Jager, R.; Russwurm, C.; Schwede, F.; Genieser, H. G.; Koesling, D.; Russwurm, M. Activation of PDE10 and PDE11 phosphodiesterases. *J Biol Chem*. 2012, *287*, 1210-1219.
  73. Zaccolo, M.; Movsesian, M. A. cAMP and cGMP signaling cross-talk: role of phosphodiesterases and implications for cardiac pathophysiology. *Circ Res*. 2007, *100*, 1569-1578.
  74. Polito, M.; Klarenbeek, J.; Jalink, K.; Paupardin-Tritsch, D.; Vincent, P.; Castro, L. R. The NO/cGMP pathway inhibits transient cAMP signals through the activation of PDE2 in striatal neurons. *Front Cell Neurosci*. 2013, *7*, 211.
  75. Gross-Langenhoff, M.; Hofbauer, K.; Weber, J.; Schultz, A.; Schultz, J. E. cAMP is a ligand for the tandem GAF domain of human phosphodiesterase 10 and cGMP for the tandem GAF domain of phosphodiesterase 11. *J Biol Chem*. 2006, *281*, 2841-2846.
  76. Kass, D. A.; Takimoto, E.; Nagayama, T.; Champion, H. C. Phosphodiesterase regulation of nitric oxide signaling. *Cardiovasc Res*. 2007, *75*, 303-314.
  77. Kass, D. A.; Champion, H. C.; Beavo, J. A. Phosphodiesterase type 5: expanding roles in cardiovascular regulation. *Circ Res*. 2007, *101*, 1084-1095.
  78. Francis, S. H.; Busch, J. L.; Corbin, J. D.; Sibley, D. cGMP-dependent protein kinases and cGMP phosphodiesterases in nitric oxide and cGMP action. *Pharmacol Rev*. 2010, *62*, 525-563.
  79. Kleppisch, T. Phosphodiesterases in the central nervous system. *Handb Exp Pharmacol*. 2009, *191*, 71-92.
  80. Menniti, F. S.; Faraci, W. S.; Schmidt, C. J. Phosphodiesterases in the CNS: targets for drug development. *Nat Rev Drug Discov*. 2006, *5*, 660-670.
  81. Straub, R. E.; Lehner, T.; Luo, Y.; Loth, J. E.; Shao, W.; Sharpe, L.; Alexander, J. R.; Das, K.; Simon, R.; Fieve, R. R. et. al. A possible vulnerability locus for bipolar affective disorder on chromosome 21q22.3. *Nat Genet*. 1994, *8*, 291-296.
  82. Sano, H.; Nagai, Y.; Miyakawa, T.; Shigemoto, R.; Yokoi, M. Increased social interaction in mice deficient of the striatal medium spiny neuron-specific phosphodiesterase 10A2. *J Neurochem*. 2008, *105*, 546-556.
  83. Schmidt, C. J.; Chapin, D. S.; Cianfrogna, J.; Corman, M. L.; Hajos, M.; Harms, J. F.; Hoffman, W. E.; Lebel, L. A.; McCarthy, S. A.; Nelson, F. R. et. al. Preclinical characterization of selective phosphodiesterase 10A inhibitors: a new therapeutic approach to the treatment of schizophrenia. *J Pharmacol Exp Ther*. 2008, *325*, 681-690.
  84. McDonald, M. L.; MacMullen, C.; Liu, D. J.; Leal, S. M.; Davis, R. L. Genetic association of cyclic AMP signaling genes with bipolar disorder. *Transl Psychiatry*. 2012, *2*, e169.
  85. Wong, M. L.; Whelan, F.; Deloukas, P.; Whittaker, P.; Delgado, M.; Cantor, R. M.; McCann, S. M.; Licinio, J. Phosphodiesterase genes are associated with susceptibility to major depression and antidepressant treatment response. *Proc Natl Acad Sci U S A*.

## References

- 2006, *103*, 15124-15129.
86. Andersson, K. E. PDE5 inhibitors - pharmacology and clinical applications 20 years after sildenafil discovery. *Br J Pharmacol*. 2018, *175*, 2554-2565.
  87. Buys, E. S.; Zimmer, D. P.; Chickering, J.; Graul, R.; Chien, Y. T.; Profy, A.; Hadcock, J. R.; Masferrer, J. L.; Milne, G. T. Discovery and development of next generation sGC stimulators with diverse multidimensional pharmacology and broad therapeutic potential. *Nitric Oxide*. 2018, *78*, 72-80.
  88. Sandner, P. From molecules to patients: exploring the therapeutic role of soluble guanylate cyclase stimulators. *Biol Chem*. 2018, *399*, 679-690.
  89. Schlossmann, J.; Schinner, E. cGMP becomes a drug target. *Naunyn Schmiedeberg's Arch Pharmacol*. 2012, *385*, 243-252.
  90. Oettrich, J. M.; Dao, V. T.; Frijhoff, J.; Kleikers, P.; Casas, A. I.; Hobbs, A. J.; Schmidt, H. H. Clinical relevance of cyclic GMP modulators: A translational success story of network pharmacology. *Clin Pharmacol Ther*. 2016, *99*, 360-362.
  91. Follmann, M.; Griebenow, N.; Hahn, M. G.; Hartung, I.; Mais, F. J.; Mittendorf, J.; Schafer, M.; Schirok, H.; Stasch, J. P.; Stoll, F.; Straub, A. The chemistry and biology of soluble guanylate cyclase stimulators and activators. *Angew Chem Int Ed Engl*. 2013, *52*, 9442-9462.
  92. Kawakami, R.; Lee, C. Y. W.; Scott, C.; Bailey, K. R.; Schirger, J. A.; Chen, H. H.; Benike, S. L.; Cannone, V.; Martin, F. L.; Sangaralingham, S. J.; Ichiki, T.; Burnett, J. C., Jr. A human study to evaluate safety, tolerability, and cyclic GMP activating properties of cenderitide in subjects with stable chronic heart failure. *Clin Pharmacol Ther*. 2018, *104*, 546-552.
  93. Rey, E.; Mearin, F.; Alcedo, J.; Ciriza, C.; Delgado-Aros, S.; Freitas, T.; Mascarenhas, M.; Minguez, M.; Santos, J.; Serra, J. Optimizing the use of linaclotide in patients with constipation-predominant irritable bowel syndrome: An expert consensus report. *Adv Ther*. 2017, *34*, 587-598.
  94. Schoenfeld, P.; Lacy, B. E.; Chey, W. D.; Lembo, A. J.; Kurtz, C. B.; Reasner, D. S.; Bochenek, W.; Tripp, K.; Currie, M. G.; Fox, S. M. et. al. Low-dose Linaclotide (72 mug) for chronic idiopathic constipation: a 12-week, randomized, double-blind, placebo-controlled trial. *Am J Gastroenterol*. 2018, *113*, 105-114.
  95. Yandrapalli, S.; Khan, M. H.; Rochlani, Y.; Aronow, W. S. Sacubitril/valsartan in cardiovascular disease: evidence to date and place in therapy. *Ther Adv Cardiovasc Dis*. 2018, *12*, 217-231.
  96. Legeai-Mallet, L. C-type natriuretic peptide analog as therapy for achondroplasia. *Endocr Dev*. 2016, *30*, 98-105.
  97. Ghofrani, H. A.; Galie, N.; Grimminger, F.; Grunig, E.; Humbert, M.; Jing, Z. C.; Keogh, A. M.; Langleben, D.; Kilama, M. O.; Fritsch, A.; Neuser, D.; Rubin, L. J.; Group, P.-S. Riociguat for the treatment of pulmonary arterial hypertension. *N Engl J Med*. 2013, *369*, 330-340.
  98. Garthwaite, J.; Boulton, C. L. Nitric oxide signaling in the central nervous system. *Annu Rev Physiol*. 1995, *57*, 683-706.
  99. Kleppisch, T.; Pfeifer, A.; Klatt, P.; Ruth, P.; Montkowski, A.; Fässler, R.; Hofmann, F. Long-term potentiation in the hippocampal CA1 region of mice lacking cGMP-dependent kinases is normal and susceptible to inhibition of nitric oxide synthase. *J Neurosci*. 1999, *19*, 48-55.
  100. Feil, R.; Hartmann, J.; Luo, C.; Wolfsgruber, W.; Schilling, K.; Feil, S.; Barski, J. J.; Meyer, M.; Konnerth, A.; De Zeeuw, C. I.; Hofmann, F. Impairment of LTD and cerebellar learning by Purkinje cell-specific ablation of cGMP-dependent protein kinase I. *J Cell Biol*. 2003, *163*, 295-302.
  101. Fox, K.; Stryker, M. Integrating Hebbian and homeostatic plasticity: introduction. *Philos Trans R Soc Lond B Biol Sci*. 2017, *372*, pii: 20160413.
  102. Morris, R. G. D.O. Hebb: The organization of behavior, Wiley: New York; 1949. *Brain Res Bull*. 1999, *50*, 437.
  103. Hebb, D. The organisation of behaviour. *New York, NY: John Wiley and Sons*. 1949,
  104. Shatz, C. J. The developing brain. *Sci Am*. 1992, *267*, 60-67.

## References

105. Keyzers, C.; Gazzola, V. Hebbian learning and predictive mirror neurons for actions, sensations and emotions. *Philos Trans R Soc Lond B Biol Sci.* 2014, *369*, 20130175.
106. Girouard, H.; Iadecola, C. Neurovascular coupling in the normal brain and in hypertension, stroke, and Alzheimer disease. *J Appl Physiol (1985).* 2006, *100*, 328-335.
107. Iadecola, C. Neurovascular regulation in the normal brain and in Alzheimer's disease. *Nat Rev Neurosci.* 2004, *5*, 347-360.
108. Lourenco, C. F.; Santos, R. M.; Barbosa, R. M.; Cadenas, E.; Radi, R.; Laranjinha, J. Neurovascular coupling in hippocampus is mediated via diffusion by neuronal-derived nitric oxide. *Free Radic Biol Med.* 2014, *73*, 421-429.
109. Dormanns, K.; Brown, R. G.; David, T. The role of nitric oxide in neurovascular coupling. *J Theor Biol.* 2016, *394*, 1-17.
110. Hofmann, F.; Feil, R.; Kleppisch, T.; Schlossmann, J. Function of cGMP-dependent protein kinases as revealed by gene deletion. *Physiol Rev.* 2006, *86*, 1-23.
111. Contestabile, A. Cerebellar granule cells as a model to study mechanisms of neuronal apoptosis or survival in vivo and in vitro. *Cerebellum.* 2002, *1*, 41-55.
112. Ramón y Cajal, S. Sur l'origine et la direction des prolongations nerveuses de la couche moléculaire du cervelet. *Internat Mschr Anat Physiol.* 1889, *7*, 12–31.
113. Jurado, S.; Sanchez-Prieto, J.; Torres, M. Elements of the nitric oxide/cGMP pathway expressed in cerebellar granule cells: biochemical and functional characterisation. *Neurochem Int.* 2004, *45*, 833-843.
114. Zuniga, R.; Gonzalez, D.; Valenzuela, C.; Brown, N.; Zuniga, L. Expression and cellular localization of HCN channels in rat cerebellar granule neurons. *Biochem Biophys Res Commun.* 2016, *478*, 1429-1435.
115. Lopez-Jimenez, M. E.; Gonzalez, J. C.; Lizasoain, I.; Sanchez-Prieto, J.; Hernandez-Guijo, J. M.; Torres, M. Functional cGMP-gated channels in cerebellar granule cells. *J Cell Physiol.* 2012, *227*, 2252-2263.
116. Paolillo, M.; Peters, S.; Schramm, A.; Schlossmann, J.; Feil, R. Real-time imaging reveals augmentation of glutamate-induced Ca<sup>2+</sup> transients by the NO-cGMP pathway in cerebellar granule neurons. *Int J Mol Sci.* 2018, *19*, pii: E2185.
117. Hahn, K.; Touthkine, A. Live-cell fluorescent biosensors for activated signaling proteins. *Curr Opin Cell Biol.* 2002, *14*, 167-172.
118. Thunemann, M.; Wen, L.; Hillenbrand, M.; Vachaviolos, A.; Feil, S.; Ott, T.; Han, X.; Fukumura, D.; Jain, R. K.; Russwurm, M. et. al. Transgenic mice for cGMP imaging. *Circ Res.* 2013, *113*, 365-371.
119. Russwurm, M.; Koesling, D. Measurement of cGMP-generating and -degrading activities and cGMP levels in cells and tissues: Focus on FRET-based cGMP indicators. *Nitric Oxide.* 2018, *77*, 44-52.
120. Brooker, G.; Harper, J. F.; Terasaki, W. L.; Moylan, R. D. Radioimmunoassay of cyclic AMP and cyclic GMP. *Adv Cyclic Nucleotide Res.* 1979, *10*, 1-33.
121. Sprenger, J. U.; Nikolaev, V. O. Biophysical techniques for detection of cAMP and cGMP in living cells. *Int J Mol Sci.* 2013, *14*, 8025-8046.
122. Thunemann, M.; Fomin, N.; Krawutschke, C.; Russwurm, M.; Feil, R. Visualization of cGMP with cGi biosensors. *Methods Mol Biol.* 2013, *1020*, 89-120.
123. Thunemann, M.; Schmidt, K.; de Wit, C.; Han, X.; Jain, R. K.; Fukumura, D.; Feil, R. Correlative intravital imaging of cGMP signals and vasodilation in mice. *Front Physiol.* 2014, *5*, 394.
124. Russwurm, M.; Mullershausen, F.; Friebe, A.; Jager, R.; Russwurm, C.; Koesling, D. Design of fluorescence resonance energy transfer (FRET)-based cGMP indicators: a systematic approach. *Biochem J.* 2007, *407*, 69-77.
125. Förster, T. Zwischenmolekulare Energiewanderung und Fluoreszenz. *Ann Phys.* 1948, *437*, 55-75.
126. Grynkiewicz, G.; Poenie, M.; Tsien, R. Y. A new generation of Ca<sup>2+</sup> indicators with greatly improved fluorescence properties. *J Biol Chem.* 1985, *260*, 3440-3450.
127. Grienberger, C.; Konnerth, A. Imaging calcium in neurons. *Neuron.* 2012, *73*, 862-885.
128. Waterston, R. H. et. al. Initial sequencing and comparative analysis of the mouse

## References

- genome. *Nature*. 2002, 420, 520-562.
129. Mural, R. J. et. al. A comparison of whole-genome shotgun-derived mouse chromosome 16 and the human genome. *Science*. 2002, 296, 1661-1671.
  130. Austin, C. P. et. al. The knockout mouse project. *Nat Genet*. 2004, 36, 921-924.
  131. Gupta, R. M.; Musunuru, K. Expanding the genetic editing tool kit: ZFNs, TALENs, and CRISPR-Cas9. *J Clin Invest*. 2014, 124, 4154-4161.
  132. Hsu, P. D.; Lander, E. S.; Zhang, F. Development and applications of CRISPR-Cas9 for genome engineering. *Cell*. 2014, 157, 1262-1278.
  133. Copp, A. J. Death before birth: clues from gene knockouts and mutations. *Trends Genet*. 1995, 11, 87-93.
  134. Sternberg, N.; Hamilton, D. Bacteriophage P1 site-specific recombination. I. Recombination between loxP sites. *J Mol Biol*. 1981 150, 467-486.
  135. Feil, R.; Brocard, J.; Mascrez, B.; LeMeur, M.; Metzger, D.; Chambon, P. Ligand-activated site-specific recombination in mice. *Proc Natl Acad Sci U S A*. 1996, 93, 10887-10890.
  136. Feil, R.; Wagner, J.; Metzger, D.; Chambon, P. Regulation of Cre recombinase activity by mutated estrogen receptor ligand-binding domains. *Biochem Biophys Res Commun*. 1997, 237, 752-757.
  137. Metzger, D.; Feil, R. Engineering the mouse genome by site-specific recombination. *Curr Opin Biotechnol*. 1999, 5, 470-476.
  138. Harno, E.; Cottrell, E. C.; White, A. Metabolic pitfalls of CNS Cre-based technology. *Cell Metab*. 2013, 18, 21-28.
  139. Giusti, S. A.; Vercelli, C. A.; Vogl, A. M.; Kolarz, A. W.; Pino, N. S.; Deussing, J. M.; Refojo, D. Behavioral phenotyping of Nestin-Cre mice: implications for genetic mouse models of psychiatric disorders. *J Psychiatr Res*. 2014, 55, 87-95.
  140. Wang, P. G.; Xian, M.; Tang, X.; Wu, X.; Wen, Z.; Cai, T.; Janczuk, A. J. Nitric oxide donors: chemical activities and biological applications. *Chem Rev*. 2002, 102, 1091-1134.
  141. Wu, X.; Tang, X.; Xian, M.; Wang, P. G. Glycosylated diazeniumdiolates: a novel class of enzyme-activated nitric oxide donors. *Tetrahedron Lett*. 2001, 42, 3779-3782.
  142. Valtcheva, N.; Nestorov, P.; Beck, A.; Russwurm, M.; Hillenbrand, M.; Weinmeister, P.; Feil, R. The commonly used cGMP-dependent protein kinase type I (cGKI) inhibitor Rp-8-Br-PET-cGMPS can activate cGKI in vitro and in intact cells. *J Biol Chem*. 2009, 284, 556-562.
  143. Schramm, A.; Schinner, E.; Huettner, J. P.; Kees, F.; Tauber, P.; Hofmann, F.; Schlossmann, J. Function of cGMP-dependent protein kinase II in volume load-induced diuresis. *Pflugers Arch*. 2014, 466, 2009-2018.
  144. Friebe, A.; Mergia, E.; Dangel, O.; Lange, A.; Koesling, D. Fatal gastrointestinal obstruction and hypertension in mice lacking nitric oxide-sensitive guanylyl cyclase. *Proc Natl Acad Sci U S A*. 2007, 104, 7699-7704.
  145. Barski, J. J.; Dethleffsen, K.; Meyer, M. Cre recombinase expression in cerebellar Purkinje cells. *Genesis*. 2000, 28, 93-98.
  146. Rowitch, D. H.; B, S. J.; Lee, S. M.; Flax, J. D.; Snyder, E. Y.; McMahon, A. P. Sonic hedgehog regulates proliferation and inhibits differentiation of CNS precursor cells. *J Neurosci*. 1999, 19, 8954-8965.
  147. Kuhbandner, S.; Brummer, S.; Metzger, D.; Chambon, P.; Hofmann, F.; Feil, R. Temporally controlled somatic mutagenesis in smooth muscle. *Genesis*. 2000, 28, 15-22.
  148. Casanova, E.; Fehsenfeld, S.; Mantamadiotis, T.; Lemberger, T.; Greiner, E.; Stewart, A. F.; Schutz, G. A CamKIIalpha iCre BAC allows brain-specific gene inactivation. *Genesis*. 2001, 31, 37-42.
  149. Soriano, P. Generalized lacZ expression with the ROSA26 Cre reporter strain. *Nat Genet*. 1999, 21, 70-71.
  150. Niwa, H.; Yamamura, K.; Miyazaki, J. Efficient selection for high-expression transfectants with a novel eukaryotic vector. *Gene*. 1991, 108, 193-199.
  151. Uhlirva, H.; Kilic, K.; Tian, P.; Thunemann, M.; Desjardins, M.; Saisan, P. A.; Sakadzic,

## References

- S.; Ness, T. V.; Mateo, C.; Cheng, Q. et. al. Cell type specificity of neurovascular coupling in cerebral cortex. *Elife*. 2016, 5, pii: e14315.
152. Shin, H. K.; Jones, P. B.; Garcia-Alloza, M.; Borrelli, L.; Greenberg, S. M.; Bacskai, B. J.; Frosch, M. P.; Hyman, B. T.; Moskowitz, M. A.; Ayata, C. Age-dependent cerebrovascular dysfunction in a transgenic mouse model of cerebral amyloid angiopathy. *Brain*. 2007, 130, 2310-2319.
153. Stosiek, C.; Garaschuk, O.; Holthoff, K.; Konnerth, A. In vivo two-photon calcium imaging of neuronal networks. *Proc Natl Acad Sci U S A*. 2003, 100, 7319-7324.
154. Schindelin, J.; Arganda-Carreras, I.; Frise, E.; Kaynig, V.; Longair, M.; Pietzsch, T.; Preibisch, S.; Rueden, C.; Saalfeld, S.; Schmid, B. et. al. Fiji: an open-source platform for biological-image analysis. *Nat Methods*. 2012, 9, 676-682.
155. Schmidt, H.; Peters, S.; Frank, K.; Wen, L.; Feil, R.; Rathjen, F. G. Dorsal root ganglion axon bifurcation tolerates increased cyclic GMP levels: the role of phosphodiesterase 2A and scavenger receptor Npr3. *Eur J Neurosci*. 2016, 44, 2991-3000.
156. Halbrugge, M.; Friedrich, C.; Eigenthaler, M.; Schanzenbacher, P.; Walter, U. Stoichiometric and reversible phosphorylation of a 46-kDa protein in human platelets in response to cGMP- and cAMP-elevating vasodilators. *J Biol Chem*. 1990, 265, 3088-3093.
157. Miller, L. <http://lukemiller.org/index.php/2010/11/analyzing-gels-and-western-blots-with-image-j/>. 2010. Accessed on 02.02.2018.
158. Konter, J.; El-Din Ali Ahmed Hassan Abuo-Rahma, G.; El-Emam, A.; Lehmann, J. The NOTizer--a device for the convenient preparation of diazen-1-ium-1,2-diolates. *Methods Enzymol*. 2005, 396, 17-26.
159. Hornak, J. The Basics of NMR - A non-technical overview of NMR theory, equipment, and techniques. <http://www.cis.rit.edu/htbooks/nmr/inside.htm>. 1996. Accessed on 02.12.2018.
160. Smolenski, A.; Burkhardt, A. M.; Eigenthaler, M.; Butt, E.; Gambaryan, S.; Lohmann, S. M.; Walter, U. Functional analysis of cGMP-dependent protein kinases I and II as mediators of NO/cGMP effects. *Naunyn Schmiedebergs Arch Pharmacol*. 1998, 358, 134-139.
161. Butt, E.; Eigenthaler, M.; Genieser, H. G. (Rp)-8-pCPT-cGMPS, a novel cGMP-dependent protein kinase inhibitor. *Eur J Pharmacol*. . 1994, 296, 265-268.
162. Eigenthaler, M.; Ullrich, H.; Geiger, J.; Horstrup, K.; Hönig-Liedl, P.; Wiebecke, D.; Walter, U. Defective nitrovasodilator-stimulated protein phosphorylation and calcium regulation in cGMP-dependent protein kinase-deficient human platelets of chronic myelocytic leukemia. *J Biol Chem*. 1993, 268, 13526-13531.
163. Garthwaite, J.; Garthwaite, G.; Hajós, F. Amino acid neurotoxicity: relationship to neuronal depolarization in rat cerebellar slices. *Neuroscience*. 1986, 18, 449-460.
164. Contestabile, A. Roles of NMDA receptor activity and nitric oxide production in brain development. *Brain Res Brain Res Rev*. 2000, 32, 476-509.
165. Dickie, B. G.; Lewis, M. J.; Davies, J. A. NMDA-induced release of nitric oxide potentiates aspartate overflow from cerebellar slices. *Neurosci Lett*. 1992, 138, 145-148.
166. Collado-Alsina, A.; Ramirez-Franco, J.; Sanchez-Prieto, J.; Torres, M. The regulation of synaptic vesicle recycling by cGMP-dependent protein kinase type II in cerebellar granule cells under strong and sustained stimulation. *J Neurosci*. 2014, 34, 8788-8799.
167. Nonaka, S.; Hough, C. J.; Chuang, D. M. Chronic lithium treatment robustly protects neurons in the central nervous system against excitotoxicity by inhibiting N-methyl-D-aspartate receptor-mediated calcium influx. *Proc Natl Acad Sci U S A*. 1998, 95, 2642-2647.
168. Pöhler, D.; Butt, E.; Meissner, J.; Müller, S.; Lohse, M.; Walter, U.; Lohmann, S. M.; Jarchau, T. Expression, purification, and characterization of the cGMP-dependent protein kinases I beta and II using the baculovirus system. *FEBS Lett*. 1995, 374, 419-425.
169. Campbell, J. C.; Henning, P.; Franz, E.; Sankaran, B.; Herberg, F. W.; Kim, C. Structural basis of analog specificity in PKG I and II. *ACS Chem Biol*. 2017, 12, 2388-2398.

## References

170. Kouzoukas, D. E.; Bhalla, R. C.; Pantazis, N. J. Activation of cyclic GMP-dependent protein kinase blocks alcohol-mediated cell death and calcium disruption in cerebellar granule neurons. *Neurosci Lett*. 2018, *676*, 108-112.
171. Brown, R. L.; Strassmaier, T.; Brady, J. D.; Karpen, J. W. The pharmacology of cyclic nucleotide-gated channels: emerging from the darkness. *Curr Pharm Des*. 2006, *12*, 3597-3613.
172. Poppe, H.; Rybalkin, S. D.; Rehmann, H.; Hinds, T. R.; Tang, X. B.; Christensen, A. E.; Schwede, F.; Genieser, H. G.; Bos, J. L.; Doskeland, S. O. et. al. Cyclic nucleotide analogs as probes of signaling pathways. *Nat Methods*. 2008, *5*, 277-278.
173. Kleppisch, T.; Wolfsgruber, W.; Feil, S.; Allmann, R.; Wotjack, C. T.; Goebbels, S.; Nave, K. A.; Hofmann, F.; Feil, R. Hippocampal cGMP-dependent protein kinase I supports an age- and protein synthesis-dependent component of long-term potentiation but is not essential for spatial reference and contextual memory. *J Neurosci*. 2003, *23*, 6005-6012.
174. Langmesser, S.; Franken, P.; Feil, S.; Emmenegger, Y.; Albrecht, U.; Feil, R. cGMP-dependent protein kinase type I is implicated in the regulation of the timing and quality of sleep and wakefulness. *PLoS One*. 2009, *4*, e4238.
175. Butt, E.; Geiger, J.; Jarchau, T.; Lohmann, S. M.; Walter, U. The cGMP-dependent protein kinase - gene, protein, and function. *Neurochem Res*. 1993, *18*, 27-42.
176. Muller, P. M.; Gnugge, R.; Dhayade, S.; Thunemann, M.; Krippeit-Drews, P.; Drews, G.; Feil, R. H<sub>2</sub>O<sub>2</sub> lowers the cytosolic Ca<sup>2+</sup> concentration via activation of cGMP-dependent protein kinase I $\alpha$ . *Free Radic Biol Med*. 2012, *53*, 1574-1583.
177. Feil, R. Functional reconstitution of vascular smooth muscle cells with cGMP-dependent protein kinase I isoforms. *Circ Res*. 2002, *90*, 1080-1086.
178. Pfeifer, A.; Klatt, P.; Massberg, S.; Ny, L.; Sausbier, M.; Hirneiss, C.; Wang, G. X.; Korth, M.; Aszódi, A.; Andersson, K. E. et. al. Defective smooth muscle regulation in cGMP kinase I-deficient mice. *EMBO J*. 1998, *17*, 3045-3051.
179. Jurado, S.; Sanchez-Prieto, J.; Torres, M. Expression of cGMP-dependent protein kinases (I and II) and neuronal nitric oxide synthase in the developing rat cerebellum. *Brain Res Bull*. 2005, *65*, 111-115.
180. Collado-Alsina, A.; Hofmann, F.; Sanchez-Prieto, J.; Torres, M. Altered synaptic membrane retrieval after strong stimulation of cerebellar granule neurons in cyclic GMP-dependent protein kinase II (cGKII) knockout mice. *Int J Mol Sci*. 2017, *18*, 2281.
181. de Vente, J.; Asan, E.; Gambaryan, S.; Markerink-van Ittersum, M.; Axer, H.; Gallatz, K.; Lohmann, S. M.; Palkovits, M. Localization of cGMP-dependent protein kinase type II in rat brain. *Neuroscience*. 2001, *108*, 27-49.
182. Kelly, M. P. Cyclic nucleotide signaling changes associated with normal aging and age-related diseases of the brain. *Cell Signal*. 2018, *42*, 281-291.
183. Baltrons, M. A.; Saadoun, S.; Agullo, L.; García, A. Regulation by calcium of the nitric oxide/cyclic GMP system in cerebellar granule cells and astroglia in culture. *J Neurosci Res*. 1997, *49*, 333-341.
184. van Staveren, W. C.; Glick, J.; Markerink-van Ittersum, M.; Shimizu, M.; Beavo, J. A.; Steinbusch, H. W.; de Vente, J. Cloning and localization of the cGMP-specific phosphodiesterase type 9 in the rat brain. *J Neurocytol*. 2002, *31*, 729-741.
185. Reyes-Irisarri, E.; Markerink-Van Ittersum, M.; Mengod, G.; de Vente, J. Expression of the cGMP-specific phosphodiesterases 2 and 9 in normal and Alzheimer's disease human brains. *Eur J Neurosci*. 2007, *25*, 3332-3338.
186. Kelly, M. P.; Adamowicz, W.; Bove, S.; Hartman, A. J.; Mariga, A.; Pathak, G.; Reinhart, V.; Romegialli, A.; Kleiman, R. J. Select 3',5'-cyclic nucleotide phosphodiesterases exhibit altered expression in the aged rodent brain. *Cell Signal*. 2014, *26*, 383-397.
187. Patel, N. S.; Klett, J.; Pilarzyk, K.; Lee, D. I.; Kass, D.; Menniti, F. S.; Kelly, M. P. Identification of new PDE9A isoforms and how their expression and subcellular compartmentalization in the brain change across the life span. *Neurobiol Aging*. 2018, *65*, 217-234.
188. Lee, D. I.; Zhu, G.; Sasaki, T.; Cho, G. S.; Hamdani, N.; Holewinski, R.; Jo, S. H.; Danner, T.; Zhang, M.; Rainer, P. P. et. al. Phosphodiesterase 9A controls nitric-oxide-

## References

- independent cGMP and hypertrophic heart disease. *Nature*. 2015, 519, 472-476.
189. Chappie, T. A.; Humphrey, J. M.; Allen, M. P.; Estep, K. G.; Fox, C. B.; Lebel, L. A.; Liras, S.; Marr, E. S.; Menniti, F. S.; Pandit, J.; Schmidt, C. J.; Tu, M.; Williams, R. D.; Yang, F. V. Discovery of a series of 6,7-dimethoxy-4-pyrrolidylquinazoline PDE10A inhibitors. *J Med Chem*. 2007, 50, 182-185.
  190. Liu, Y.; Beyer, A.; Aebersold, R. On the dependency of cellular protein levels on mRNA abundance. *Cell*. 2016, 165, 535-550.
  191. Wong, E. H.; Kemp, J. A.; Priestley, T.; Knight, A. R.; Woodruff, G. N.; Iversen, L. L. The anticonvulsant MK-801 is a potent N-methyl-D-aspartate antagonist. *Proc Natl Acad Sci U S A*. 1986, 83, 7104-7108.
  192. Haynes, L. W. Block of the cyclic GMP-gated channel of vertebrate rod and cone photoreceptors by l-cis-diltiazem. *J Gen Physiol*. 1992, 100, 783-801.
  193. Shelly, M.; Lim, B. K.; Cancedda, L.; Heilshorn, S. C.; Gao, H.; Poo, M. M. Local and long-range reciprocal regulation of cAMP and cGMP in axon/dendrite formation. *Science*. 2010, 327, 547-552.
  194. Brescia, M.; Zaccolo, M. Modulation of compartmentalised cyclic nucleotide signalling via local inhibition of phosphodiesterase activity. *Int J Mol Sci*. 2016, 17, pii: E1672.
  195. Pietrobon, M.; Zamparo, I.; Maritan, M.; Franchi, S. A.; Pozzan, T.; Lodovichi, C. Interplay among cGMP, cAMP, and Ca<sup>2+</sup> in living olfactory sensory neurons in vitro and in vivo. *J Neurosci*. 2011, 31, 8395-8405.
  196. Kobayashi, T.; Nagase, F.; Hotta, K.; Oka, K. Crosstalk between second messengers predicts the motility of the growth cone. *Sci Rep*. 2013, 3, 3118.
  197. Akiyama, H.; Fukuda, T.; Tojima, T.; Nikolaev, V. O.; Kamiguchi, H. Cyclic nucleotide control of microtubule dynamics for axon guidance. *J Neurosci*. 2016, 36, 5636-5649.
  198. Wang, Z.; Lu, Y.; Qin, K.; Wu, Y.; Tian, Y.; Wang, J.; Zhang, J.; Hou, J.; Cui, Y.; Wang, K.; Shen, J.; Xu, Q.; Kong, D.; Zhao, Q. Enzyme-functionalized vascular grafts catalyze in-situ release of nitric oxide from exogenous NO prodrug. *J Control Release*. 2015, 210, 179-188.
  199. Winther, A. K.; Fejerskov, B.; Ter Meer, M.; Jensen, N. B. S.; Dillion, R.; Schaffer, J. E.; Chandrawati, R.; Stevens, M. M.; Schultze Kool, L. J.; Simonsen, U.; Zelikin, A. N. Enzyme Prodrug Therapy Achieves Site-Specific, Personalized Physiological Responses to the Locally Produced Nitric Oxide. *ACS Appl Mater Interfaces*. 2018, 10, 10741-10751.
  200. Deng, L.; Zhang, E.; Chen, C. Synergistic interaction of beta-galactosyl-pyrrolidinyldiazoniumdiolate with cisplatin against three tumor cells. *Arch Pharm Res*. 2013, 36, 619-625.
  201. Arancio, O.; Kiebler, M.; Lee, C. J.; Lev-Ram, V.; Tsien, R. Y.; Kandel, E. R.; Hawkins, R. D. Nitric oxide acts directly in the presynaptic neuron to produce long-term potentiation in cultured hippocampal neurons. *Cell*. 1996, 87, 1025-1035.
  202. Ohki, E. C.; Tilkins, M. L.; Ciccarone, V. C.; Price, P. J. Improving the transfection efficiency of post-mitotic neurons. *J Neurosci Methods*. 2001, 112, 95-99.
  203. Shuhaibar, L. C.; Egbert, J. R.; Norris, R. P.; Lampe, P. D.; Nikolaev, V. O.; Thunemann, M.; Wen, L.; Feil, R.; Jaffe, L. A. Intercellular signaling via cyclic GMP diffusion through gap junctions restarts meiosis in mouse ovarian follicles. *Proc Natl Acad Sci U S A*. 2015, 112, 5527-5532.
  204. Stroppel, A. S.; Paolillo, M.; Ziegler, T.; Feil, R.; Stafforst, T. Npom-protected NONOate enables light-triggered NO/cGMP signalling in primary vascular smooth muscle cells. *Chembiochem*. 2018, 19, 1312-1318.
  205. Barski, J. J.; Hartmann, J.; Rose, C. R.; Hoebeek, F.; Mörl, K.; Noll-Hussong, M.; De Zeeuw, C.; Konnerth, A.; Meyer, M. Calbindin in cerebellar Purkinje cells is a critical determinant of the precision of motor coordination. *J Neurosci*. 2003, 23, 3469-3477.
  206. Mathias, E. J.; Plank, M. J.; David, T. A model of neurovascular coupling and the BOLD response: PART I. *Comput Methods Biomech Biomed Engin*. 2017, 20, 508-518.
  207. Linden, D. J.; Connor, J. A. Long-term depression of glutamate currents in cultured cerebellar Purkinje neurons does not require nitric oxide signalling. *Eur J Neurosci*. 1992, 4, 10-15.

## References

208. Daniel, H.; Hemart, N.; Jaillard, D.; Crepel, F. Long-term depression requires nitric oxide and guanosine 3':5' cyclic monophosphate production in rat cerebellar Purkinje cells. *Eur J Neurosci.* 1993, 5, 1079-1082.
209. Hartell, N. A. cGMP acts within cerebellar Purkinje cells to produce long term depression via mechanisms involving PKC and PKG. *Neuroreport.* 1994, 5, 833-836.
210. Lev-Ram, V.; Makings, L. R.; Keitz, P. F.; Kao, J. P.; Tsien, R. Y. Long-term depression in cerebellar Purkinje neurons results from coincidence of nitric oxide and depolarization-induced Ca<sup>2+</sup> transients. *Neuron.* 1995, 15, 407-415.
211. Shibuki, K.; Okada, D. Endogenous nitric oxide release required for long-term synaptic depression in the cerebellum. *Nature.* 1991, 349, 326-328.
212. Luong, T. N.; Carlisle, H. J.; Southwell, A.; Patterson, P. H. Assessment of motor balance and coordination in mice using the balance beam. *J Vis Exp.* 2011, pii: 2376.
213. Lies, B.; Groneberg, D.; Gambaryan, S.; Friebe, A. Lack of effect of ODQ does not exclude cGMP signalling via NO-sensitive guanylyl cyclase. *Br J Pharmacol.* 2013, 170, 317-327.
214. Montoliu, C.; Rodrigo, R.; Monfort, P.; Llansola, M.; Cauli, O.; Boix, J.; Elmili, N.; Agusti, A.; Felipo, V. Cyclic GMP pathways in hepatic encephalopathy. Neurological and therapeutic implications. *Metab Brain Dis.* 2010, 25, 39-48.
215. van der Staay, F. J.; Rutten, K.; Barfacker, L.; Devry, J.; Erb, C.; Heckroth, H.; Karthaus, D.; Tersteegen, A.; van Kampen, M.; Blokland, A.; Prickaerts, J.; Reymann, K. G.; Schroder, U. H.; Hendrix, M. The novel selective PDE9 inhibitor BAY 73-6691 improves learning and memory in rodents. *Neuropharmacology.* 2008, 55, 908-918.
216. Boess, F. G.; Hendrix, M.; van der Staay, F. J.; Erb, C.; Schreiber, R.; van Staveren, W.; de Vente, J.; Prickaerts, J.; Blokland, A.; Koenig, G. Inhibition of phosphodiesterase 2 increases neuronal cGMP, synaptic plasticity and memory performance. *Neuropharmacology.* 2004, 47, 1081-1092.
217. Rutten, K.; Prickaerts, J.; Hendrix, M.; van der Staay, F. J.; Sik, A.; Blokland, A. Time-dependent involvement of cAMP and cGMP in consolidation of object memory: studies using selective phosphodiesterase type 2, 4 and 5 inhibitors. *Eur J Pharmacol.* 2007, 558, 107-112.
218. Rutten, K.; Prickaerts, J.; Blokland, A. Rolipram reverses scopolamine-induced and time-dependent memory deficits in object recognition by different mechanisms of action. *Neurobiol Learn Mem.* 2006, 85, 132-138.
219. Zhang, H. T.; O'Donnell, J. M. Effects of rolipram on scopolamine-induced impairment of working and reference memory in the radial-arm maze tests in rats. *Psychopharmacology (Berl).* 2000, 150, 311-316.
220. Prickaerts, J.; Sik, A.; van Staveren, W. C.; Koopmans, G.; Steinbusch, H. W.; van der Staay, F. J.; de Vente, J.; Blokland, A. Phosphodiesterase type 5 inhibition improves early memory consolidation of object information. *Neurochem Int.* 2004, 45, 915-928.
221. Barad, M.; Bourtchouladze, R.; Winder, D. G.; Golan, H.; Kandel, E. Rolipram, a type IV-specific phosphodiesterase inhibitor, facilitates the establishment of long-lasting long-term potentiation and improves memory. *Proc Natl Acad Sci U S A.* 1998, 95, 15020-15025.
222. Baratti, C. M.; Boccia, M. M. Effects of sildenafil on long-term retention of an inhibitory avoidance response in mice. *Behav Pharmacol.* 1999, 10, 731-737.
223. Rutten, K.; Vente, J. D.; Sik, A.; Ittersum, M. M.; Prickaerts, J.; Blokland, A. The selective PDE5 inhibitor, sildenafil, improves object memory in Swiss mice and increases cGMP levels in hippocampal slices. *Behav Brain Res.* 2005, 164, 11-16.
224. Rutten, K.; Basile, J. L.; Prickaerts, J.; Blokland, A.; Vivian, J. A. Selective PDE inhibitors rolipram and sildenafil improve object retrieval performance in adult cynomolgus macaques. *Psychopharmacology (Berl).* 2008, 196, 643-648.
225. Reichel, J. M.; Bedenk, B. T.; Gassen, N. C.; Hafner, K.; Bura, S. A.; Almeida-Correa, S.; Genewsky, A.; Dedic, N.; Giesert, F.; Agarwal, A.; Nave, K. A.; Rein, T.; Czisch, M.; Deussing, J. M.; Wotjak, C. T. Beware of your Cre-Ation: lacZ expression impairs neuronal integrity and hippocampus-dependent memory. *Hippocampus.* 2016, 26, 1250-1264.

## References

226. Price, J.; Turner, D.; Cepko, C. Lineage analysis in the vertebrate nervous system by retrovirus-mediated gene transfer. *Proc Natl Acad Sci U S A*. 1987, *84*, 156-160.
227. Nolan, G. P.; Fiering, S.; Nicolas, J. F.; Herzenberg, L. A. Fluorescence-activated cell analysis and sorting of viable mammalian cells based on beta-D-galactosidase activity after transduction of *Escherichia coli lacZ*. *Proc Natl Acad Sci U S A*. 1988, *85*, 2603-2607.
228. Cruz, F. C.; Babin, K. R.; Leao, R. M.; Goldart, E. M.; Bossert, J. M.; Shaham, Y.; Hope, B. T. Role of nucleus accumbens shell neuronal ensembles in context-induced reinstatement of cocaine-seeking. *J Neurosci*. 2014, *34*, 7437-7446.
229. Cruz, F. C.; Koya, E.; Guez-Barber, D. H.; Bossert, J. M.; Lupica, C. R.; Shaham, Y.; Hope, B. T. New technologies for examining the role of neuronal ensembles in drug addiction and fear. *Nat Rev Neurosci*. 2013, *14*, 743-754.
230. Engeln, M.; Bastide, M. F.; Toulme, E.; Dehay, B.; Bourdenx, M.; Doudnikoff, E.; Li, Q.; Gross, C. E.; Boue-Grabot, E.; Pisani, A.; Bezard, E.; Fernagut, P. O. Selective inactivation of striatal FosB/DeltaFosB-expressing neurons alleviates L-DOPA-induced dyskinesia. *Biol Psychiatry*. 2016, *79*, 354-361.
231. Comley, L. H.; Wishart, T. M.; Baxter, B.; Murray, L. M.; Nimmo, A.; Thomson, D.; Parson, S. H.; Gillingwater, T. H. Induction of cell stress in neurons from transgenic mice expressing yellow fluorescent protein: implications for neurodegeneration research. *PLoS One*. 2011, *6*, e17639.
232. Shields, B. C.; Kahuno, E.; Kim, C.; Apostolides, P. F.; Brown, J.; Lindo, S.; Mensh, B. D.; Dudman, J. T.; Lavis, L. D.; Tadross, M. R. Deconstructing behavioral neuropharmacology with cellular specificity. *Science*. 2017, *356*, pii: eaaj2161.

## 7 Curriculum vitae

### Michael Paolillo

#### Education

---

<b>Tübingen University, Germany</b> Doctoral Candidate in Cellular and Molecular Neuroscience	Graduation: 2019
<b>Tübingen University, Germany</b> M.Sc. Cellular and Molecular Neuroscience	Graduation: 2015
<b>Binghamton University, New York, USA</b> B.Sc. Biochemistry and B.Sc. Integrative Neuroscience With Honors in Chemistry	Graduation: 2013

#### Work Experience

---

**Interfaculty Institute of Biochemistry (IFIB) at Tübingen University, Germany**  
**Biochemistry/Neuroscience Researcher, PhD (Dr. rer. nat.)** Aug. 2015 – Dec. 2018

- Investigated cGMP signal transduction in cardiovascular and neurological disease models in collaboration with domestic and international colleagues culminating in 4 scientific publications.
- Communication of scientific results domestically and internationally to both scientific and lay audiences (written and oral).
- Supervised research students to the successful completion of bachelor and master theses.
- Established a new method to study cell specific nitric oxide release in vivo.
- Experienced in Microsoft products, OriginPro, ImageJ, Axiovert, and other scientific software.

**Founder of the science magazine *The Neuromag*** 2015 – present

- Founded *Neuromag.net*, established and led a team of 8 scientists to publish 40+ scientific articles for both scientific and lay audiences.

**UC San Diego School of Medicine in San Diego, USA**

**Visiting Researcher** May 2018 – July 2018

- Investigated neurovascular coupling in transgenic mice with two-photon microscopy.
- Awarded a travel grant to conduct a collaboration between Tübingen University, Germany and UC San Diego, USA.

**Interfaculty Institute of Biochemistry (IFIB) at Tübingen University, Germany**

**Biochemistry / Neuroscience Researcher, M.Sc.** Nov. 2013 - July 2015

- Investigated cGMP signal transduction in cardiovascular and neurological disorders in collaboration with colleagues culminating in a written thesis and an oral defense.
- Synthesized an organic NO-compound and demonstrated its utility in cell culture.
- Utilized advanced microscopy techniques (e.g. FRET and spinning disc microscopy) and identified an interplay between cGMP and Ca<sup>2+</sup>.

**Hertie Institute for Clinical Brain Research (HIH) in Tübingen, Germany**

**Neuroimmunology Research Student** Sept. 2014 - Nov. 2014

- Investigation of multiple sclerosis disease models and the mechanisms of T cell induced neuronal cell death via the interplay between T cells, astrocytes, and neurons.
- Written and oral presentation of data to colleagues, superiors and collaborators.

**Chemistry Department at Binghamton University, New York, USA**

**RNA / DNA Research, B.Sc.** Sept. 2010 – May 2013

- Determination of the thermodynamic stability of modified and native strand RNA and DNA resulting in a research award and a high impact publication.

## References

### Leadership Experience

---

- Founded Neuromag.net, established and led a team of 8 scientists to publish 40+ articles.
- Co-founded a doctoral run committee to serve as liaisons between students and faculty.
- Led the organization of 6+ international scientific meetings in teams of 7+ colleagues
- Designed and oversaw the successful completion of internships and theses of students.
- Supervised practical laboratory courses of 10+ students and conducted oral exams.
- Supervised and coached 40+ teaching assistants for a class of 600+ students.

### Selected Awards, Presentations, and Certificates

---

European Business Competence License (EBCL)	2017
Course in Biostatistics of Clinical Studies	2017
Awarded a travel grant for an international collaboration	2018
Awarded best talk at the 2017 Tübingen Biochemistry Meeting	2017
Awarded the Hertie Foundation Scholarship for high academic performance	2013 & 2014
Talk at a biochemistry meeting in Würzburg, Germany	2017
Talk at a neuroscience conference in Schramberg, Germany	2017
Talk at a biochemistry conference in Chiemsee, Germany	2016
Poster presentation at the Society for Neuroscience Conference, San Diego	2016
Poster presentation at a neuroscience conference in Schramberg, Germany	2015

### Publications

---

1. Peters S, **Paolillo M**, Mergia E, Koesling D, Kennel L, Schmidtko A, Russwurm M, Feil R. cGMP imaging in brain slices reveals brain region-specific activity of NO-sensitive guanylyl cyclases (NO-GCs) and NO-GC stimulators. *Int J Mol Sci.* 2018;19 pii: E2313.
2. **Paolillo M**, Peters S, Schramm A, Schlossmann J, Feil R. Real-time imaging reveals augmentation of glutamate-induced Ca<sup>2+</sup> transients by the NO-cGMP pathway in cerebellar granule neurons. *Int J Mol Sci.* 2018;19 pii: E2185.
3. Stroppel AS, **Paolillo M**, Ziegler T, Feil R, Stafforst T. Npom-protected NONOate enables light-triggered NO/cGMP signalling in primary vascular smooth muscle cells. *Chembiochem.* 2018;19:1312-1318.
4. Patra A, **Paolillo M**, Charisse K, Manoharan M, Rozners E, Egli M. 2'-Fluoro RNA shows increased Watson-Crick H-bonding strength and stacking relative to RNA: evidence from NMR and thermodynamic data. *Angew Chem Int Ed Engl.* 2012;51:11863-6.

### Languages

---

English – native; German – professional fluency; Spanish – proficient user; Italian – beginner